

XDP Hybrid-flyback Controller XDPS2201

Product Overview

Product Highlights

- Digital Hybrid-flyback controller with integrated half-bridge driver in DSO-14 (150mil) package
- 600V high voltage start-up cell for fast charging and low stand-by power
- Peak current mode control for robust and fast line and load control
- Burst mode entry/exit operation based on output current estimation
- Primary side output overvoltage protection
- Supports lowest no-load stand-by power < 75mW
- Wide range of configurable parameters via one pin UART interface
- Lowest necessary bill of material

Features

- Configurable brown-in and brown-out protection
- Configurable built-in soft-start
- Configurable burst mode entry and exit current thresholds with small hysteresis
- Configurable overcurrent protection with two levels for peak and transient load
- Configurable output overvoltage protection
- Configurable frequency reduction with cycle skipping for improved low load efficiency
- Configurable jitter for switching frequency
- Configurable propagation delay compensation for accurate peak current control
- Pb-free lead plating; RoHS compliant
- Halogen-free according to IEC61249-2-21

Target Applications

- AC/DC SMPS
- Ultra high power density adapter > 20W/inch³
- Ultra high efficiency SMPS > 93%

Product validation

Qualified for industrial applications according to the relevant tests of JEDEC47/20/22.

Description

The XDPS2201 contains a Hybrid-flyback controller that is based on an asymmetrical half-bridge control. The half-bridge is driving a conventional flyback transformer in conjunction with a serial capacitor. The main inductance of the flyback transformer and the serial capacitor are building a resonant tank, which is used for achieving zero voltage switching (ZVS) behavior of the half-bridge power switches and is providing in addition a resonant power transmission during the conventional demagnetization phase of the flyback transformer. During normal operation the charge period and associated power is controlled by direct peak current control, whereas the demagnetization phase is timing controlled to ensure proper negative premagnetization, which is required for ZVS condition at the half-bridge power switches. Beside the continuous resonant mode (CRM) operation the IC also provides an advanced zero voltage resonant valley switching (ZV-RVS) and burst mode to support highest efficiency over the whole load and wide output voltage range.

| Sales Code | Package | SP-Ordering Code |
|------------|-----------|------------------|
| XDPS2201 | PG-DSO-14 | SP005417712 |

Typical Application

Typical Application

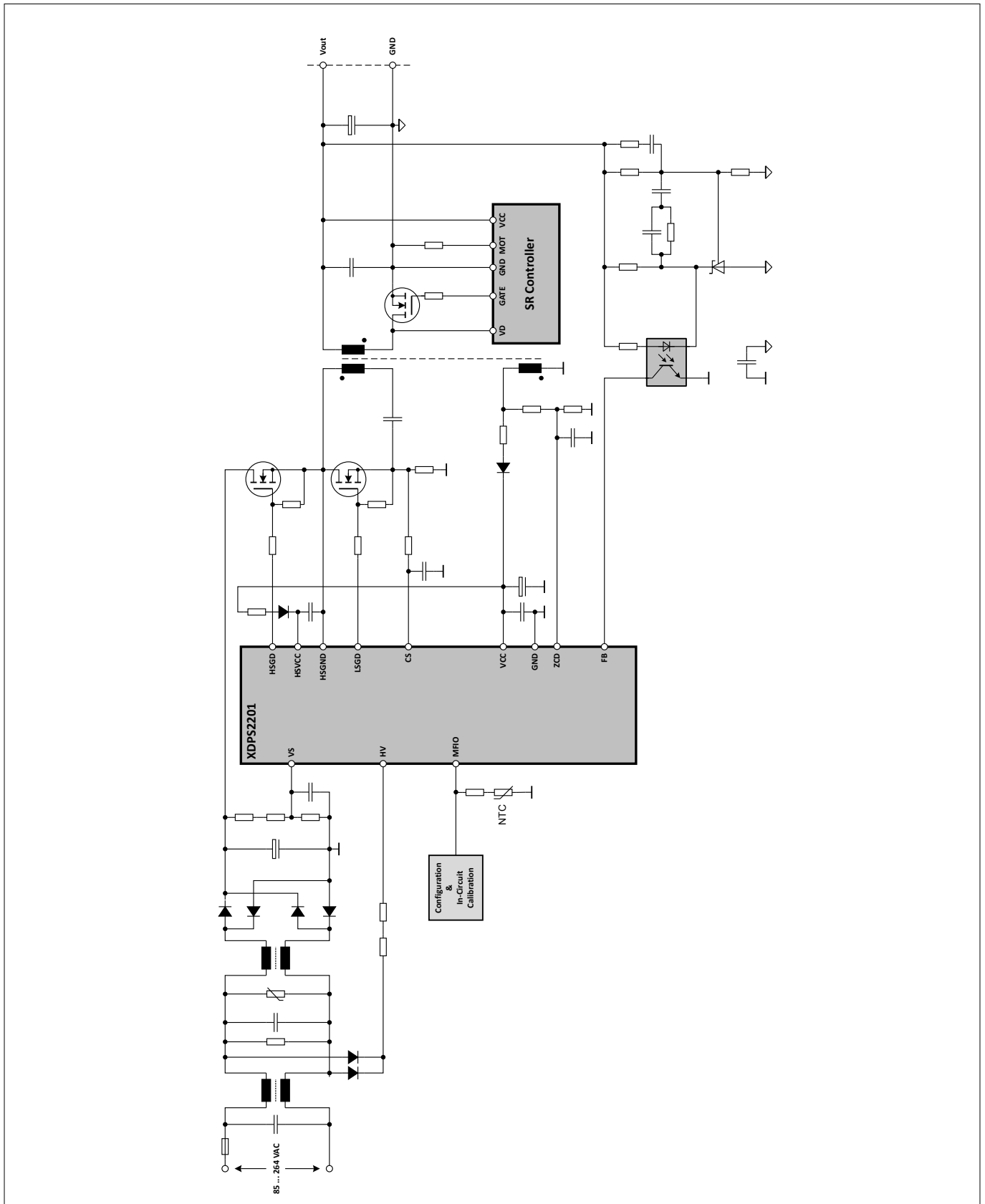


Figure 1 High density adapter < 75W

Table of contents

Table of contents

| | | |
|-----------|--|----|
| | Product Overview | 1 |
| | Product validation | 1 |
| | Description | 1 |
| | Typical Application | 2 |
| | Table of contents | 3 |
| 1 | Pin configuration | 6 |
| 2 | Block diagram | 8 |
| 3 | Functional description | 9 |
| 3.1 | Introduction | 9 |
| 3.1.1 | Continuous resonant mode (CRM) | 10 |
| 3.1.2 | Boundary conditions for ZVS operation | 13 |
| 3.1.3 | Zero voltage resonant valley switching mode (ZV-RVS) | 14 |
| 3.1.4 | Output control methods | 16 |
| 3.2 | Power supply management | 18 |
| 3.2.1 | VCC capacitor charge-up and start-up sequence | 18 |
| 3.2.2 | Bang-bang mode operation during brown-in phase | 19 |
| 3.2.3 | Bang-bang mode during protection mode operation | 21 |
| 3.2.4 | VCC supply during burst mode (BM) operation | 22 |
| 3.3 | Control features | 24 |
| 3.3.1 | Output control | 24 |
| 3.3.1.1 | Keeping ZVS operation for wide input voltage range | 25 |
| 3.3.1.2 | Keeping ZVS operation for wide output voltage range | 26 |
| 3.3.1.2.1 | Cycle by cycle ZVS operation during CRM operation | 26 |
| 3.3.1.3 | Output current control law | 27 |
| 3.3.1.3.1 | Current control during CRM | 30 |
| 3.3.1.3.2 | Current control during ZV-RVS mode | 31 |
| 3.3.1.4 | Propagation delay compensation (PDC) | 31 |
| 3.3.2 | PWM control schemes | 32 |
| 3.3.2.1 | CRM control scheme | 33 |
| 3.3.2.2 | ZV-RVS control scheme | 34 |
| 3.3.2.2.1 | Valley skipping control | 35 |
| 3.3.2.3 | DCM control scheme | 36 |
| 3.3.2.4 | Mode transition control | 37 |
| 3.3.2.5 | Overcurrent control | 37 |
| 3.3.3 | Vout start-up control | 37 |
| 3.3.4 | Burst mode control | 41 |
| 3.3.4.1 | Burst mode entry | 41 |

Table of contents

| | | |
|-----------|---|-----------|
| 3.3.4.2 | Burst mode operation | 42 |
| 3.3.4.3 | Burst mode bootstrap precharge | 43 |
| 3.3.4.4 | Burst mode exit control | 44 |
| 3.3.4.4.1 | Burst mode slow exit | 45 |
| 3.3.4.4.2 | Burst mode fast exit | 46 |
| 3.3.5 | Frequency jitter | 46 |
| 3.3.6 | Half-bridge gate driver | 47 |
| 3.4 | Protection features | 49 |
| 3.4.1 | Protection modes | 50 |
| 3.4.2 | VCC undervoltage lockout (UVOFF) | 50 |
| 3.4.3 | HSVCC undervoltage lockout (HSUVOFF) | 50 |
| 3.4.4 | Input voltage V_{in} protection | 50 |
| 3.4.4.1 | Brown-in protection (BIP) | 51 |
| 3.4.4.2 | Fast brown-out protection (FBOP) | 51 |
| 3.4.4.3 | Slow brown-out protection (SBOP) | 51 |
| 3.4.4.4 | V_{in} overvoltage protection (V_{inOVP}) | 51 |
| 3.4.5 | Start-up timeout protection (STTOP) | 52 |
| 3.4.6 | CS pin short circuit protection (CSSCP) | 52 |
| 3.4.7 | Overcurrent protection | 52 |
| 3.4.7.1 | Output overcurrent protection OCP1 level 1 (OCP1lev1) | 53 |
| 3.4.7.2 | Output overcurrent protection OCP1 level 2 (OCP1lev2) | 54 |
| 3.4.7.3 | Output maximum current protection (OCP1max) | 54 |
| 3.4.7.4 | Primary peak overcurrent protection OCP2 (OCP2) | 55 |
| 3.4.8 | V_{out} voltage protection | 55 |
| 3.4.8.1 | V_{out} undervoltage protection (V_{outUVP}) | 55 |
| 3.4.8.2 | V_{out} overvoltage protection (V_{outOVP}) | 56 |
| 3.4.8.3 | V_{out} short circuit protection (V_{outSCP}) | 56 |
| 3.4.9 | External overtemperature protection (extOTP) | 56 |
| 3.4.10 | Watchdog timer | 56 |
| 4 | Configuration | 57 |
| 4.1 | Configurable parameters and functions | 57 |
| 4.1.1 | System settings | 57 |
| 4.1.2 | Dimensioning | 57 |
| 4.1.3 | Half-bridge | 58 |
| 4.1.4 | ZV-RVS/DCM operation | 59 |
| 4.1.5 | Burst | 59 |
| 4.1.6 | Start-up | 59 |
| 4.1.7 | Protections | 60 |
| 4.1.8 | Mode thresholds | 62 |
| 4.1.9 | Jitter | 62 |
| 4.1.10 | Others | 62 |

Table of contents

| | | |
|----------|---|-----------|
| 4.2 | Tolerance classes for configurable parameters | 63 |
| 5 | Electrical characteristics | 65 |
| 5.1 | Definitions | 65 |
| 5.2 | Absolute maximum ratings | 65 |
| 5.3 | Package characteristics | 67 |
| 5.4 | Operating range | 67 |
| 5.5 | DC electrical characteristics | 68 |
| 6 | Package dimensions | 73 |
| | Revision history | 74 |
| | Disclaimer | 75 |

Pin configuration

1 Pin configuration

The pin configuration is shown in [Figure 2](#) and [Table 1](#). The pin functions are described in the sequel.

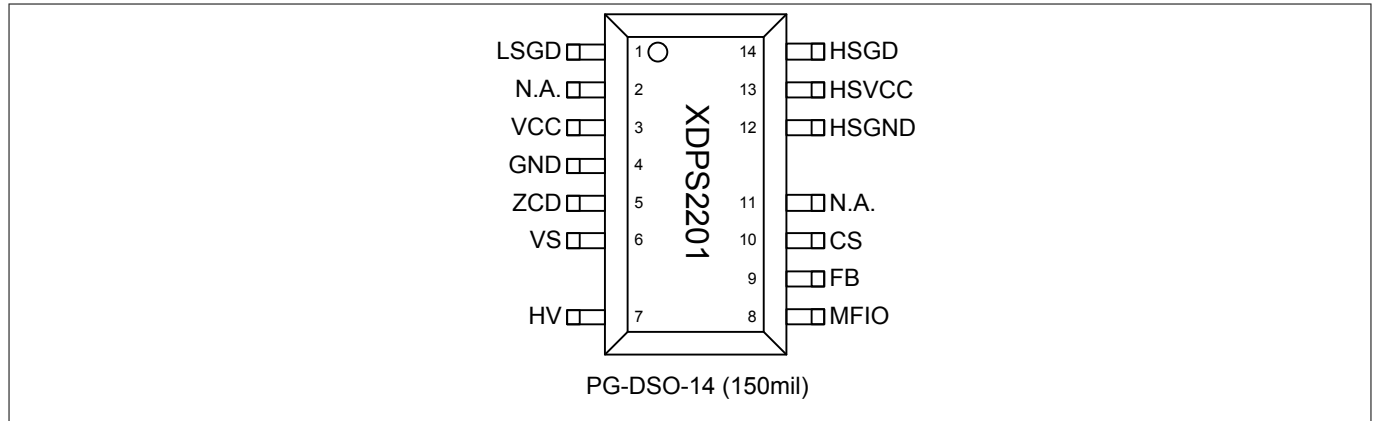


Figure 2 Pin configuration

Table 1 Pin definitions and functions

| Symbol | Pin | Type | Function |
|--------|-----|------|--|
| LSGD | 1 | O | Low-side gate driver Low-side gate driver of half-bridge driver stage |
| N.A. | 2 | — | Not available This pin is internally connected but not used, and should be connected to GND |
| VCC | 3 | I | Positive voltage supply IC power supply |
| GND | 4 | O | Ground Combined power and signal ground |
| ZCD | 5 | I | Zero-crossing detection ZCD pin provides zero-crossing detection after the low-side gate driver is turned off, during pause phase in skip cycle and burst mode. Furthermore, the reflected output voltage at auxiliary winding can be measured during the low-side gate driver turn-on phase |
| VS | 6 | I | Voltage sensing Low leakage input voltage sensing pin for controlling the negative magnetization and protections. VS pin is connected to a resistor divider for measuring the bulk voltage |
| HV | 7 | I | High-voltage input HV pin is connected to the AC line via external resistors and 2 diodes. An internally connected 600 V HV start-up cell is used for the initial VCC charge |
| MFIO | 8 | IO | Multi-functional input-output UART communication for parameter configuration and failure mode reporting is provided by this pin. In addition, a connected NTC can be measured |
| FB | 9 | I | Feedback Input pin receiving the feedback control signal from the optocoupler |
| CS | 10 | I | Current sensing |

Pin configuration**Table 1** Pin definitions and functions (continued)

| Symbol | Pin | Type | Function |
|--------|-----|------|---|
| | | | Input pin for current sensing during the high-side gate driver turn-on phase |
| N.A. | 11 | — | Not available This pin is internally connected but not used, and should be connected to GND |
| HSGND | 12 | O | High-side ground Ground reference node for floating driver domain |
| HSVCC | 13 | I | High-side power supply Power supply input for floating driver domain |
| HSGD | 14 | O | High-side gate driver Floating high-side gate driver of half-bridge driver stage |

Block diagram

2 Block diagram

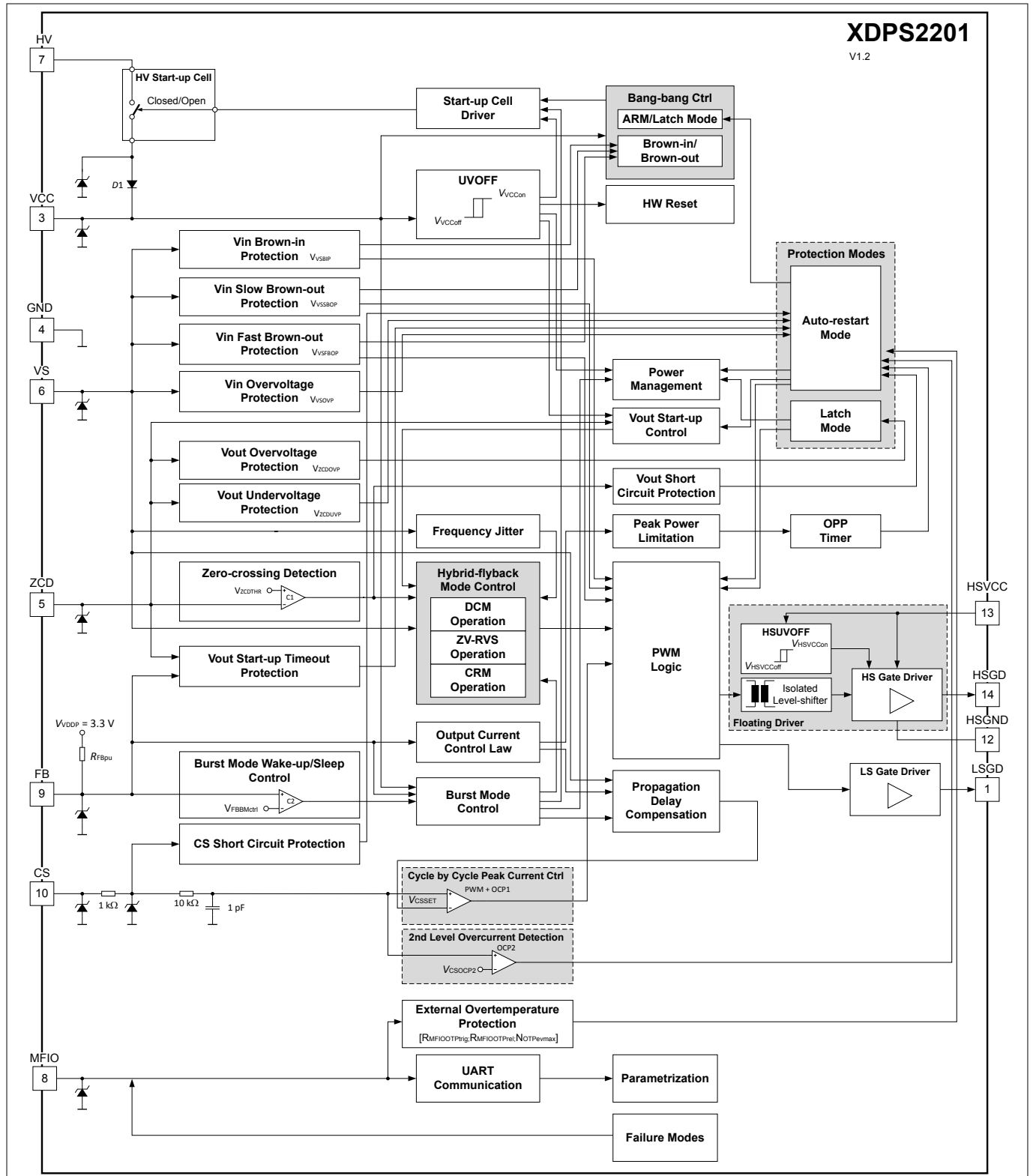


Figure 3 Block diagram

Functional description

3 Functional description

The functional description gives an overview about the integrated functions and features and their relationship. The mentioned parameters are based on either configurable parameters shown in [Chapter 4.1](#) or fixed parameters shown in [Chapter 5.5](#).

This chapter contains following main descriptions:

- Introduction ([Chapter 3.1](#))
- Power supply management ([Chapter 3.2](#))
- Control features ([Chapter 3.3](#))
- Protection features ([Chapter 3.4](#))

3.1 Introduction

In the following a brief introduction is given for the hybrid-flyback converter, which is based on a resonant asymmetrical half-bridge flyback topology shown in [Figure 4](#).

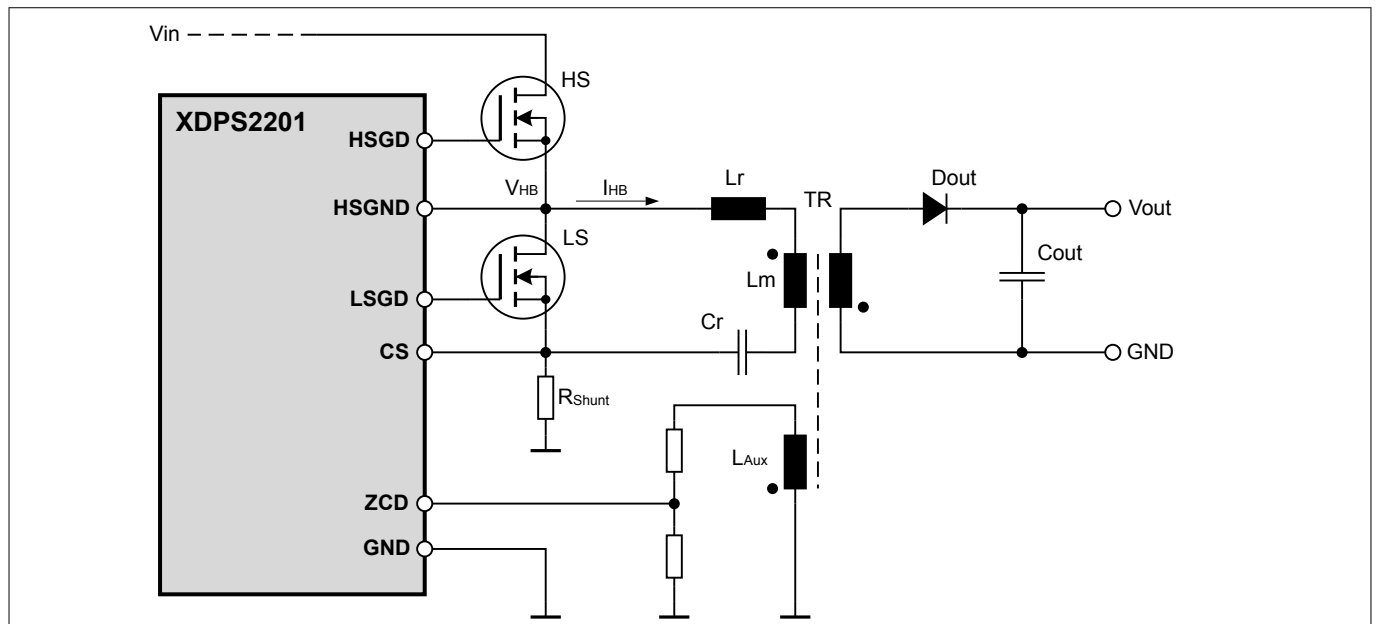


Figure 4 Hybrid-flyback power stage

The main advantage of this hybrid-flyback topology is the extended energy storage approach, which enables the usage of a smaller transformer at the same switching frequency compared to the standard and active clamp flyback topologies. In hybrid-flyback the total energy is not only stored in the transformer. In addition an amount of energy is stored in an external capacitor C_r , which is connected in series with the transformer. The proportion of the amount of energy that is stored in transformer and capacitor is depending on the input voltage. For lower input voltage more energy is getting stored in the capacitor. The switching frequency is also depending on the input voltage similar to a critical conduction mode flyback operation (see [Figure 5](#)).

Functional description

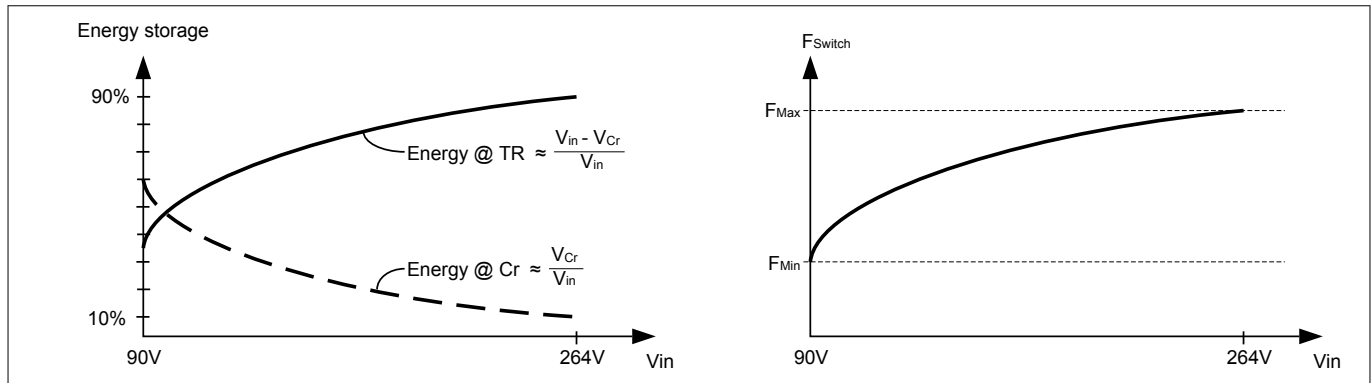


Figure 5 Hybrid-flyback energy storage sharing and switching frequency dependency

The resonant asymmetrical half-bridge flyback power stage can achieve zero voltage switching (ZVS) operation on primary side and zero current switching (ZCS) operation on secondary side under all conditions of input voltage V_{in} and output voltage V_{out} . The power circuit in the primary side is realized by an LC tank, built by the resonant inductor L_r and resonant capacitor C_r , which is driven by a half-bridge similar to an LLC converter. L_r represents the series inductance, being L_r either only the transformer leakage inductance or the leakage inductance plus an optional external inductor. With this configuration the transformer leakage energy is recycled avoiding the switching losses of traditional single switch flyback converter.

In order to achieve lowest switching losses by means of ZVS operation over the whole load range, two control methods are implemented to support maximum efficiency over wide V_{in} , wide V_{out} and whole output load ranges. The control methods are based on measured current signal V_{CS} at shunt resistor R_{shunt} , voltage signal V_{ZCD} and valley detection N_{RVSval} at auxiliary winding L_{Aux} and input voltage V_{in} .

Following operating modes are supported by the two control methods for ensuring ZVS operation:

- Continuous resonant mode (CRM) operation (see [Chapter 3.1.1](#))
- Zero voltage resonant valley switching (ZV-RVS) operation (see [Chapter 3.1.3](#))

3.1.1 Continuous resonant mode (CRM)

The operation phases of the resonant asymmetrical flyback duty cycle can be divided into 6 phases as shown in [Figure 6](#) and [Figure 7](#). In continuous resonant mode (CRM) the switching of high-side switch HS and low-side switch LS is done in an alternating manner without blanking phases. Only short dead-times t_{deadHS} for the high-side switch turn-on and t_{deadLS} for the LS switch turn-on apply during the soft resonant switch-over of the half-bridge middle node.

Functional description

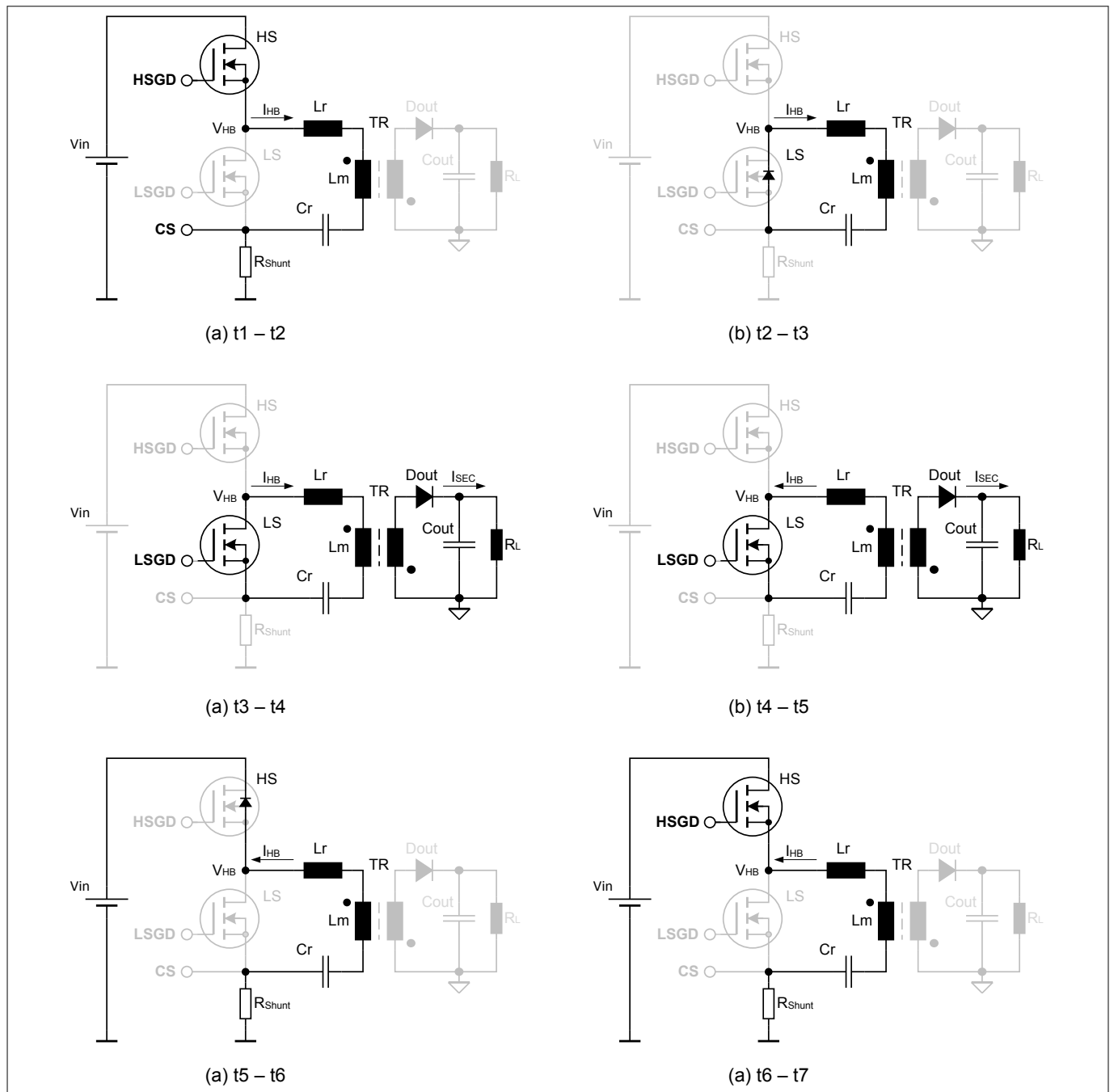


Figure 6 Hybrid-flyback converter operation phases in CRM

Phase 1, t1 to t2:

Phase 1 starts when the half-bridge current I_{HB} is changing in direction to a positive value. In this phase HS switch is turned on and LS switch is turned off since time t_0 . The increasing positive current I_{HB} is magnetizing the transformer TR and charging the resonant capacitor Cr . The output diode $Dout$ is biased inversely blocking any energy transfer to the secondary side. The magnitude of I_{HB} is measured via the shunt resistor R_{Shunt} . Phase 1 is finished once I_{HB} exceeds an internal peak current set-point, which turns off the HS switch.

Phase 2, t2 to t3:

At time t_2 HS switch is also turned off, which disconnects the charging path from V_{in} . The magnetizing current I_{HB} in the transformer TR keeps flowing and forces the voltage at the half-bridge node V_{HB} to drop until the body diode of LS switch starts to conduct. At this time t_3 the primary side of the transformer TR has the same voltage level as capacitor Cr .

Functional description**Phase 3, t3 to t4:**

During phase 3 *HS* switch is kept turned off. At time *t3* *LS* switch is turned on under zero voltage (ZVS) condition. The voltage at secondary winding of transformer *TR* is now equal to the voltage across the resonant capacitor *Cr*, divided by the transformer turns ratio. The secondary side current I_{SEC} starts flowing through output diode *Dout*. The resonant sine wave shape and period of I_{SEC} is determined by the resonant tank formed by the transformer leakage inductance *Lr* and *Cr*. The primary half-bridge current I_{HB} is the sum of the transformer *TR* magnetizing current I_{MAG} plus the reflected secondary side current I_{SEC} . The current in the resonant *LrCr* tank is still positive and mainly driven by the transformer magnetizing inductance *Lm*, which charges further the resonant capacitor *Cr*. In this manner the energy stored in the transformer and *Cr* is transferred to the output.

Phase 4, t4 to t5:

Phase 4 starts when the primary side half-bridge current I_{HB} inverts its direction, which is driven by the resonant *LrCr* tank. During this time period the energy is still being transferred to the secondary side. At the same time also bringing down the transformer magnetizing current I_{MAG} to a negative level equivalent with I_{MAGneg} is supported as long *LS* switch is kept turned on.

Phase 5, t5 to t6:

At the beginning of phase 5 *LS* switch is also getting turned off. The negative current I_{MAGneg} in the transformer *TR* induced during the previous phase 4 is forcing the half-bridge bridge voltage V_{HB} to rise until clamping is taking place by the body diode of *HS* switch.

Phase 6, t6 to t7:

Phase 6 starts with turning on *HS* switch at ZVS condition. As the transformer resonant tank *LmCr* current I_{MAG} is still negative the excess of energy in the tank is sent back to the input.

Functional description

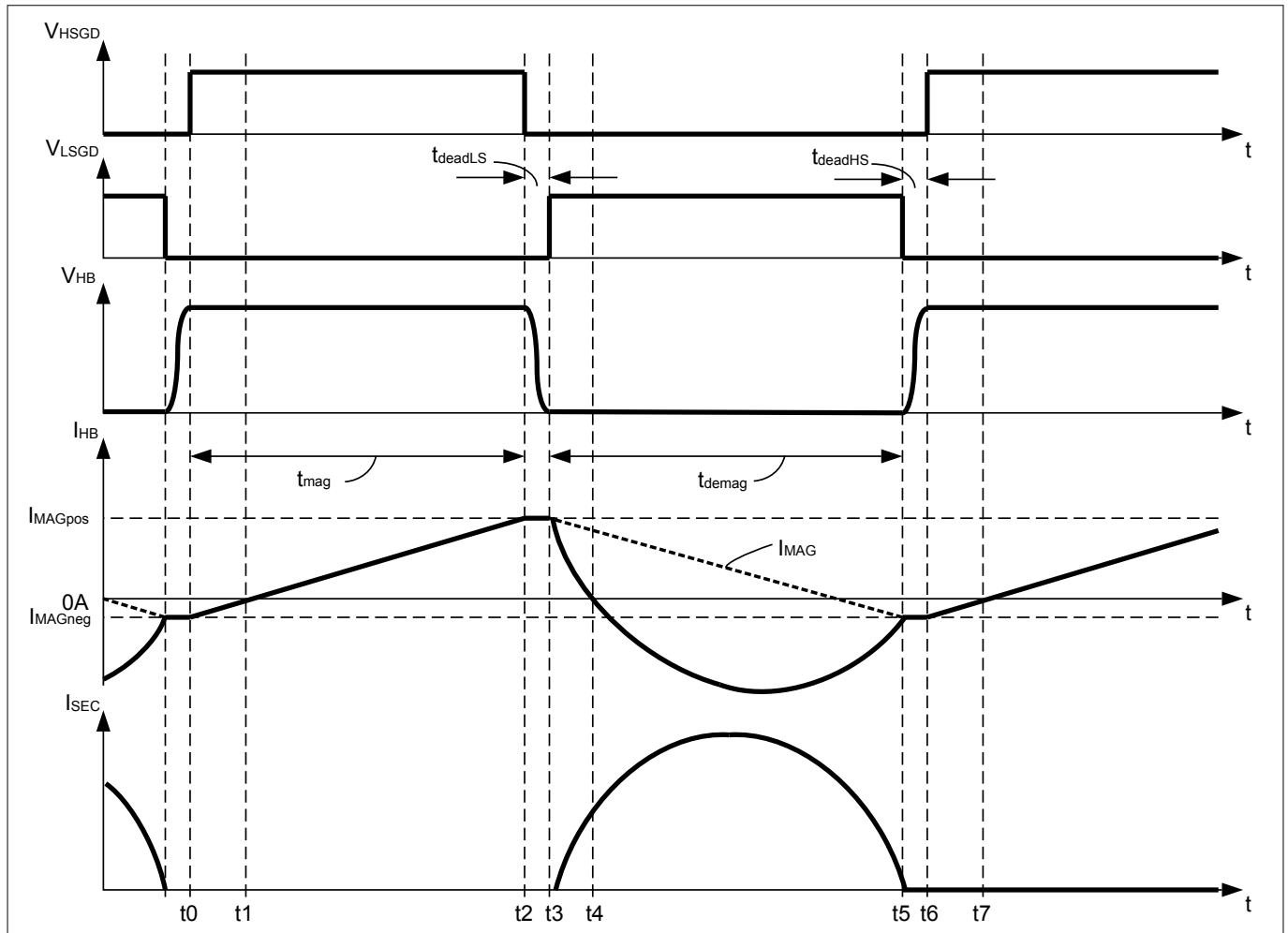


Figure 7 Hybrid-flyback converter signals

3.1.2 Boundary conditions for ZVS operation

Achieving a zero voltage switching (ZVS) turn-on condition for both *HS* and *LS* switches requires the right polarity of the resonant tank *LmCr* current I_{MAG} . Furthermore a sufficient energy level in the resonant tank *LmCr* is needed to switch-over the half-bridge voltage V_{HB} during the dead-times t_{deadLS} and t_{deadHS} . By ensuring ZVS operation, hard switching with undesired oscillations and, in worst case, body diode cross conduction can be properly avoided.

Switching over from *HS* switch to *LS* switch under ZVS condition is properly supported by the positive magnetization level (see [Figure 7](#)). Forcing ZVS condition for switch-over from *LS* switch to *HS* switch is covered by regulating the negative magnetization level depending on the input voltage V_{in} .

Wide V_{out} voltage range operation

When operating with variable output voltage there is an application requirement for adapting the switching phase between *HS* switch turn-on phases to ensure ZVS condition. [Figure 8](#) shows an example for a potential body diode cross conduction when output voltage is reduced and the timings for *LS* switch turn-on phase t_{LSon} and start of *HS* turn-on are not adapted. At time t_3 the slope of demagnetization current I_{MAG} is flatter compared to time period before t_0 due to lower V_{out} level. This leads to a larger demagnetization period t_{demag} of the transformer (see [Equation 7](#)). Keeping the pulse pattern for t_{LSon} and dead-time t_{deadHS} for turning on the *HS* switch constant would result in a body diode cross conduction of *LS* switch at time t_5 (see [Figure 8](#)). Here I_{MAG} is still positive and therefore not switching-over the half-bridge node and not finishing the conduction of the *LS* switch body diode. By adapting the pulse pattern depending on V_{out} ZVS condition is reached for all output voltage and load conditions (see [Chapter 3.3.1.2.1](#)).

Functional description

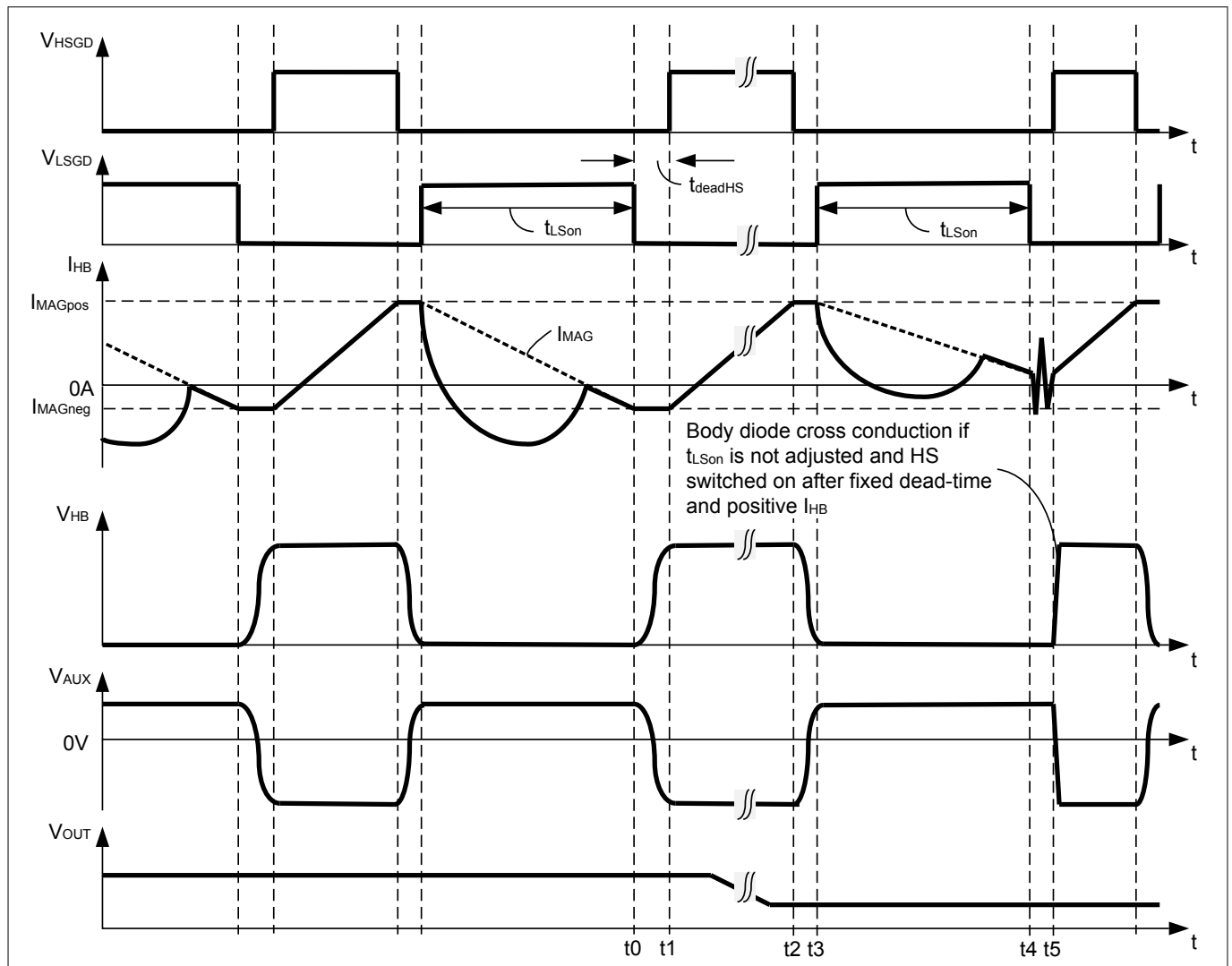


Figure 8 Body diode cross conduction at low V_{out} and fixed LS switch on-time

3.1.3 Zero voltage resonant valley switching mode (ZV-RVS)

When decreasing the load the amount of circulating magnetization energy is proportionally increasing compared to the transmitted energy in CRM operation. When decreasing V_{out} the demagnetization time is becoming longer than half of the resonant period of the $LrCr$ tank, which can lead to further resonant half-bridge oscillations. Turning off the LS switch during an ongoing I_{HB} oscillation can lead to oscillations on the secondary side due to the secondary side leakage inductance.

The higher circulation half-bridge current at low output load is limiting the achievable efficiency in CRM operation.

To overcome the mentioned issues the zero voltage resonant valley switching (ZV-RVS) mode is implemented to fix the peak to peak magnetization current and support a frequency foldback operation to reduce the average amount of circulating magnetization current.

ZV-RVS mode is based on valley detection of the signal at auxiliary winding L_{AUX} via ZCD pin zero-crossing detection. The free-wheeling oscillation, which is observed after demagnetization of transformer has finished, is the same as seen in the standard flyback topology. Figure 4 shows the auxiliary winding L_{AUX} used for zero-crossing detection, the falling edge indicating a rising half-bridge voltage V_{HB} and vice versa.

For optimum operation a waiting time gap $t_{waitgap}$ is introduced after a HS and LS switching cycle, which increases the associated half-bridge switching period. The time period $t_{waitgap}$ is depending on the set number

Functional description

for skipping valley detection before the next zero-crossing rising edge detection leads to a dedicated ZVS pulse. The number of skipped valleys is increasing with decreasing output load. After the ZVS pulse only one *HS* and *LS* half-bridge switching cycle with subsequent t_{waitgap} is performed. The ZVS pulse is generated by turning on *LS* switch under ZVS condition and forcing a negative half-bridge current level I_{MAGneg} to create a negative magnetization of the transformer. This leads to the same ZVS condition for turning on *HS* switch similar to CRM operation (see [Chapter 3.1.1](#)).

The operation can be divided into 8 phases as shown in [Figure 9](#).

Phase 1, t_0 to t_1 :

Phase 1 starts with finishing the demagnetization of the transformer. In this phase both switches are kept turned off and the half-bridge current I_{HB} is only determined by the free-wheeling oscillation due to parasitic capacities and inductivities connected to the half-bridge node. Phase 1 ends with a zero-crossing rising edge detection, which is depending on the set valley skipping number. A zero-crossing rising edge detection via *ZCD* pin indicates that V_{HB} is dropping to 0V as base for reaching ZVS condition for turning on *LS* switch.

Phase 2, t_1 to t_2 :

Phase 2 is a predefined delay time for turning on *LS* switch after the zero-crossing rising edge detection at time t_1 . The predefined delay time is depending on the free-wheeling oscillation period and provides ZVS condition for V_{HB} .

Phase 3, t_2 to t_3 :

At time t_2 *LS* switch is turned on under ZVS condition. *HS* switch is still kept turned off. The voltage on the resonant capacitor *Cr* is applied to the primary winding of the transformer forcing a negative flowing half-bridge current level I_{HBneg} , which magnetizes the transformer in the negative direction. The injected current during ZVS pulse on-time t_{ZVS} needs to provide the right amount of energy for switching over the half-bridge node voltage V_{HB} .

Note: Depending on the voltage of the resonant capacitor *Cr* and the output capacitor *Cout*, a secondary side synchronous controller (*SR*) may get triggered at the same time when ZVS pulse is generated. To avoid a shoot-through with *SR* controller being turned on when subsequently turning on *HS* switch, the minimum on-time of the *SR* controller must be shorter than the minimum pulse width of ZVS pulse t_{ZVS} (see [Figure 29](#)).

Phase 4, t_3 to t_4 :

At time t_3 *LS* switch is turned off. The negative half-bridge current keeps flowing and pulls up the half-bridge node. Once the half-bridge voltage V_{HB} is clamped by the body diode in *HS* switch ZVS condition is reached for turning on *HS* switch. Phase 4 is similar to the phase 5 in [Chapter 3.1.1](#).

Phase 5, t_4 to t_5 :

At time t_4 *HS* switch is turned on. Once the half-bridge current I_{HB} changes in polarity, energy is taken from the input capacitor and stored in the transformer and the resonant capacitor *Cr*. I_{HB} is rising and increasing the voltage at *Cr*. During this phase the secondary diode is inversely polarized and blocking a flowing current.

Phase 6, t_5 to t_6 :

At time t_5 *HS* switch is turned off. The half-bridge current I_{HB} keeps flowing and decreases the half-bridge voltage V_{HB} down to 0V, leading to ZVS condition for *LS* switch.

Phase 7, t_6 to t_7 :

In phase 7 the main energy transmission to the secondary side is taking place. Once the half-bridge current I_{HB} starts to decrease, the secondary side diode *Dout* is getting forward polarized and charging the output capacitor *Cout*. I_{MAG} is then demagnetizing the transformer. In addition a resonant current is superimposed, which is generated by the transformer leakage inductance and the resonant capacitor acting as resonant tank *LrCr*. As *Lr* is significant smaller than *Lm* the resonant period of *LrCr* tank is much shorter and can be seen as an oscillation. The very large resonant period of *LmCr* tank can be seen as a linear decrease of magnetizing current in this relative short time phase.

Functional description

Phase 8, t7 to t8:

Phase 8 shows an example of the half-bridge current signal when the $LrCr$ tank half resonant period is shorter than the demagnetization phase at LS switch turn-off. This shape of current is depending on the operation conditions determining the demagnetization period and low-side on-time. At time t8 the demagnetization of the transformer is finished. The secondary side diode $Dout$ is again inversely polarized and the free-wheeling oscillation at the half-bridge node is starting.

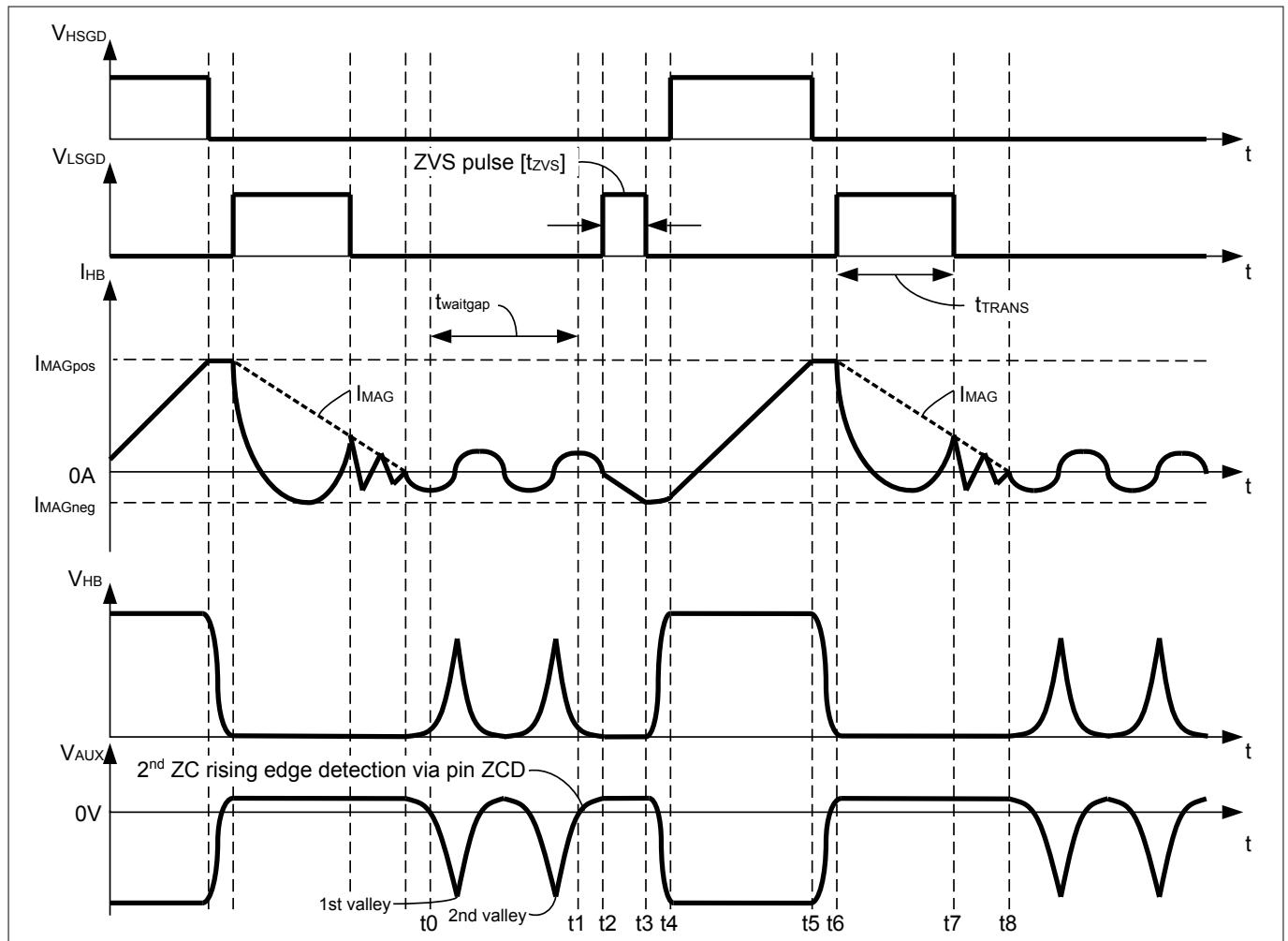


Figure 9 Hybrid-flyback operating in zero voltage resonant valley switching mode (ZV-RVS)

3.1.4 Output control methods

Output current control in CRM

The hybrid-flyback topology can be controlled either by duty cycle control or a combination of peak current control for HS switch and on-time control for LS switch. When looking on duty cycle control for HS switch a relationship between output voltage V_{out} and input voltage V_{in} is given as shown in the following equation. All equations in the sequel are based on considering ideal lossless components and neglecting any dead-times.

$$V_{out} = D \times \frac{V_{in}}{N} \times \frac{L_m}{L_m + L_r}$$

Equation 1

The duty cycle D is determined by

Functional description

$$D = \frac{t_{HSon}}{t_{HSon} + t_{LSon}}$$

Equation 2

with t_{HSon} and t_{LSon} being the on-times for *HS* and *LS* switches. *N* represents the winding turns ratio between primary and secondary side of the transformer.

Equation 1 shows that V_{out} is independent of the output current I_{out} .

Same as for standard flyback controllers primary peak current control is implemented to support a 1st order system for easier control loop compensation. The taken input power per half-bridge switching cycle is depending on the voltage at the resonant capacitor *Cr* that is charged by the half-bridge current I_{HB} during the on-time t_{HSon} . The input power can be calculated as shown in the following equation.

$$P_{in} = \frac{1}{2} \times V_{Cr_avg} \times (I_{MAGpos} + I_{MAGneg})$$

Equation 3

V_{Cr_avg} is the average voltage on the resonant capacitor *Cr*, which is the reflected output voltage V_{out} multiplied with the transformer turns ratio. The output voltage is reflected at winding L_{AUX} during the on-time period of *LS* switch.

$$V_{Cr_avg} = N \times V_{out}$$

Equation 4

Assuming an ideal system with no losses, the taken output power P_{out} can be seen as the transferred input power $P_{in} = P_{out}$. Both leads to a direct correlation between input half-bridge current I_{HB} and average output current I_{out} as shown following.

$$I_{out} = \frac{P_{out}}{V_{out}} = \frac{1}{2} \times N \times (I_{MAGpos} + I_{MAGneg})$$

Equation 5

Equation 5 shows that I_{out} can be controlled only by controlling I_{MAG} and can then be independent of V_{in} and V_{out} . This is different compared to a standard flyback controller, where by means of peak current control the output power P_{out} is controlled independent on output voltage.

The hybrid-flyback is controlling the magnetization time t_{mag} and demagnetization time t_{demag} (see **Figure 7**) in 2 different ways. t_{mag} is mainly controlled by the positive half-bridge current level I_{MAGpos} by means of peak current control at shunt resistor R_{shunt} via CS pin. Whereas t_{demag} is controlled by adjusting the on-time t_{LSon} . Increasing t_{demag} increases the negative magnetizing current level I_{MAGneg} when keeping I_{MAGpos} level constant. During output overcurrent condition t_{demag} can be temporarily longer than t_{LSon} due to waiting for the zerocrossing detection before turning on the *HS* switch. The correlations between t_{mag} , t_{demag} and I_{MAGpos} , I_{MAGneg} are shown in following equations:

$$t_{mag} = \frac{L_m \times (I_{MAGpos} - I_{MAGneg})}{V_{in} - V_{Cr_avg}}$$

Equation 6

$$t_{demag} = \frac{L_m \times (I_{MAGpos} - I_{MAGneg})}{N \times V_{out}}$$

Equation 7

Functional description

Output current control in ZV-RVS mode

Compared to CRM operation the ZV-RVS mode is adding waiting time gaps $t_{waitgap}$, where no energy is either taken from the input nor energy is transferred to the output. This extends the minimum off-time, which is determined by the on-time of the LS switch. The average output current I_{out} is decreasing with increasing $t_{waitgap}$ derived by following equation from **Figure 10**. This provides 2 degree of freedom to control the output current by means of half-bridge current I_{HB} and extended half-bridge switching period $t_{HBperiodex}$ adjustment.

$$I_{out} = \frac{P_{out}}{V_{out}} = \frac{t_{HBperiod}}{t_{HBperiodex}} \times \frac{1}{2} \times N \times (I_{MAGpos} + I_{MAGneg})$$

Equation 8

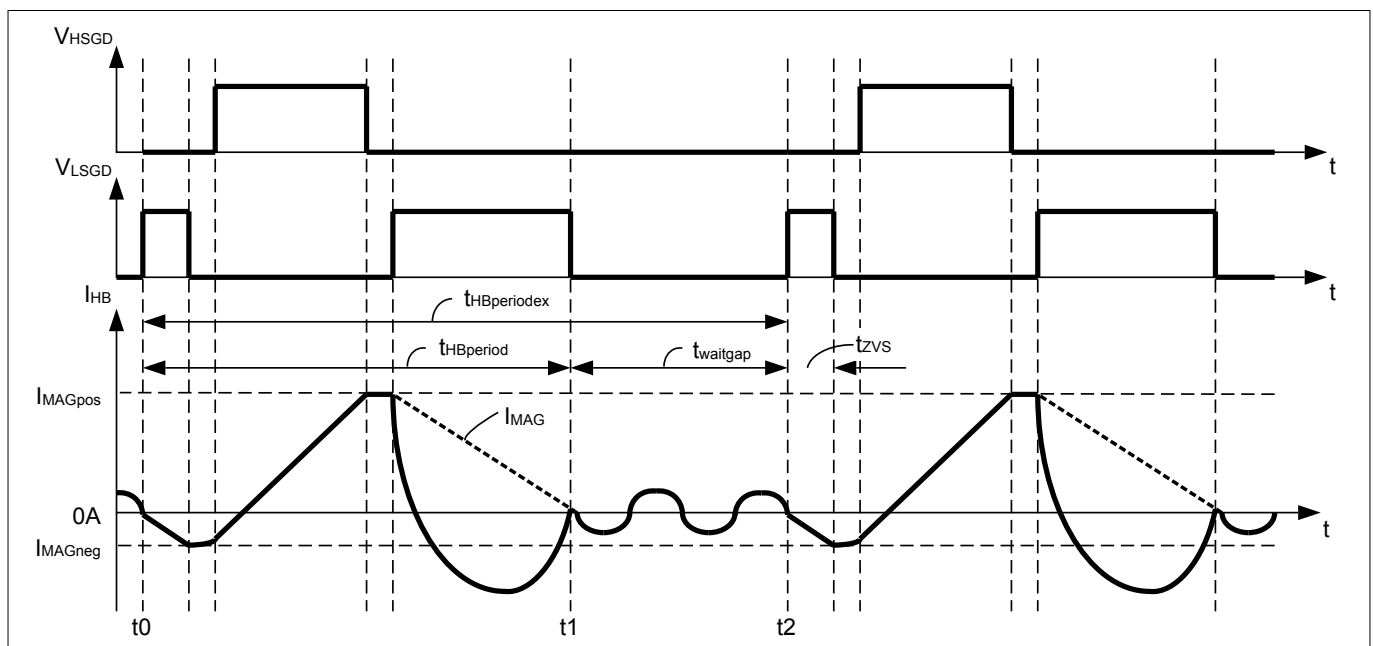


Figure 10 *LrCr* tank and I_{MAG} currents during ZV-RVS mode operation

3.2 Power supply management

The power supply management ensures a reliable and robust IC operation. Depending on the operation mode of the control IC, the power supply management unit runs in different ways for VCC supply, which are described as in the sequel.

- VCC capacitor charge-up and start-up sequence (**Chapter 3.2.1**)
- Bang-bang mode operation during brown-in phase (**Chapter 3.2.1**)
- Bang-bang mode operation during protection mode (**Chapter 3.2.3**)
- VCC supply during burst mode (BM) operation (**Chapter 3.2.4**)

3.2.1 VCC capacitor charge-up and start-up sequence

At VCC start-up the capacitor C_{VCC} is being charged by the internal HV start-up cell via HV pin (see **Figure 11**). The high voltage HV pin is connected to an external resistor R_{HV} , which is in series with 2 diodes connected to VAC. The internal HV start-up cell is turned on for V_{VCC} lower than the IC deactivation voltage threshold V_{VCCoff} (see **Chapter 3.4.2**). Once the voltage at VCC pin exceeds the threshold V_{VCCon} at time t_0 the HV start-up cell is turned off and the IC is starting the internal hardware initialization procedure (see **Figure 12**). Subsequently the IC starts with half-bridge gate driver operation after brown-in condition is reached at time t_2 (see **Chapter**

Functional description

3.4.4.1). During this period of time the VCC capacitor is discharging until the external VCC self-supply takes over at time t_3 and start regulating the voltage at VCC pin for V_{VCCSS} .

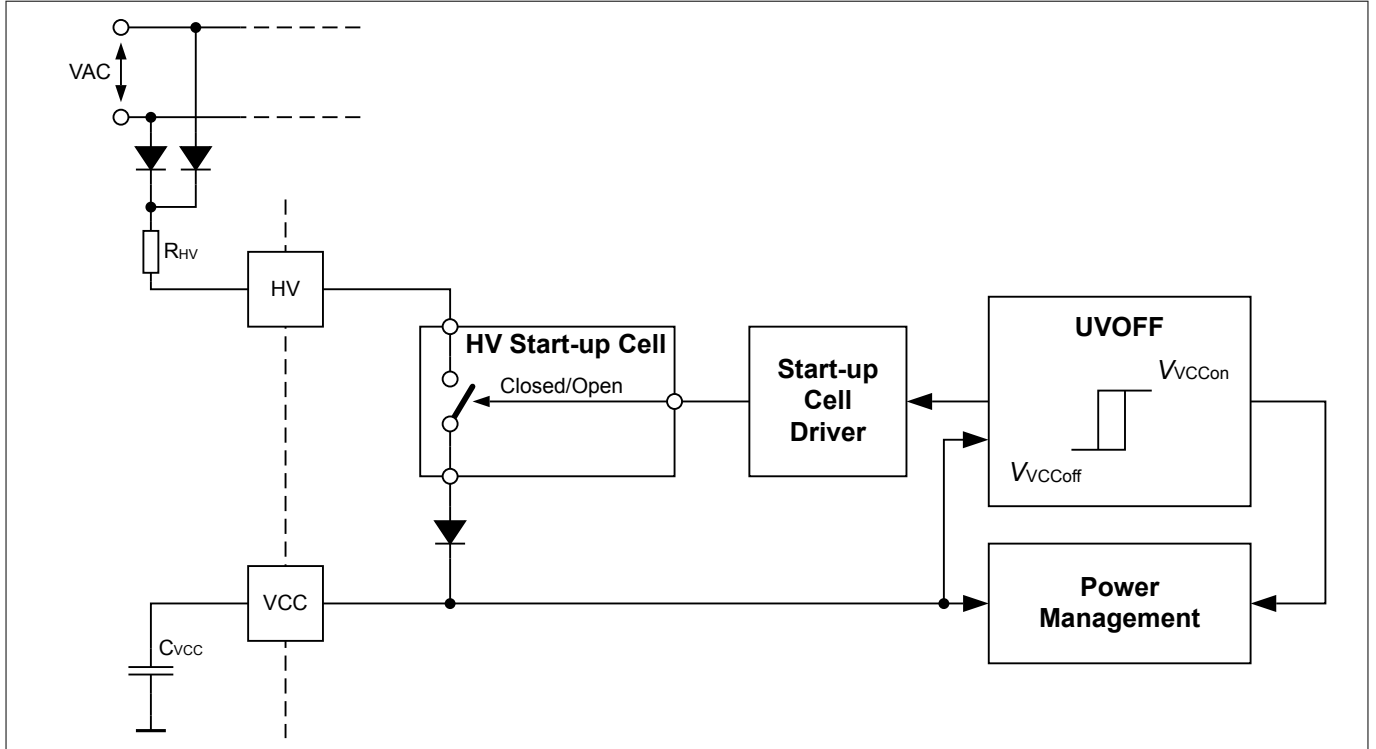


Figure 11 VCC capacitor charge-up control

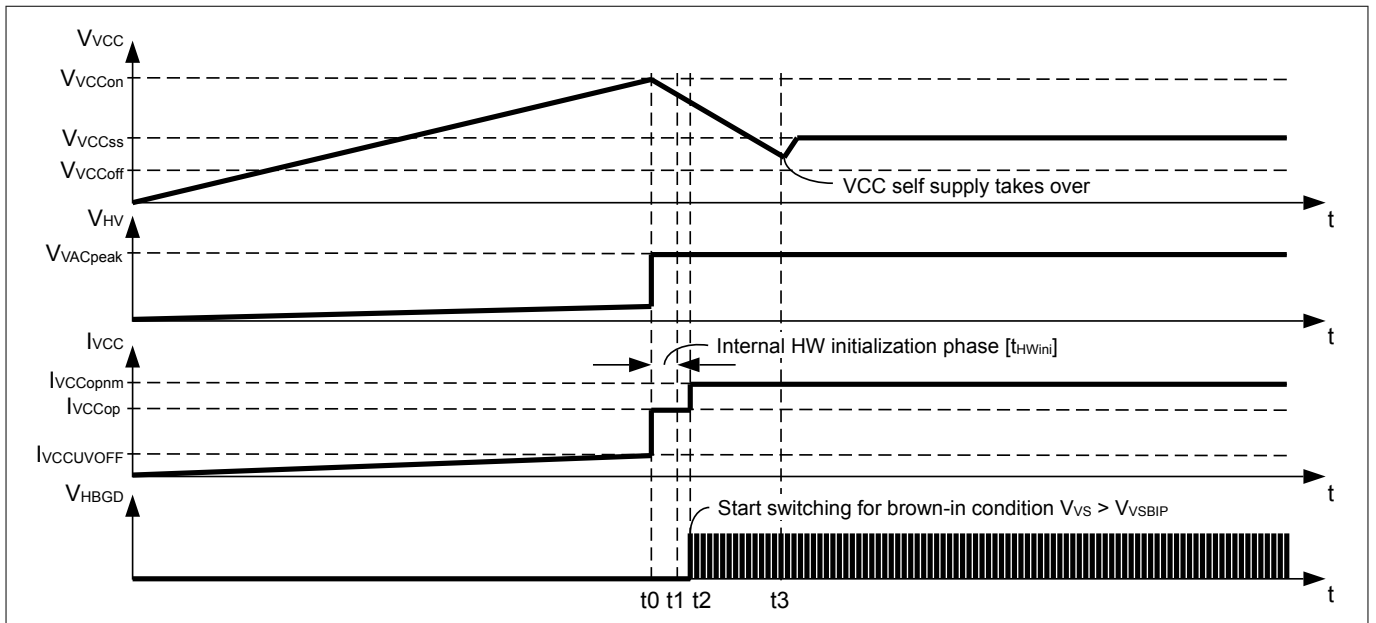


Figure 12 Typical start-up sequence

3.2.2 Bang-bang mode operation during brown-in phase

During brown-in phase the IC is observing the voltage at VS pin for reaching Vin brown-in condition. During this time VCC is not yet self-supplied via the transformer. To support a fast activation of switching operation when Vin brown-in condition is getting reached, the VCC voltage needs to be kept at a high level to support immediate operation with having enough time for take-over by VCC self-supply. A bang-bang mode operation

Functional description

for V_{in} brown-in phase is ensuring a high VCC level, which can be either triggered by V_{in} brown-in protection or the fast and slow V_{in} brown-out protection (see [Figure 13](#) and [Chapter 3.4.4](#)).

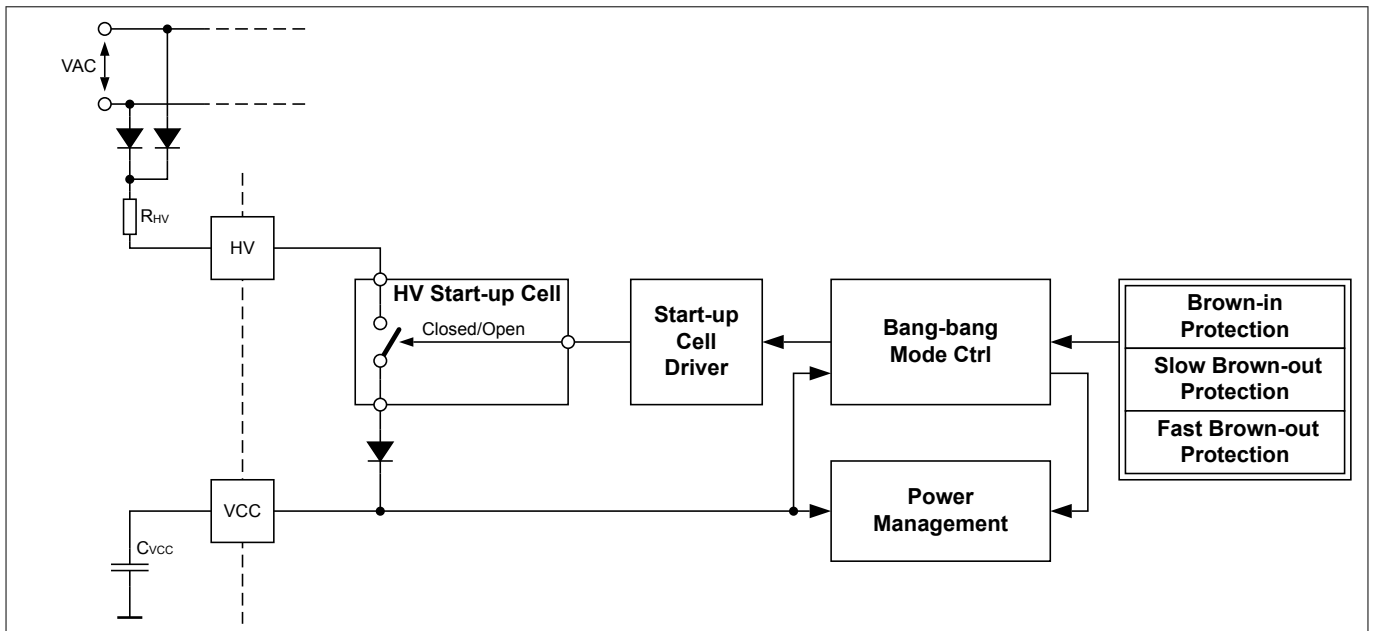


Figure 13 Bang-bang mode triggered by brown-in and brown-out

[Figure 14](#) shows the bang-bang mode operation after a brown-out detection event. Once brown-out is detected at time t_0 the IC enters immediately a sleep mode with reduced current consumption I_{VCCBB} . The HV start-up cell turns on and charges up the VCC voltage until the threshold V_{VCCOn} . Then the IC is activated for a time period $t_{VSBIdet}$ in order to detect a V_{in} brown-in condition. Subsequently the IC is entering again the sleep mode. At time t_1 V_{in} brown-in condition is reached but the IC is still inactive. The IC is detecting the V_{in} brown-in condition after being activated with VCC exceeding V_{VCCOn} at time t_2 .

Functional description

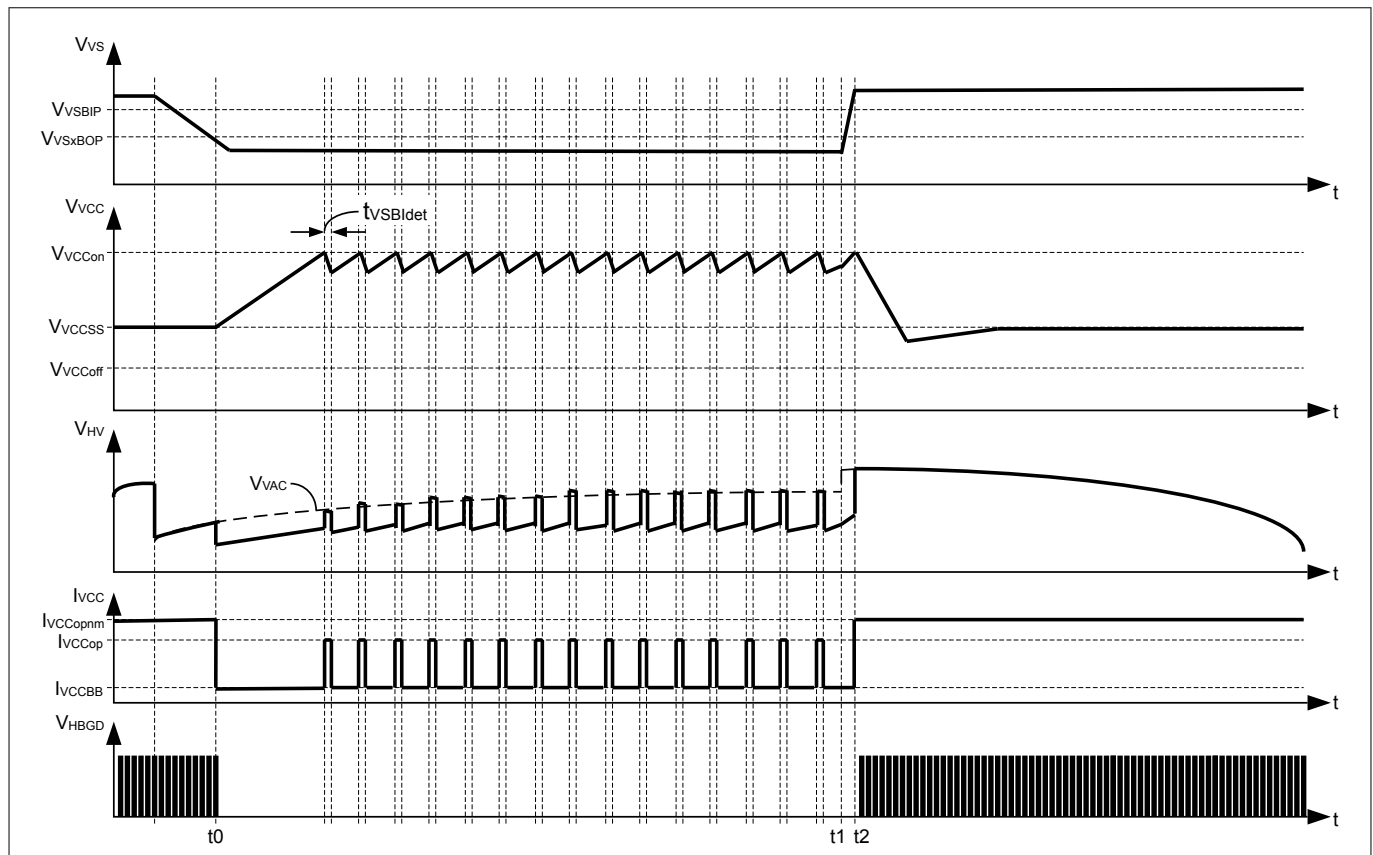


Figure 14 Bang-bang mode operation during brown-in phase

3.2.3 Bang-bang mode during protection mode operation

The bang-bang mode triggered by auto-restart mode or latch mode supports an IC operation without external VCC supply during the latched and auto-restart operation (see [Chapter 3.4.1](#)). It directly controls the HV start-up cell by turning off at VCC pin threshold V_{VCCOn} and turning on after a time period $t_{ARMbase}$ (see [Figure 15](#)). During this bang-bang mode operation the VCC is kept at a high voltage level in order to support a proper restart, once triggered. The VCC current consumption is reduced to I_{VCCBB} .

In auto-restart mode, there is also in addition a counter activated, which initiates a restart after a set number of $N_{ARMstep}$ HV start-up cell charge cycles (see [Figure 16](#)).

In latched operation a mode reset can only be achieved by disconnecting the AC line. A HW reset is taking place once the VCC voltage drops below the threshold V_{VCCoff} .

Functional description

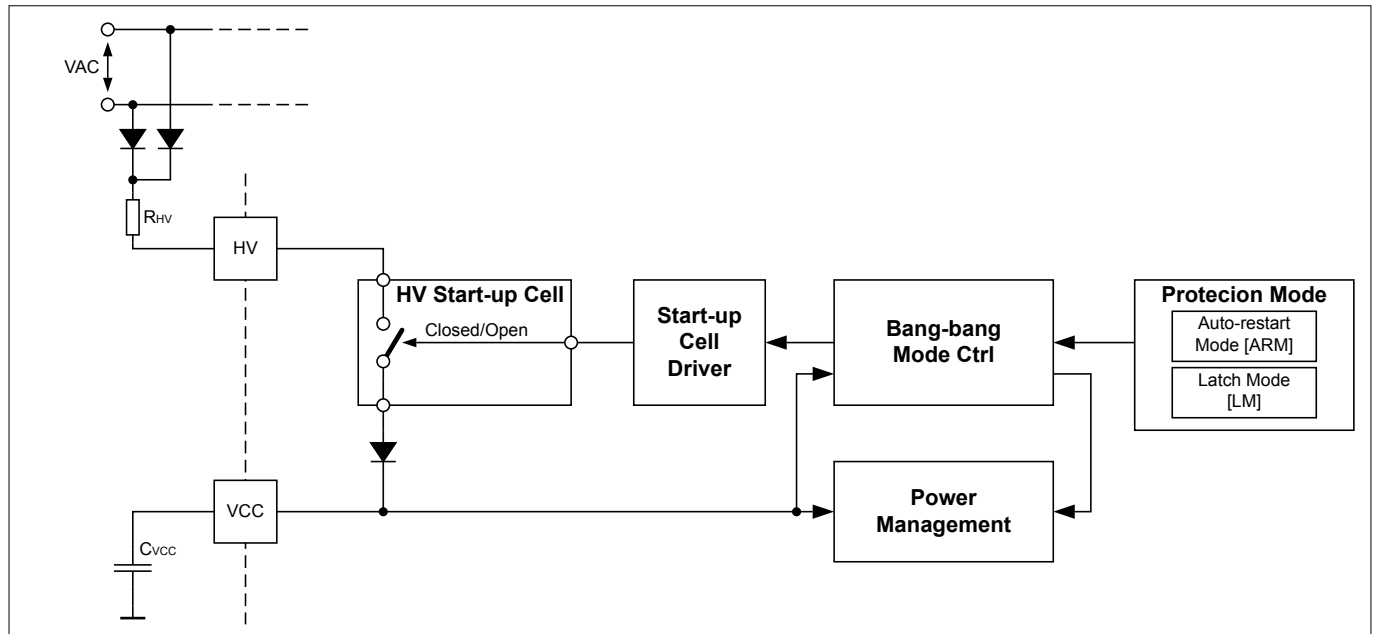


Figure 15 Bang-bang mode during protection mode

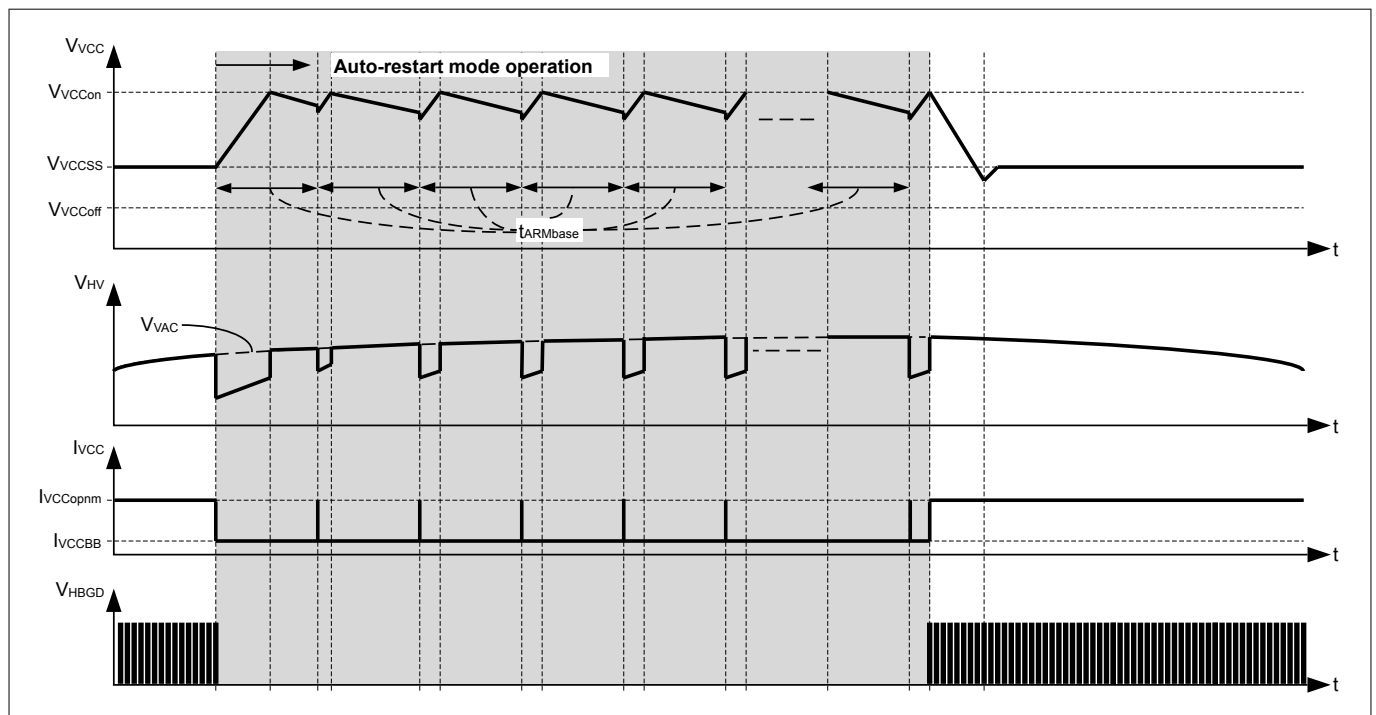


Figure 16 Auto-restart mode operation

3.2.4 VCC supply during burst mode (BM) operation

During burst mode operation the IC enters repeatedly a power saving mode, in which the IC current consumption is reduced to $I_{VCCBMpsm}$. Waking up from and entering this power saving mode is controlled by the feedback voltage at *FB* pin by comparing the voltage level with the wake-up and sleep control threshold $V_{FBBMctrl}$ (see [Chapter 3.3.4.2](#)). In addition a wake-up threshold $V_{VCCslpHVon}$ is enabled at *VCC* pin, which turns-on the HV start-up cell once V_{VCC} drops below $V_{VCCslpHVon}$. This shall support a higher voltage level at *HSVCC* pin than the threshold $V_{HSVCCon}$. The HV start-up cell is turned off when either the IC is waked up via *FB* pin or

Functional description

V_{VCC} is exceeding the threshold V_{VCCOn} . In addition there is always only one HV start-up cell VCC charge up cycle initiated once entering the burst mode.

Note: The system dimensioning should ensure that during steady state burst mode operation V_{VCC} stays always well above the VCC wake-up threshold $V_{VCCslpHVon}$ in order to avoid increasing bias losses due to charging the VCC capacitor from input high voltage.

Figure 17 shows a typical burst mode operation signal for V_{VCC} and correlated current consumption I_{VCC} during steady state burst mode operation once feedback voltage has dropped below the burst mode entry threshold V_{FBMen} . A large decrease of V_{VCC} can occur for a large output load drop at time t_0 , when optocoupler feedback network is entering saturation due to V_{out} overshoot. This can lead to a significant longer rising time period of feedback voltage V_{FB} until time t_2 . At time t_1 the VCC voltage is dropping below the threshold $V_{VCCslpHVon}$ and turning on the HV start-up cell. The average current $I_{HV(avg)}$ flowing into pin HV is depending on VAC and charging via VCC pin with $I_{VCCchg(avg)}$ the capacitor at VCC. At time t_2 the IC is waked up via FB pin and the HV start-up cell is turned off. When feedback voltage is dropping below $V_{FBMctrl}$ at time t_3 the IC is entering the power saving mode.

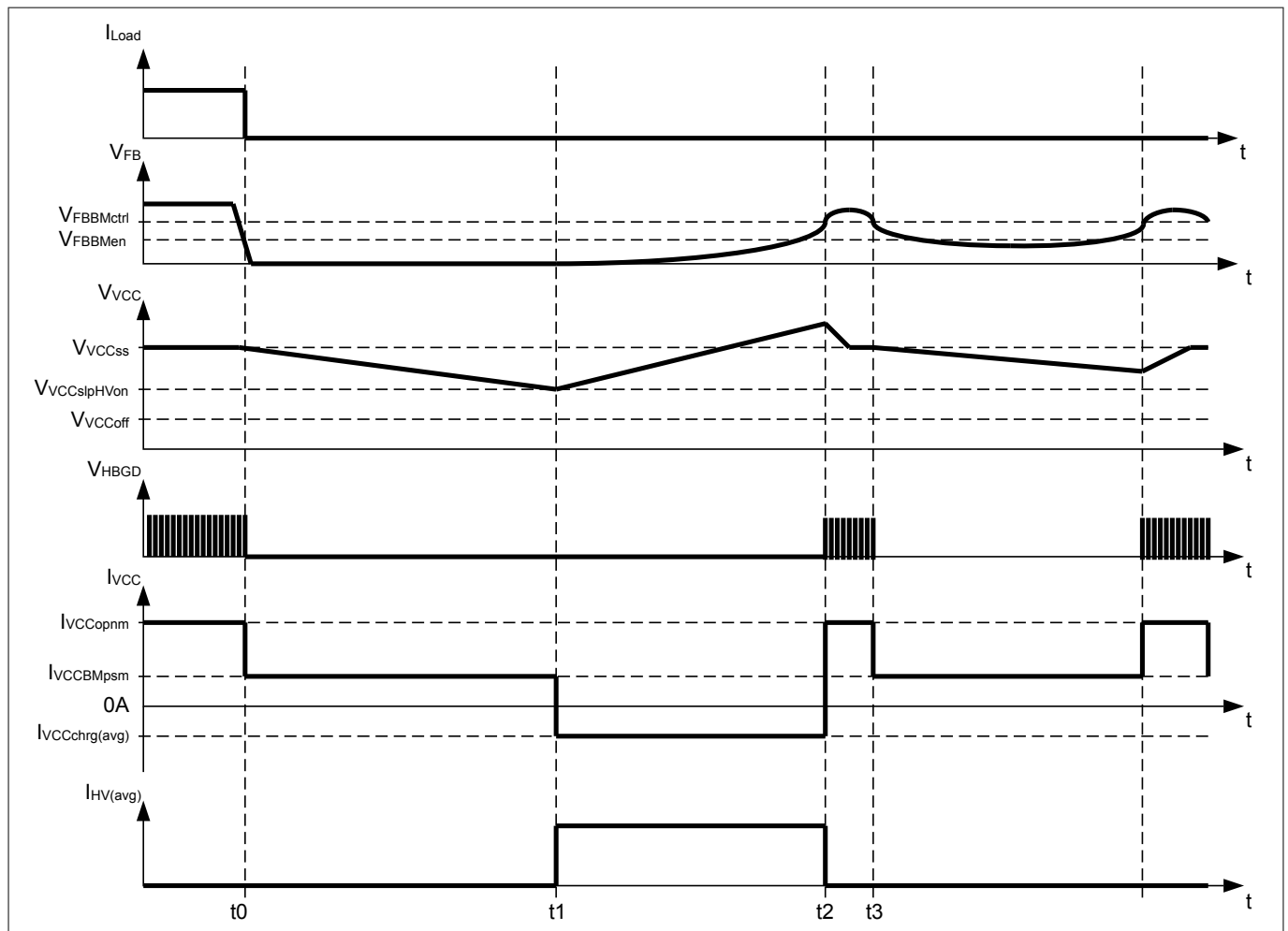


Figure 17 Burst mode operation

Functional description

3.3 Control features

The control features chapter contains all functions for the hybrid-flyback PWM generation and the half-bridge gate driver listed in [Table 2](#). The hybrid-flyback PWM generation consists mainly of the mode control and output current control. The output current control is determining that part of the PWM control, which is taking place during high-side switch on-time t_{HSon} by means of peak current control (see [Figure 18](#)) for the positive magnetization level I_{MAGpos} . Furthermore it provides the decision for changing the valley number in ZV-RVS operation. The PWM control ensures cycle by cycle ZVS switching operation. The mode control feature focus on controlling directly the timings of the half-bridge PWM scheme associated with the dead-times t_{deadLS} , t_{deadHS} and the low-side switch on-time t_{LSon} to determine the negative magnetization level I_{MAGneg} for the different operation modes like CRM, ZV-RVS and DCM.

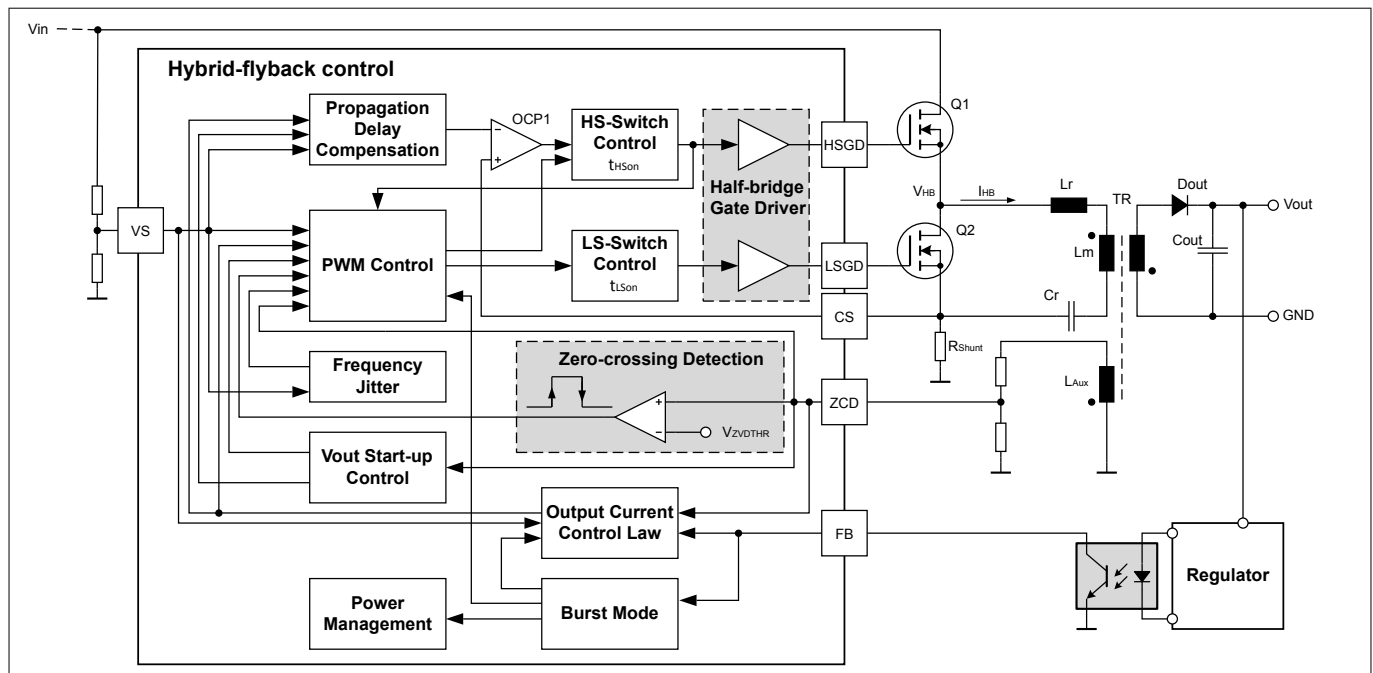


Figure 18 Hybrid-flyback control structure

Table 2 Control features

| Feature | Chapter |
|-------------------------|-------------------------------|
| Output control | Chapter 3.3.1 |
| Mode control | Chapter 3.3.2 |
| Burst mode control | Chapter 3.3.4 |
| Vout start-up control | Chapter 3.3.3 |
| Frequency jitter | Chapter 3.3.5 |
| Half-bridge gate driver | Chapter 3.3.6 |

3.3.1 Output control

During continuous switching operation the output current is only controlled by means of the positive and negative magnetization current levels I_{MAGpos} and I_{MAGneg} following [Equation 5](#). During continuous operation the output current I_{out} is controlled by means of a linear relationship between the feedback voltage at FB pin and the associated internal current set-point I_{SET} , which is described in [Chapter 3.3.1.3](#). The linear relationship is achieved by adjusting I_{MAGneg} cycle by cycle via the turn-on time of LS switch t_{LSon} depending on the input

Functional description

voltage V_{in} (see [Chapter 3.3.1.1](#)) and the output voltage V_{out} (see [Chapter 3.3.1.2](#)). The positive magnetization level I_{MAGpos} equals the positive half-bridge peak current that is controlled via CS pin at the shunt resistor R_{Shunt} (see [Figure 19](#)):

$$V_{CSpeak} = I_{HBpeak} \times R_{Shunt} = I_{MAGpos} \times R_{Shunt}$$

Equation 9

The output voltage is measured via ZCD pin at the auxiliary winding and taken for protection features (see [Chapter 3.4.8](#)) and for compensating the peak to peak magnetizing current I_{MAGpp} to ensure ZVS operation over wide output voltage range (see [Chapter 3.3.1.2](#)).

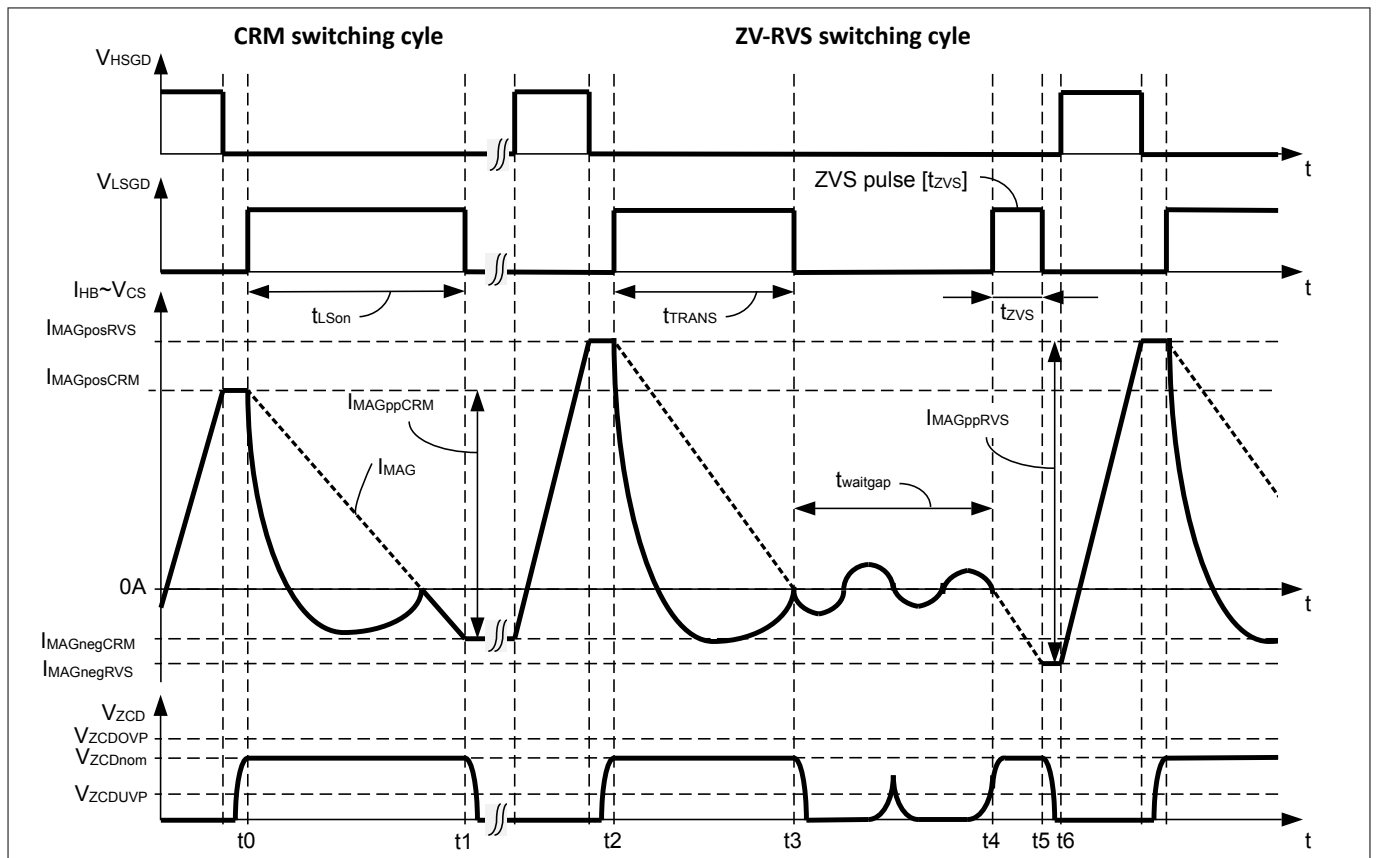


Figure 19 Negative magnetization controlled by low-side gate driver

3.3.1.1 Keeping ZVS operation for wide input voltage range

ZVS operation for wide input voltage range is achieved by V_{in} feed-forward compensation of negative magnetization level I_{MAGneg} during the different operation modes (see [Chapter 3.3.2](#)). This is supported by several configurable parameters introduced in the sequel.

The implemented output current control is based on the dimensioning for the nominal output current level I_{outnom} ¹⁾ following [Equation 5](#):

$$I_{outnom} = \frac{N}{2} \times (I_{MAGposnom}(V_{in}; V_{out}; Mode) + I_{MAGneg}(V_{in}; Mode))$$

Equation 10

The peak current control at CS pin for adjusting I_{MAGpos} is therefore depending on the input, output voltage and the mode operation that are directly impacting the negative magnetization level I_{MAGneg} .

¹⁾ configurable, see [Table 5](#)

Functional description

I_{MAGneg} is compensated for a changing output voltage (see [Chapter 3.3.1.2](#)). Therefore the compensation for input voltage requires only set-points for minimum and maximum V_{in} (see [Figure 20](#)).

Minimum V_{in}

For minimum V_{in} the natural freewheeling oscillation caused by $I_{MAGnegnom}^{2)}$ (see [Figure 19](#)) shall support the complete switch-over of the half-bridge node.

Maximum V_{in}

For maximum V_{in} the additional required negative magnetization is set for CRM with $I_{MAGnegmaxCRM}^{2)}$ and for ZV-RVS with $I_{MAGnegmaxRVS}^{2)}$, which might be different.

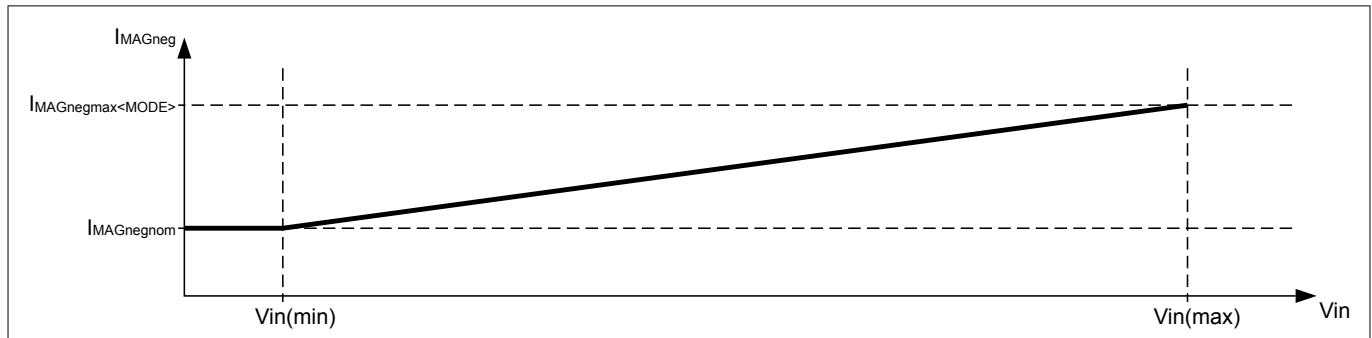


Figure 20 V_{in} feed-forward compensation for I_{MAGneg}

3.3.1.2 Keeping ZVS operation for wide output voltage range

When output voltage V_{out} is decreasing the demagnetization time of the transformer t_{demag} is prolonging, which leads to a longer time period t_{TRANS} . ZVS operation is ensured by adjusting the turn-on time of the LS switch t_{Lson} to match with the changed time period for t_{TRANS} in order to keep the same negative magnetization level I_{MAGneg} for a constant output load (see [Figure 21](#)). $t_{TRANSRVS0V}$ means the time period for $V_{out} = 0V$ and is derived from $t_{TRANSRVS0V\%}^{3)}$ by the following equation:

$$t_{TRANSRVS0V} = t_{TRANSRVS0V\%} \times t_{TRANSnom}$$

Equation 11

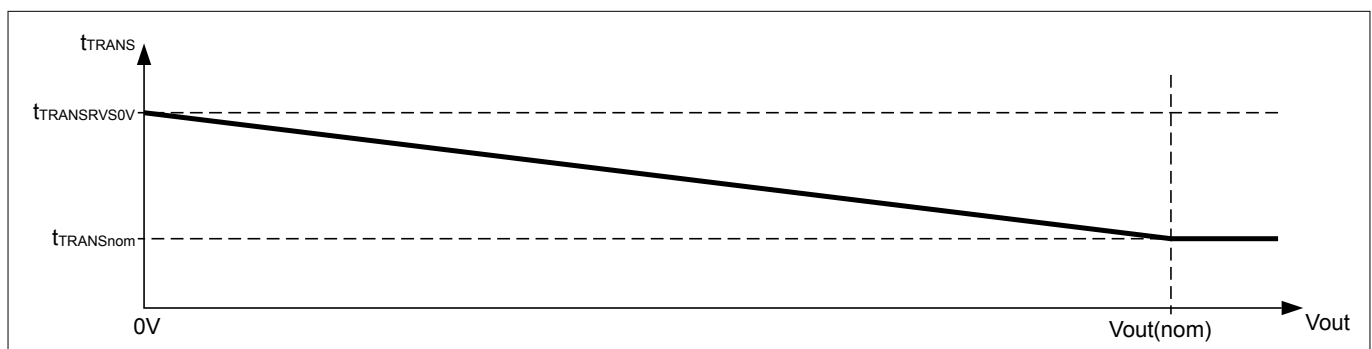


Figure 21 V_{out} compensation for t_{TRANS}

3.3.1.2.1 Cycle by cycle ZVS operation during CRM operation

When fast decreasing the output voltage V_{out} (see [Figure 8](#)) or fast increasing the positive magnetization level I_{MAGpos} (see [Chapter 3.3.2.5](#)) the demagnetization time t_{demag} of the transformer can be too short when operating with fixed LS switch on-time period. This can cause hard switching or even body diode cross conduction if transformer is still positive magnetized.

²⁾ configurable, see [Table 6](#)

³⁾ configurable, see [Table 6](#)

Functional description

To ensure a cycle by cycle ZVS switching condition, the controller only activates the *HS* switch when the voltage signal at *ZCD* pin (see [Figure 18](#)) indicates a changing half-bridge voltage V_{HB} . By this body diode cross conduction is properly avoided. This is achieved by regulating I_{MAGneg} for a target delay time t_{LS2ZCD} between falling edge of *LS* switch and subsequently occurring falling edge at *ZCD* pin (see [Figure 22](#)).

The polarity of the transformer auxiliary winding L_{AUX} has to be considered in such a way that a rising V_{HB} is leading to a falling V_{ZCD} . The time between turning off the *LS* switch until zero-crossing detection for turning on the high-side switch t_{LS2ZCD} is observed and determining a prolongation of next turn-on phase for *LS* switch if required to ensure reliable ZVS operation.

An example is shown with phase t2-t3 in comparison to phase t6-t7. The dead-time $t_{deadHS1}$ is determined by the negative half-bridge current level $I_{MAGneg1}$. The small level of $I_{MAGneg1}$ leads to a rather slow rising slope of V_{HB} . The detection of zero-crossing at *ZCD* pin is delayed and turn-on of *HS* switch is not taking place under full ZVS condition at time t3. The increased delay of zero-crossing after having turned off *LS* switch is taken as input for increasing indirectly the negative half-bridge current level to $I_{MAGneg2}$ by extending the turn-on time of *LS* switch in phase t5-t6. ZVS condition for turning on the *LS* switch are reached by properly dimensioning the dead-time t_{deadLS} (see [Chapter 3.3.2.1](#)).

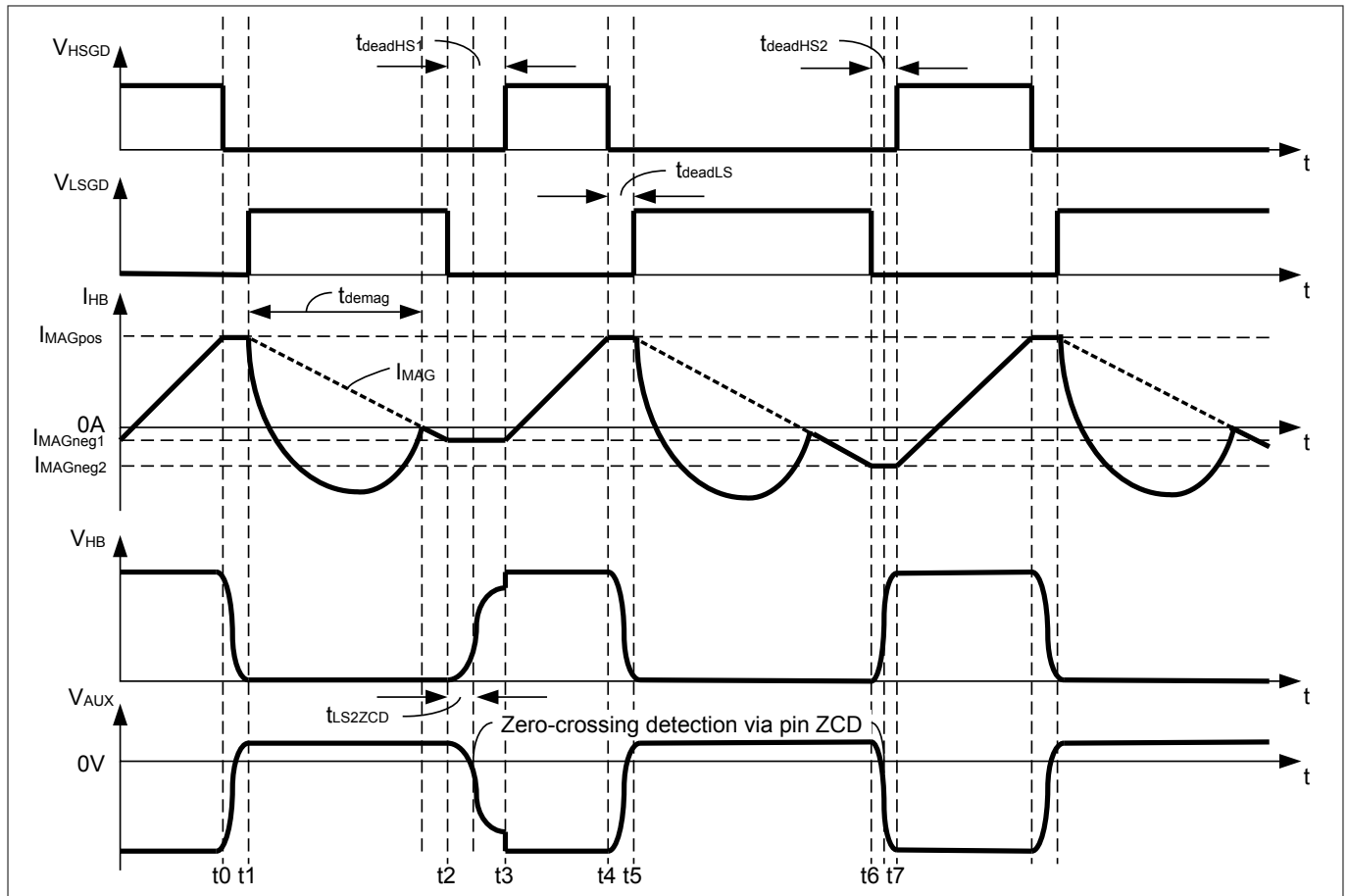


Figure 22 Using zero-crossing detection at L_{AUX} to ensure ZVS operation

Only in DCM operation at very light-load partial hard switching can occur for the first *LS* switching cycle turn-on. This is only taking place after a long waiting period when demagnetization of the transformer is finished not causing a body diode conduction issue (see [Chapter 3.3.2.3](#)).

3.3.1.3 Output current control law

[Figure 23](#) shows the control path from feedback signal input at *FB* pin to peak current setting at *CS* pin. The requested output current equals to the internal I_{SET} for the corresponding feedback signal. The required peak current setting is then calculated based on V_{in} measurement and mode operation.

Functional description

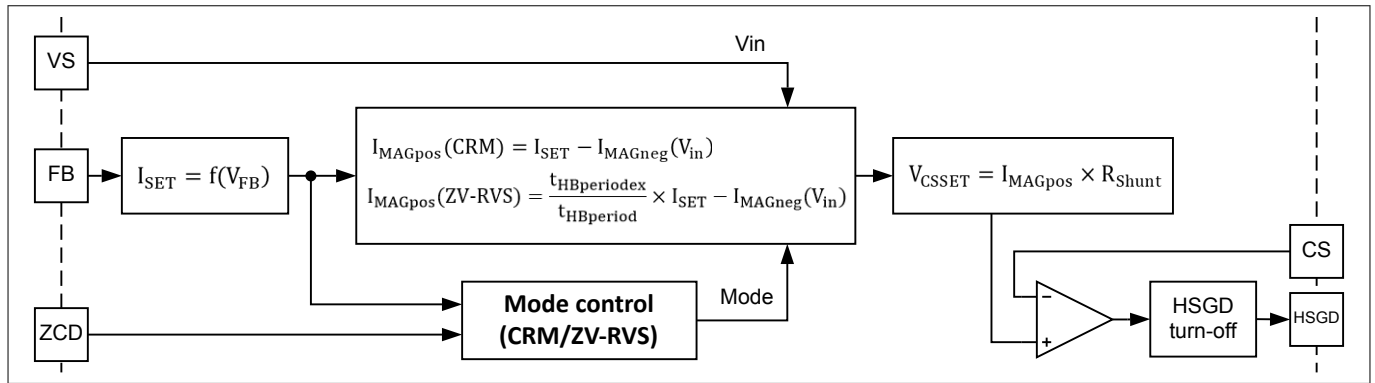


Figure 23 Control path from feedback input to peak current setting

The feedback voltage V_{FB} has a linear correlation with the output current I_{out} between the borders for maximum output current $I_{outOC1max}$ and burst mode entry current level $I_{outBMen}$. **Figure 24** is showing output current levels for various functions.

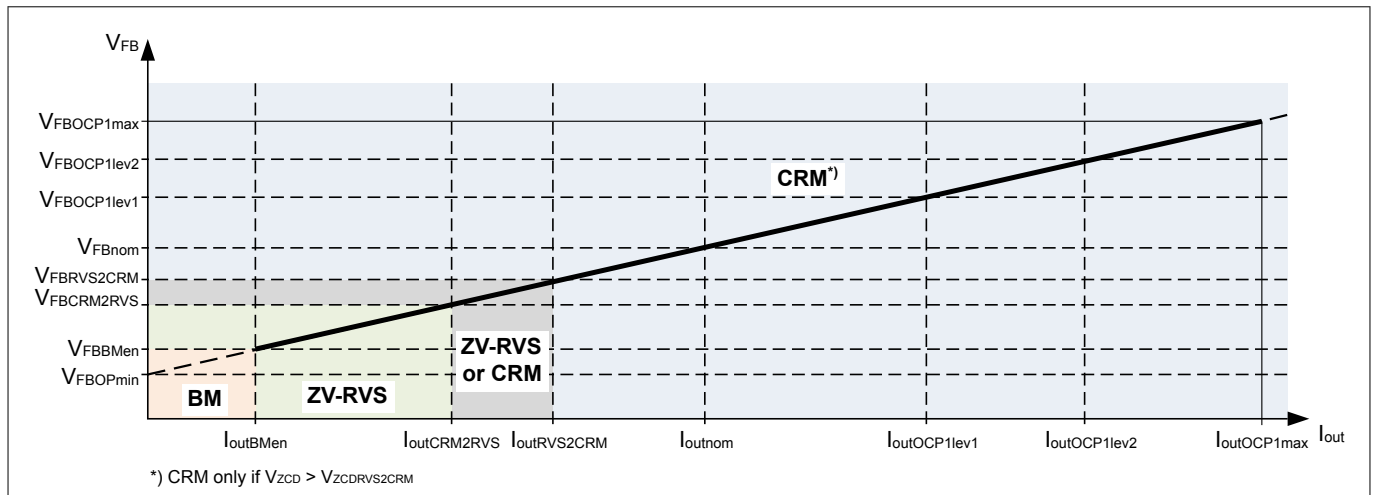


Figure 24 Control law for feedback voltage at FB pin

Controlling the output current I_{out} is determined by the equivalent internal current set-point I_{SET} , which is then taken for the peak current setting at CS pin to adjust the positive magnetization level I_{MAGpos} . The correlation between I_{SET} and I_{MAGpos} is different for CRM (see [Chapter 3.3.1.3.1](#)) and ZV-RVS mode (see [Chapter 3.3.1.3.2](#)) in order to ensure a smooth transition between the CRM and ZV-RVS mode. **Figure 25** shows the configurable current set-points for various functions and their correlation with the feedback voltage.

The configurable current set-points $I_{SETxxx\%}$ are defined in percentage with respect to the nominal current set-point $I_{SETnom\%}$ that determines in percentage of the FB pin operating voltage range $V_{FBOPmax}$ the associated voltage level V_{FBnom} . Here $I_{SETnom\%}$ is set to 50% used as a factor without unit.

$$V_{FBnom} = (I_{SETnom\%} \times V_{FBOPmax}) + V_{FBOPmin}$$

Equation 12

Note: The current set-point for burst mode exit threshold $I_{SETBMex\%}$ is only active during burst mode operation and only used as an internal parameter for comparison, which is not associated with a feedback voltage level (see [Chapter 3.3.4.4.1](#)). The same applies for $I_{SETstmax\%}$ that is only active during V_{out} start-up control (see [Chapter 3.3.3](#)) to provide additional output charge current.

Functional description

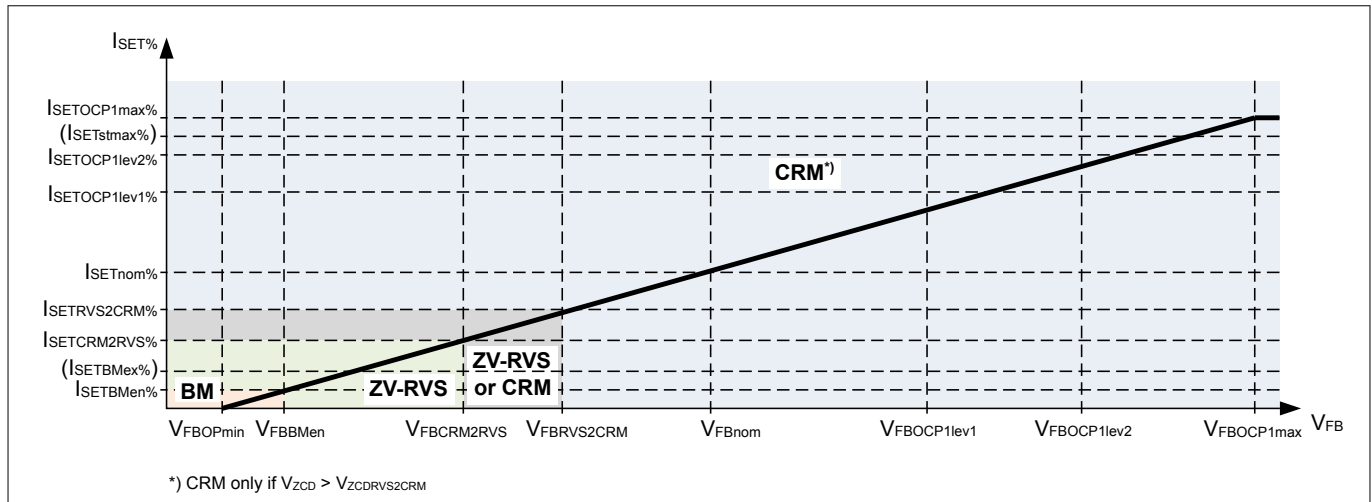


Figure 25 Configurable internal current set-points $I_{SETxxx}\%$ and correlation with V_{FB}

For all other current set-points $I_{SETxxx}\%$ the correlated feedback voltage V_{FBxxx} can be calculated as following:

$$V_{FBxxx} = (I_{SETxxx}\% \times I_{SETnom}\% \times V_{FBOPmax}) + V_{FBOPmin}$$

Equation 13

The offset $V_{FBOPmin}$ considers the minimum operating voltage level of the opto-coupler output before entering saturation.

The peak current setting at CS pin is done by comparing the voltage at the shunt resistor R_{Shunt} with the internally derived threshold V_{CSxxx} :

$$I_{MAGxxx} = \frac{V_{CSxxx}}{R_{Shunt}}$$

Equation 14

V_{CSxxx} is beside $I_{SET}\%$ also depending on V_{in} and the mode operation (see [Chapter 3.3.1.1](#)) shown by following relationship:

CRM operation

$$V_{CSxxx} = (I_{SETxxx}\% \times I_{SETnom}\% \times V_{CSOPmax}) + (I_{MAGneg}(V_{in}) \times R_{Shunt})$$

Equation 15

ZV-RVS operation

$$V_{CSxxx} = \frac{t_{HBperiodx}}{t_{HBperiod}} \times [(I_{SETxxx}\% \times I_{SETnom}\% \times V_{CSOPmax}) + (I_{MAGneg}(V_{in}) \times R_{Shunt})]$$

Equation 16

Hereby $V_{CSOPmax}$ is the maximum operating voltage range at CS pin. R_{Shunt} dimensioning is based on nominal output current I_{outnom} at nominal current set-point $I_{SETnom}\%$, where $I_{SETnom}\%$ also determines in percentage of $V_{CSOPmax}$ at CS pin the associated voltage level $V_{CSOPnom}$.

$$R_{Shunt} = \frac{N}{2} \times \frac{I_{SETnom}\% \times V_{CSOPmax}}{I_{Outnom}}$$

Equation 17

Functional description

At the corners for $V_{in}(min)$ and $V_{in}(max)$ the expected peak current setting for nominal current set-point $I_{SETnom\%}$ can be calculated with:

Minimum peak current setting $V_{CSnom}(min)$ for nominal load at $V_{in}(min)$

CRM operation

$$V_{CSnom}(min) = (I_{SETnom\%} \times V_{CSOPmax}) + \left(\left(I_{MAGnegnom\%} \times \frac{2 \times I_{Outnom}}{N} \right) \times R_{Shunt} \right)$$

Equation 18

ZV-RVS operation

$$V_{CSnom}(min) = \frac{t_{HBperiodex}}{t_{HBperiod}} \times \left(\left(I_{SETnom\%} \times V_{CSOPmax} \right) + \left(\left(I_{MAGnegnom\%} \times \frac{2 \times I_{Outnom}}{N} \right) \times R_{Shunt} \right) \right)$$

Equation 19

Maximum peak current setting $V_{CSnom}(max)$ for nominal load at $V_{in}(max)$

CRM operation

$$V_{CSnom}(max) = (I_{SETnom\%} \times V_{CSOPmax}) + \left(\left(I_{MAGnegmaxCRM\%} \times \frac{2 \times I_{Outnom}}{N} \right) \times R_{Shunt} \right)$$

Equation 20

ZV-RVS operation

$$V_{CSnom}(max) = \frac{t_{HBperiodex}}{t_{HBperiod}} \times \left(\left(I_{SETnom\%} \times V_{CSOPmax} \right) + \left(\left(I_{MAGnegmaxRVS\%} \times \frac{2 \times I_{Outnom}}{N} \right) \times R_{Shunt} \right) \right)$$

Equation 21

3.3.1.3.1 Current control during CRM

During CRM operation the negative magnetization I_{MAGneg} is controlled for a target value only depending on input voltage V_{in} (see [Chapter 3.3.1.1](#)). Here the negative magnetization I_{MAGneg} is controlled by adjusting the on-time t_{Lson} , which leads to a linear correlation between I_{out} and the set positive magnetization level I_{MAGpos} :

$$I_{out} = \frac{N}{2} \times (I_{MAGpos}(V_{in}) + I_{MAGneg}(V_{in}))$$

Equation 22

I_{MAGpos} is then controlled by the peak current control at CS pin based on the correlation with the internal target current set-point I_{SET} , which is a proportional representation of the output current I_{out} :

$$I_{SET} = \frac{2}{N} \times I_{out}$$

Equation 23

$$I_{MAGpos}(I_{SET}; V_{in}) = I_{SET} - I_{MAGneg}(V_{in})$$

Equation 24

When reducing the load the on-time of LS switch is getting reduced until the minimum time period $t_{TRANSnom}$. For further reduction in load the on-time of LS is kept constant, which results in a constant peak to peak magnetization I_{MAGpp} (see [Figure 19](#)):

Functional description

$$I_{MAGpp} = I_{MAGpos} - I_{MAGneg}$$

Equation 25

3.3.1.3.2 Current control during ZV-RVS mode

As in ZV-RVS mode the peak current control for I_{MAGpos} shall be kept almost constant (see [Chapter 3.3.2.2.1](#)) to ensure that the demagnetization time is longer than half of the resonant period of the $LrCr$ tank, a waiting time gap $t_{waitgap}$ is introduced directly after the end of $t_{TRANSnom}$ period (see [Figure 19](#)), which is extending the half-bridge period to $t_{HBperiodex}$. This results in a reduced output current I_{out} that can be expressed as:

$$I_{out} = \frac{t_{HBperiod}}{t_{HBperiodex}} \times \frac{N}{2} \times (I_{MAGpos} + I_{MAGneg})$$

Equation 26

The control for $t_{HBperiodex}$ is performed by means of valley skipping control (see [Chapter 3.3.2.2.1](#)) depending on I_{SET} and Vin :

$$t_{HBperiodex}(I_{SET}; Vin) = t_{HBperiod} \times \frac{(I_{MAGpos} + I_{MAGneg}(Vin))}{I_{SET}}$$

Equation 27

3.3.1.4 Propagation delay compensation (PDC)

During peak current control a propagation delay is impacting the resulting peak current limitation (see [Figure 26](#)). The higher reached peak current is then compensated to a lower level by the closed application control loop via the feedback signal at FB pin. The magnitude of I_{MAGpos} overshoot is depending on the voltage at the transformer input winding Lm , which is depending on input voltage Vin and reflected output voltage at resonant capacitor V_{Cr} . A higher voltage amplitude at the transformer input winding leads to a steeper rising slope of I_{MAGpos} and vice versa. A total delay of $t_{PDCOCP1}$ leads then to a delta overshoot of $\Delta I_{MAGposcomp}$:

$$\Delta I_{MAGposcomp} = \frac{(Vin - V_{Cr})}{Lm} \times t_{PDCOCP1}$$

Equation 28

$t_{PDCOCP1}$ consists of an internal delay t_{PDint} caused by the OCP1 comparator, gate driver and an external delay t_{PDext} caused by the power switch turn-off and parasitic capacitance connected to the half-bridge node.

$$t_{PDCOCP1} = t_{PDint} + t_{PDext}$$

Equation 29

Functional description

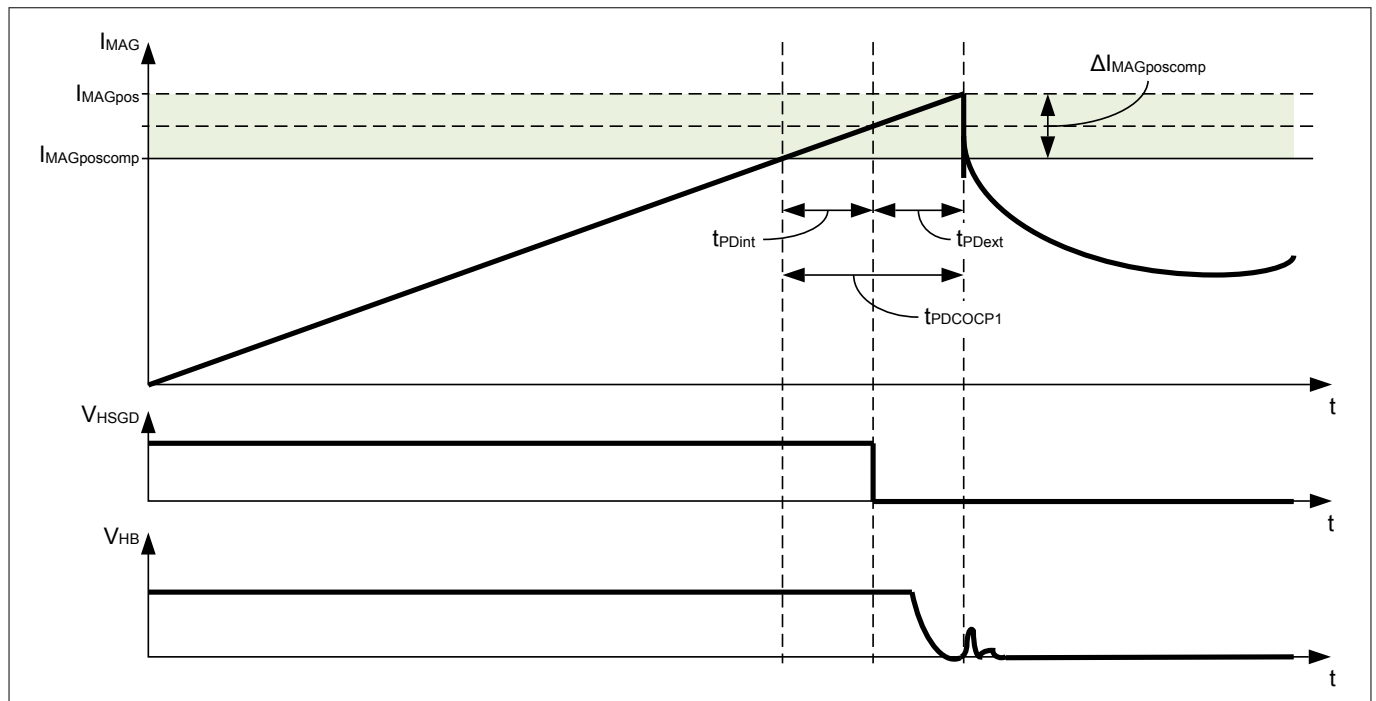


Figure 26 Propagation delay compensation of peak current control for I_{MAGpos}

This dependency on V_{in} and V_{Cr} impacts the current set-point threshold accuracy seen in the application and is therefore compensated to avoid errors on the feedback signal V_{FB} .

The propagation delay compensation uses [Equation 28](#) to calculate $\Delta I_{MAGposcomp}$ based on the parameter $t_{PDCOCP1}$ ⁴⁾, the measured input voltage at VS pin and measured reflected output voltage at ZCD pin. Lm is extracted from other configurable parameters as following:

$$Lm = \frac{V_{VS} V_{Cr} \times t_{TRANSnom}}{I_{MAGpp}}$$

Equation 30

The peak current setting is then compensated by reducing the internal target peak current set-point I_{MAGpos} with $\Delta I_{MAGposcomp}$:

$$I_{MAGposcomp} = I_{MAGpos} - \Delta I_{MAGposcomp}$$

Equation 31

3.3.2 PWM control schemes

[Table 3](#) shows the list of features that describes the pulse width modulation (PWM) control methods for the different control modes and the associated mode transition. Depending on load, output voltage, and input voltage (see [Chapter 3.3.1](#)) the control scheme is adjusted to ensure ZVS operation for both low-side and high-side switches.

⁴ configurable, see [Table 21](#)

Functional description

Table 3 PWM control

| Feature | Chapter |
|----------------------------|---------------------------------|
| CRM control scheme | Chapter 3.3.2.1 |
| ZV-RVS mode control scheme | Chapter 3.3.2.2 |
| DCM control scheme | Chapter 3.3.2.3 |
| Mode transition control | Chapter 3.3.2.4 |
| Overcurrent control | Chapter 3.3.2.5 |

3.3.2.1 CRM control scheme

The PWM control targets a ZVS operation for every half-bridge switching cycle by cycle by tuning the negative current level I_{MAGneg} (see [Figure 27](#)). The dead-time t_{deadLS} ⁵⁾ between HS and LS switch is fixed as the peak current is high enough to provide proper ZVS operation for LS switch.

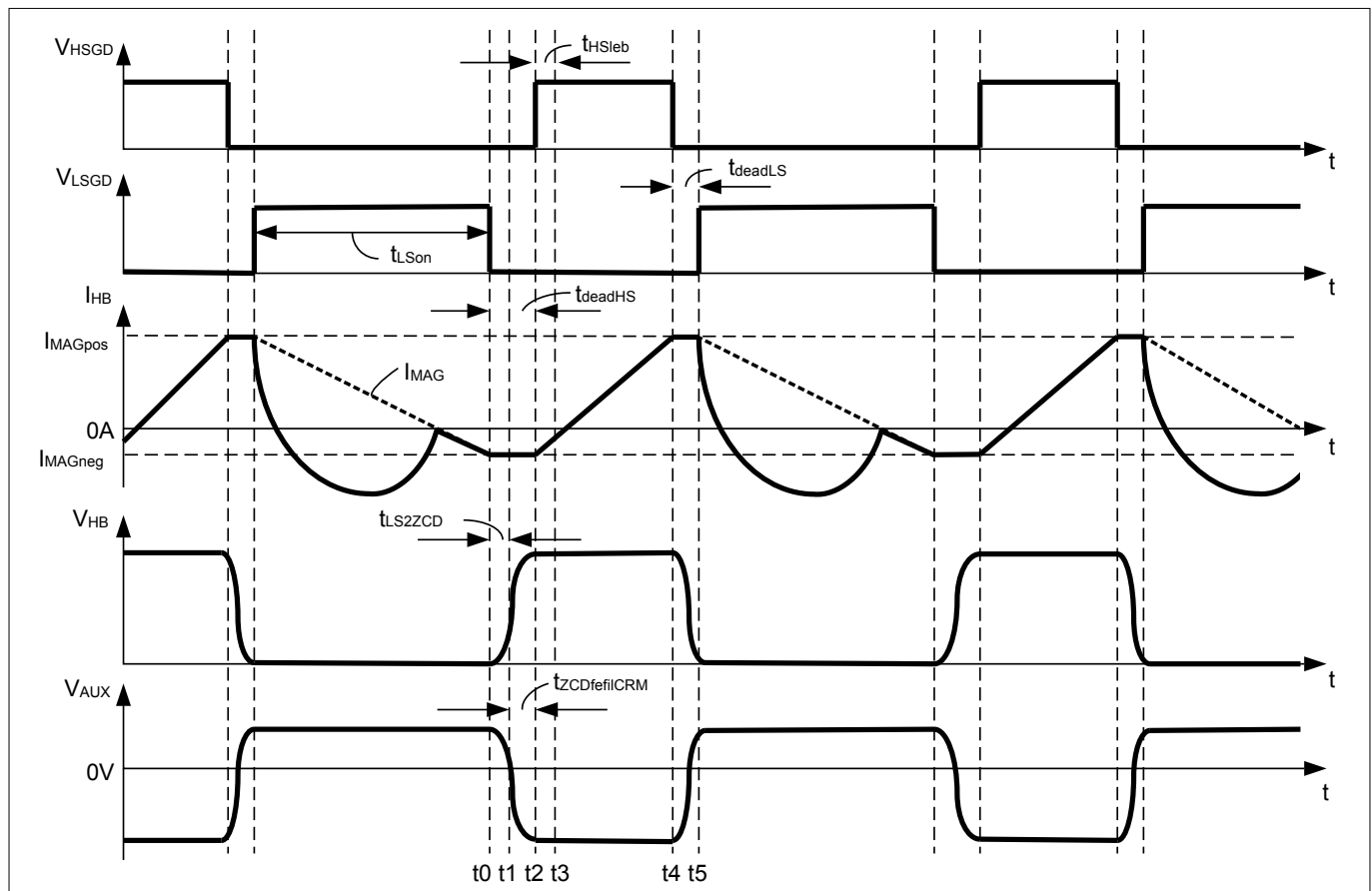


Figure 27 Half-bridge timings for CRM operation

The dead-time t_{deadHS} is depending on input voltage and mode operation. In CRM operation it consists of 2 time periods:

⁵⁾ configurable, see [Table 7](#)

Functional description

$$t_{\text{deadHS}}(V_{\text{in}}; \text{CRM}) = t_{\text{LS2ZCD}}(V_{\text{in}}) + t_{\text{ZCDrefiICRM}}$$

Equation 32

The time period t_{LS2ZCD} is captured after turning off *LS* switch at time t_0 until zero-crossing detection at time t_1 and compared with a target value based on V_{in} . The shortest time period $t_{\text{LS2ZCDmin}}$ ⁵⁾ occurs at maximum input voltage, whereas the longest time period $t_{\text{LS2ZCDnom}}$ ⁵⁾ is correlated with minimum input voltage (see **Figure 28**).

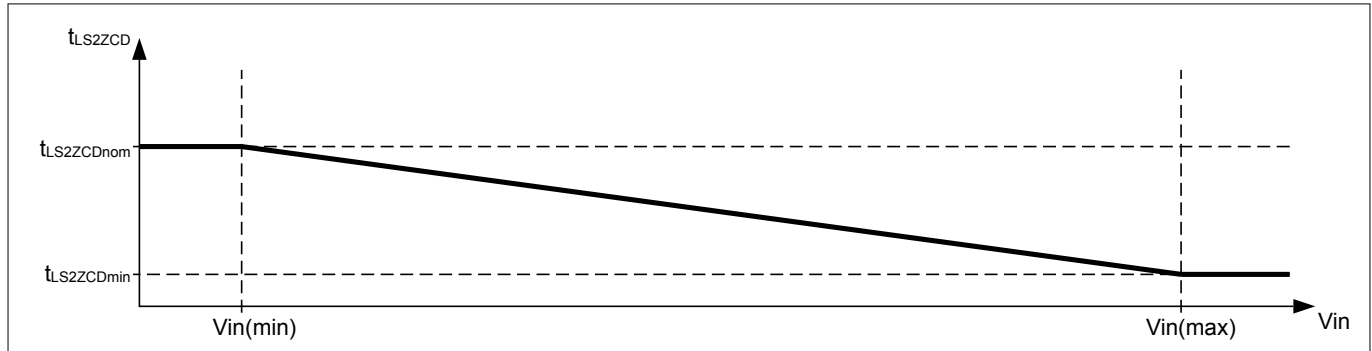


Figure 28 Adaptive target time period for t_{LS2ZCD}

In the subsequent half-bridge switching cycle the *LS* switch on-time t_{LSon} is adjusted by Δt_{LSon}

$$\Delta t_{\text{LSon}} = t_{\text{LS2ZCD}}(V_{\text{in}}) - t_{\text{LS2ZCDcap}}$$

Equation 33

with $t_{\text{LS2ZCDcap}}$ being the captured time period.

Extending t_{LSon} increases the negative magnetization level I_{MAGneg} , which then reduces the time for switching-over the half-bridge node. In this way the negative magnetization is being self-adjusted to the defined target value as shown in **Chapter 3.3.1.1** and supporting an internal accurate output current estimation for peak current setting at *CS* pin.

When reducing t_{LSon} the minimum is determined by t_{TRANSnom} ⁵⁾ at maximum output voltage level.

The 2nd part of t_{deadHS} is defined by the fixed time period $t_{\text{ZCDrefiICRM}}$ ⁵⁾, which is delaying the *HS* switch turn-on at time t_2 after zero-crossing detection at time t_1 (see **Figure 27**).

After *HS* switch is turned on the peak current limitation only takes place after a leading edge spike blanking period t_{HSleb} ⁵⁾, which determines also the minimum on-time of *HS* switch operation.

3.3.2.2 ZV-RVS control scheme

The relevant timings for ZV-RVS mode operation with ZVS pulse generation are shown in **Figure 29**). During ZV-RVS mode a waiting time gap t_{waitgap} is inserted at time t_0 after a *HS* and *LS* switch half-bridge cycle to control the output current (see **Chapter 3.3.1.3.2**). The ZVS pulse t_{ZVS} is initiated by turning on the *LS* switch after the rising edge zero-crossing detection target number at time t_1 and a delay time period $t_{\text{ZCDrefilRVS}}$ ⁶⁾. The dead-time for turning on the *HS* switch after the ZVS pulse is fixed with $t_{\text{deadHSRVS}}$ ⁶⁾. The subsequent dead-time t_{deadLS} is same as in CRM operation.

The required ZVS pulse length t_{ZVS} is determined by the target negative magnetization level I_{MAGneg} , the transformer magnetizing inductance L_m and depending on output voltage V_{out} :

⁵⁾ configurable, see **Table 7**

⁶⁾ configurable, see **Table 8**

Functional description

$$t_{ZVS} = \frac{I_{MAGneg} \times L_m}{N \times V_{OUT}}$$

Equation 34

I_{MAGneg} is adapted for changes in input voltage (see [Chapter 3.3.1.1](#)). The minimum ZVS pulse length occurs when both lowest input voltage and highest output voltage applies. Here the parameter $t_{ZVSmin}^{7)}$ is limiting the minimum adjustable ZVS pulse length.

Note: The minimum t_{ZVSmin} shall be equal or longer than the minimum on-time of the SR controller for proper operation.

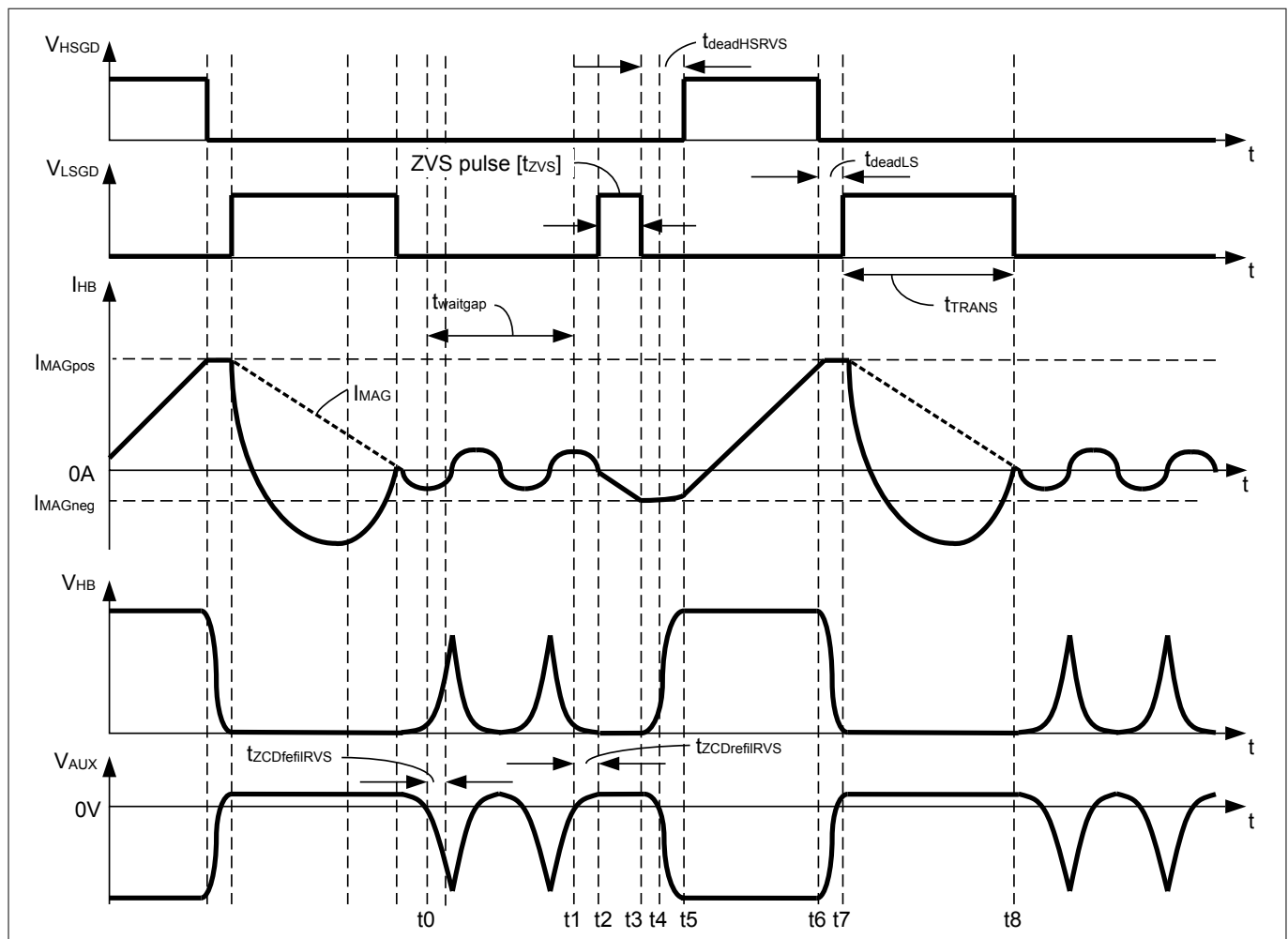


Figure 29 Half-bridge timings for ZV-RVS mode operation

3.3.2.2.1 Valley skipping control

When operating in ZV-RVS mode, valley detection is taking place to determine the time for turning on the ZVS pulse (see [Figure 29](#)). The waiting time after transformer demagnetization $t_{waitgap}$ is controlled based on the target number of detected valleys. A valley is counted once a falling edge of the ZCD signal is detected after a filter $t_{ZCDrefilRVS}^{8)}$. The target number for valley detection is adjusted every half-bridge switching cycle depending on exceeding the thresholds $I_{MAGposRVS(+)}$ or $I_{MAGposRVS(-)}$. The target valley number is increased once

⁷ configurable, see [Table 8](#)
⁸ configurable, see [Table 8](#)

Functional description

the internally derived peak current setting I_{MAGpos} is dropping below $I_{MAGposRVS(+)}$ and decreased when exceeding $I_{MAGposRVS(-)}$. Hence a hysteresis is built in order to avoid value jumping during steady state operation. The hysteresis magnitude can be calculated with:

$$I_{MAGposRVShys} = \frac{1}{3} \times I_{MAGposnom}$$

Equation 35

Both thresholds are depending on the output voltage measured via ZCD pin. The value is decreasing with decreasing output voltage as shown in [Figure 30](#). As a result the peak current setting at CS pin is kept almost constant between the two thresholds $I_{MAGposRVS(-)}$ and $I_{MAGposRVS(+)}$ for a given output voltage. The threshold $I_{MAGposRVS(+)}$ is determined by the two points for $I_{MAGposnom}$ at nominal output voltage and $I_{MAGposRVS0V}$ for $V_{out} = 0V$. $I_{MAGposRVS0V}$ is defined by $I_{MAGposRVS0V\%}$ ⁹⁾ with following equation:

$$I_{MAGposRVS0V} = I_{MAGposRVS0V\%} \times I_{MAGposnom}$$

Equation 36

The maximum number of requested target valleys is limited and leads to a mode change to DCM (see [Chapter 3.3.2.4](#)).

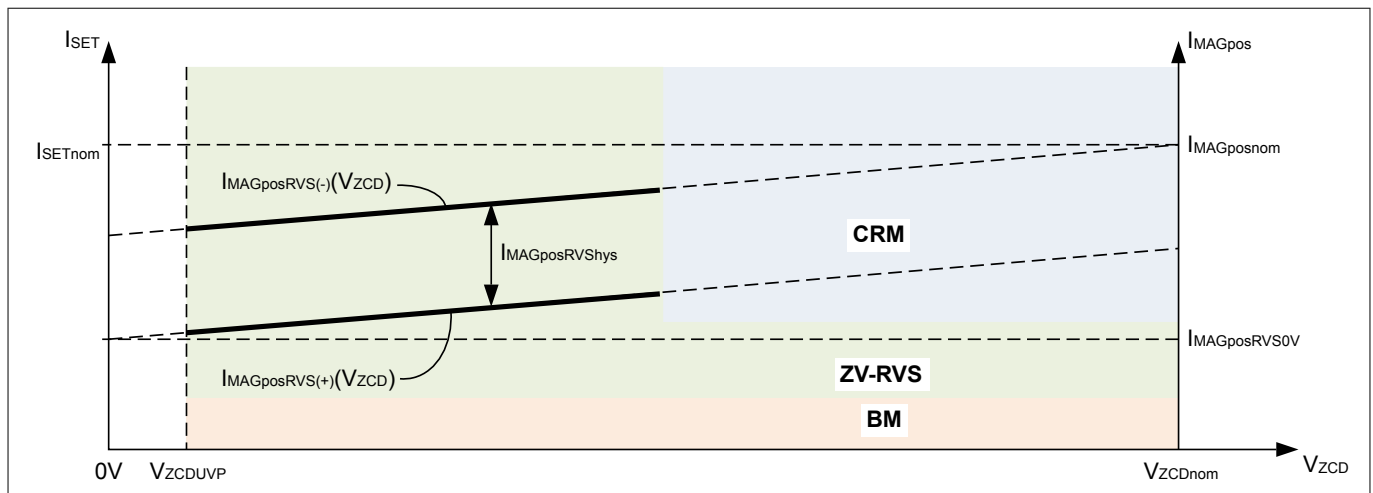


Figure 30 Valley skipping control for adjusting $t_{waitgap}$

3.3.2.3 DCM control scheme

The DCM control is associated with triggering the ZVS pulse in ZV-RVS mode operation. ZV-RVS mode operation at light-load is limited by the maximum number of detectable zero-crossings at ZCD due to decreasing oscillation magnitude with prolongation of the inserted waiting time gap $t_{waitgap}$ (see [Figure 10](#)). When further reducing the output current the waiting time gap $t_{waitgap}$ is further increased until the ZVS pulse is initiated without zero-crossing detection. The subsequent half-bridge cycle is then again performed under ZVS condition (see [Chapter 3.3.2.2](#)).

Increasing $t_{waitgap}$ takes only place until the extended half-bridge period $t_{HBperiodex}$ (see [Chapter 3.3.2.2](#)) reaches the associated minimum half-bridge switching frequency F_{DCMmin} ¹⁰⁾. When output current is further decreased, the feedback voltage V_{FB} drops until it exceeds the burst mode entry threshold (see [Chapter 3.3.4.1](#)).

The DCM operation can be disabled by means of EN_{DCM} ¹⁰⁾.

⁹⁾ configurable, see [Table 6](#)

¹⁰⁾ configurable, see [Table 9](#)

Functional description

3.3.2.4 Mode transition control

Mode transition between CRM and ZV-RVS mode

The mode transition control observes the signal levels at *FB* and *ZCD* pins for exceeding thresholds that define the changeover from CRM to ZV-RVS mode and vice versa. The feedback signal V_{FB} is determining the internal current set-point $I_{SET\%}$ and compared with the current set-point thresholds (see [Chapter 3.3.1.3](#)). During operating in CRM the thresholds $I_{SETCRM2RVS\%}^{11)}$ and $V_{ZCDCRM2RVS}^{11)}$ at *ZCD* pin are determining the switchover to ZV-RVS mode. Operating in ZV-RVS mode the thresholds $I_{SETRVS2CRM\%}^{11)}$ and $V_{ZCDRVS2CRM}^{11)}$ at *ZCD* pin are determining the switchover to CRM.

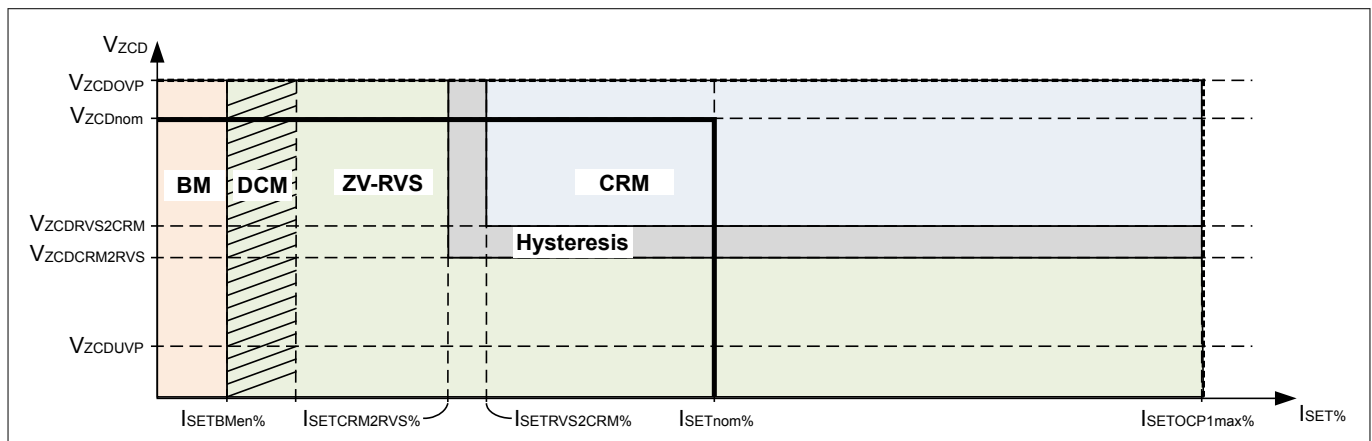


Figure 31 Mode transition between CRM and ZV-RVS mode

Mode transition between ZV-RVS mode and DCM

The DCM operation takes place once the control loop requests for operating beyond the maximum number of valley switching $N_{RVSvalmax}^{12)}$ (see [Chapter 3.3.2.2.1](#)). After entering DCM operation the peak current setting is slightly increased by adding an offset of 25% of the set $I_{MAGposRVS(+)}$. During DCM operation the number of occurring valleys is observed. When ZVS pulse is initiated within a time period with lower number of valleys than $N_{RVSvalmax}$ a switch-over to valley synchronized ZV-RVS mode operation is taking place. After leaving the DCM operation the 25% offset is removed again. This ensures a hysteresis between entering and leaving DCM.

3.3.2.5 Overcurrent control

The hybrid-flyback topology supports high level overcurrent operation with high efficiency. In such case CRM operation is taking place based on the equations shown in [Chapter 3.3.1.3.1](#). The additionally required circulating current is achieved by increasing the peak current setting for current set-points higher than I_{SETnom} , as requested by the feedback signal at *FB* pin. Hereby the energy transmission time t_{TRANS} is extended to provide increased negative magnetization level I_{MAGneg} to reach ZVS condition for turning on the *HS* switch (see [Chapter 3.3.1.2.1](#)). If the estimated overcurrent is exceeding overcurrent set-points for a defined time period, a protection mode is entered (see [Chapter 3.4.7](#)).

3.3.3 Vout start-up control

The IC contains a *Vout* start-up control by observing the output voltage via the reflected voltage at *ZCD* pin, which is shown in [Figure 34](#).

¹¹ configurable, see [Table 19](#)
¹² configurable, see [Table 9](#)

Functional description

A start-up request takes place after an IC HW reset or entered auto-restart mode when VCC is charged up and exceeded the threshold V_{VCCon} (see [Chapter 3.2.1](#)). At that moment following 4 conditions are checked to be valid:

1. Brown-in condition with $V_{VS} > V_{VSBIp}$ (see [Chapter 3.4.4.1](#))
2. No Input overvoltage with $V_{VS} < V_{VSOVP}$ (see [Chapter 3.4.4.4](#))
3. Feedback signal out of regulation range $V_{FB} > V_{FBBMctrl}$
4. No overtemperature condition with $R_{MFIO} > R_{MFIOOTPre}$ (see [Chapter 3.4.9](#))

The conditions 1-3 needs to be valid within the time period $t_{stupcheck}$. Once conditions 1-3 are valid condition 4 is checked.

In case one of those conditions is not met the IC enters bang-bang during brown-in phase (see [Chapter 3.2.2](#)). After all 4 conditions are valid the IC prepares for the first *HS* switch pulse. Here a maximum on-time $t_{Hsonmax}$ is calculated based on V_{in} to check for a R_{Shunt} short circuit at CS pin (CSSCP, see [Chapter 3.4.6](#)), when turning on the *HS* switch. But before turning on the *HS* switch a first initial *LS* switch pulse is generated with $t_{ZVSst1st}$ ¹³⁾ to precharge the bootstrap capacitor at *HSVCC* pin. Afterwards the length of ZVS pulse is fixed to the time period $t_{ZVSstup}$ until the voltage at *ZCD* pin exceeds the threshold $V_{ZCDtZVSstup}$.

$$t_{ZVSstup} = \frac{I_{MAGneg} \times L_m}{k \times V_{ZCDtZVSstup}}$$

Equation 37

Then t_{ZVS} is decreased depending on increasing V_{ZCD} (see [Figure 32](#)).

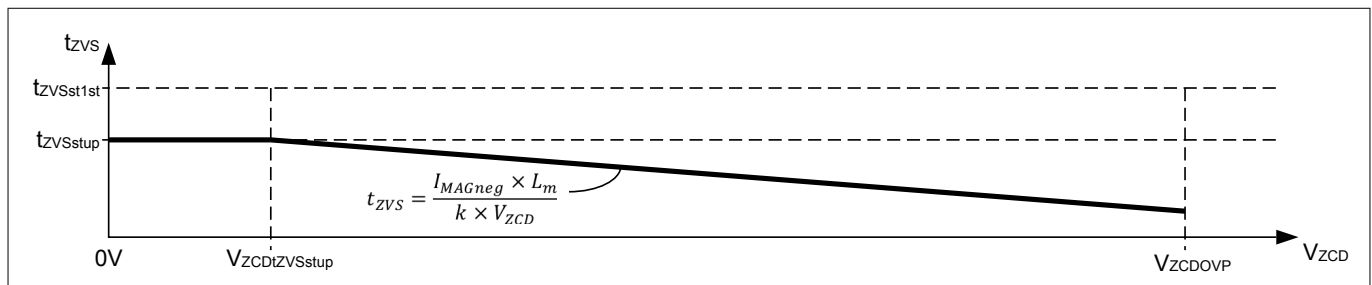


Figure 32 Adaptive t_{ZVS} depending on V_{ZCD}

During ZCD search phase the number of generated half-bridge switching cycles is counted. If no zero-crossing detection is taking place after the *HS* switch is turned off, a next ZVS pulse is generated after a time period $t_{startzcdto}$ ¹³⁾. When ZCD signal is missing, the counted number of half-bridge switching cycles is exceeding $N_{HBcyclemax}$ ¹³⁾ a protection mode for *Vout* short circuit detection (*VoutSCP*, see [Chapter 3.4.8.3](#)) is entered.

With entering the ZCD search phase the very first peak current setting at CS pin is starting based on overcurrent set-point $I_{SETOCP1lev1\%}$. The further peak current setting is kept constant until V_{ZCD} is exceeding the threshold $V_{ZCDtZVSstup}$. Then *Vout* start-up control is determining the peak current control setting based on comparing the measured voltage at *ZCD* pin with target voltage set-point $V_{ZCDtarget}$. The peak current control is cycle by cycle linearly increasing V_{CS} until target voltage level at *ZCD* pin is reached or linearly decreasing V_{CS} if V_{ZCD} is over the target voltage level for *ZCD* pin. Here the IC increases step by step after a time period $t_{SLWTASK}$ the incremental target value $V_{ZDtarget}$ (see [Figure 33](#)). During start-up the current set-point maximum control range is limited by $I_{SETstmax\%}$ ¹³⁾.

The incremental voltage step $\Delta V_{ZCDstinc}$ is determined by the ramp-up time period $t_{startramp}$ ¹³⁾:

¹³⁾ configurable, see [Table 11](#)

Functional description

$$\Delta V_{ZCDstinc} = \frac{V_{ZCDnom} \times t_{SLWTASK}}{t_{startramp}}$$

Equation 38

By this the IC ramps up the output voltage in a primary side controlled manner. When the voltage at ZCD pin exceeds the threshold $V_{ZCDRVS2CRM}$ the PWM operation is switched over to CRM scheme.

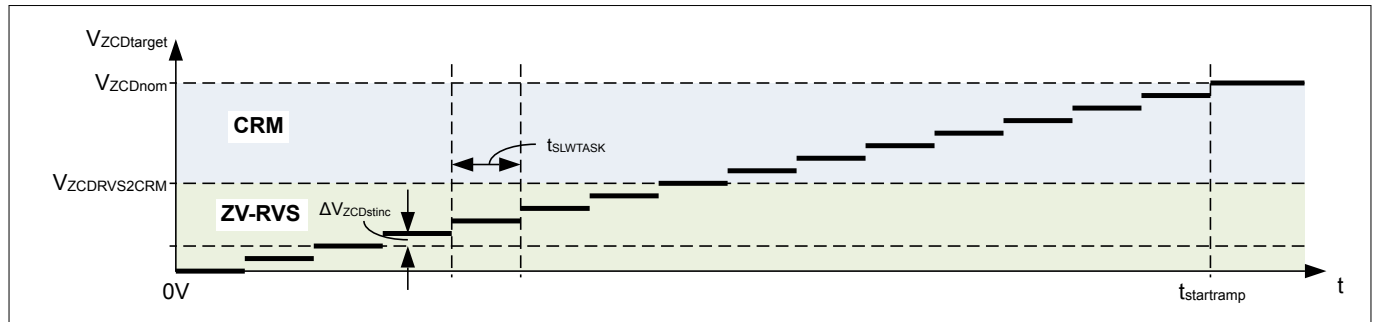


Figure 33 $V_{ZCDtarget}$ control during start-up phase

The start-up phase is finished once the feedback loop at FB pin takes over the peak current control. This takes place when the peak current setting at CS pin determined by V_{FB} is dropping below the peak current setting determined by V_{ZCD} ramp-up control. The maximum time period for the start-up phase is limited by a timer when exceeding $t_{startto}$, which leads to a start-up timeout (STTOP, see [Chapter 3.4.5](#)).

Functional description

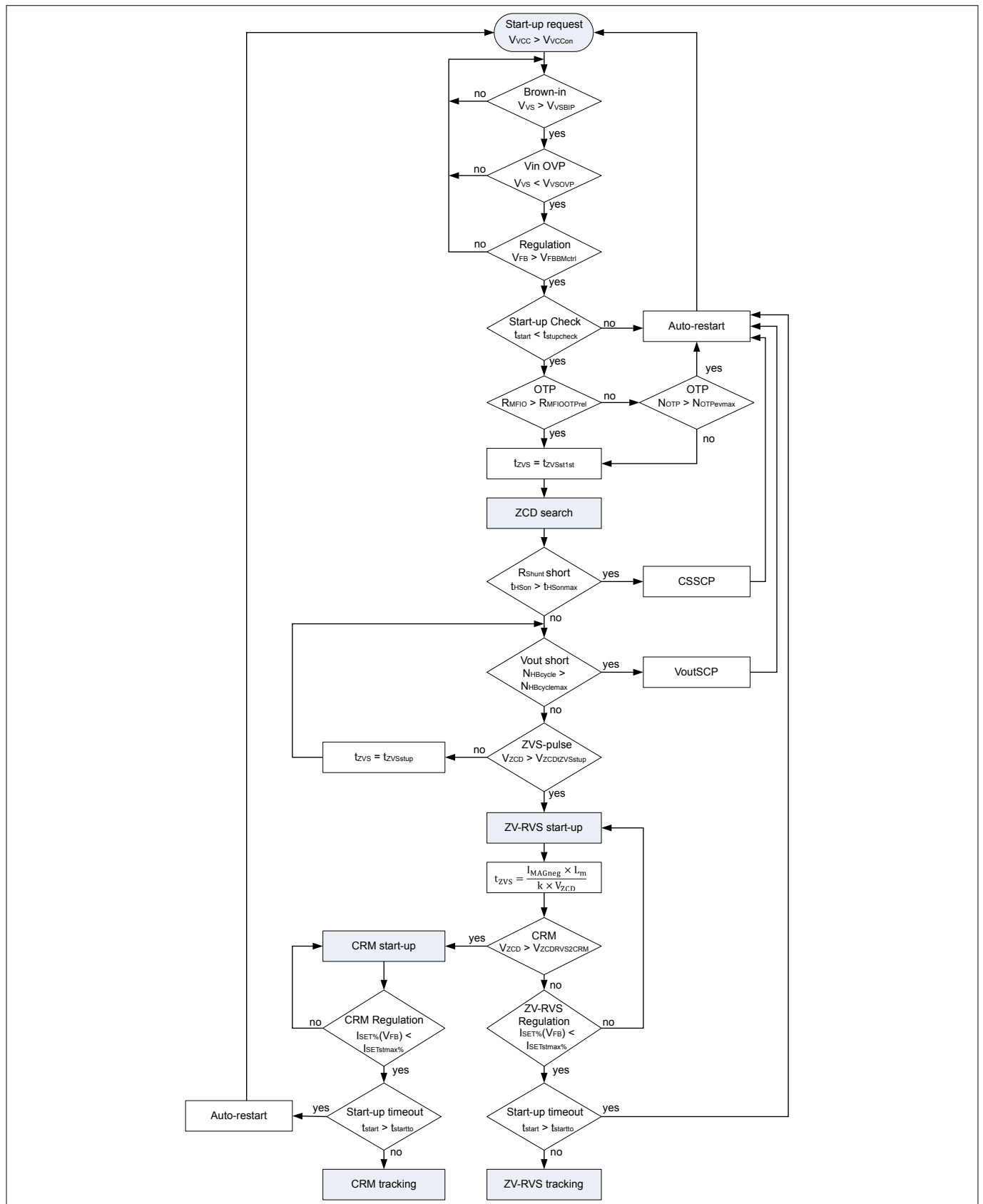


Figure 34 Start-up sequence

Functional description

3.3.4 Burst mode control

The IC contains a burst mode control block to enter a highly efficient operation mode at light-load. By introducing longer non-switching phases with IC entering a sleep mode the average switching and bias losses are reduced during burst mode operation. A slow and fast burst mode exit is supported in order to have a smooth take-over for feedback voltage regulation, when changing back from hysteretic burst frame on/off control to linear feedback loop control. **Figure 35** shows the main functions for the burst mode control as listed and described in the following:

- Burst mode entry (see [Chapter 3.3.4.1](#))
- Burst mode operation (see [Chapter 3.3.4.2](#))
- Burst mode bootstrap precharge (see [Chapter 3.3.4.3](#))
- Burst mode exit control (see [Chapter 3.3.4.4](#))

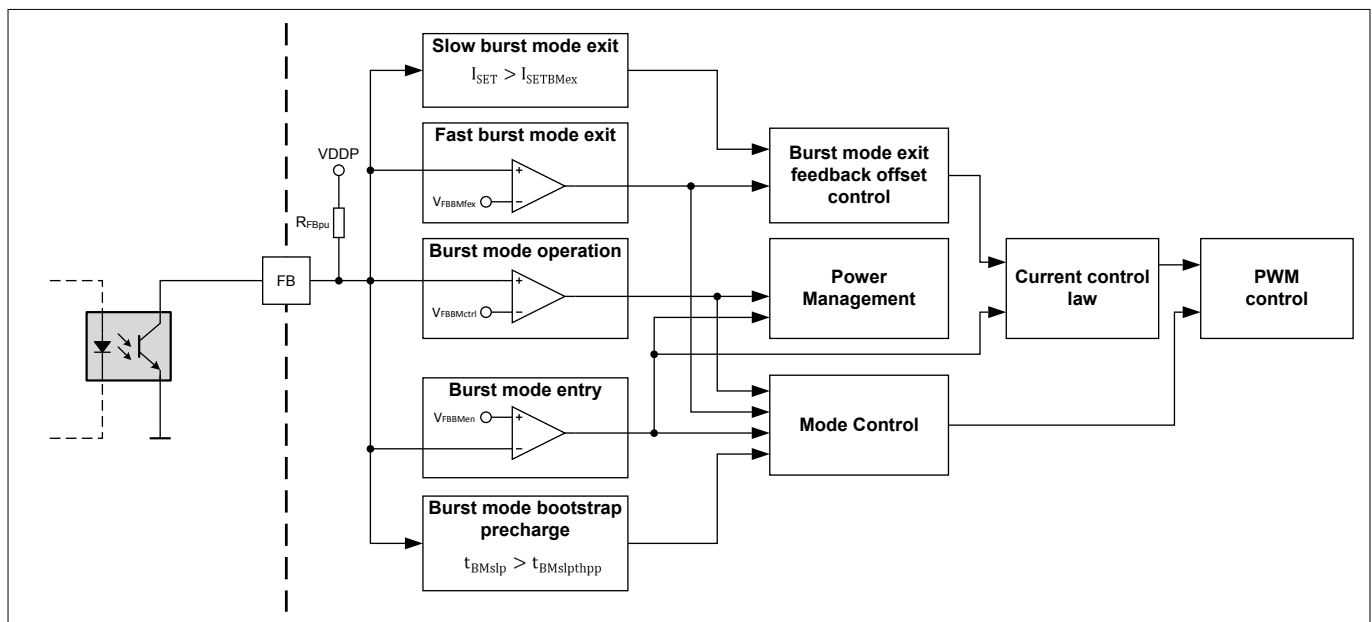


Figure 35 Burst mode control block

3.3.4.1 Burst mode entry

The burst mode entry is based on comparing the voltage at *FB* pin with the threshold V_{FBBMen} . Once V_{FB} is dropping below V_{FBBMen} the generation of next switching pulse is stopped and burst mode is enabled by entering sleep mode with the reduced current consumption $I_{VCCBMpsm}$. V_{FBBMen} is correlated with the current set-point $I_{SETBMen\%}^{14}$, which is defined by the output current control law (see [Chapter 3.3.1.3](#)).

$$V_{FBBMen} = (I_{SETBMen\%} \times I_{SETnom\%} \times V_{FBOPmax}) + V_{FBOPmin}$$

Equation 39

Once entered burst mode the current control law is switched over to a minimum fixed peak current setting at CS pin, which is based on $I_{MAGposRVS(+)} + I_{MAGneg}$ (see [Figure 30](#)).

At burst mode entry the HV start-up cell is used once to charge up the VCC and VCC current consumption is reduced during the sleep phases (see [Chapter 3.2.4](#)).

¹⁴ configurable, see [Table 10](#)

Functional description

3.3.4.2 Burst mode operation

The steady state burst mode operation is based on a burst frame on/off control by means of comparing the voltage at *FB* pin with the feedback burst mode control threshold $V_{FBMctrl}$. This threshold determines when the IC enters the sleep phase (falling edge) after having generated at least one switching pulse during the active phase. The same comparator is also used during the sleep phase for waking up (rising edge) by triggering a burst on-frame pattern t_{BMfon} (see [Figure 36](#)). During sleep phase $V_{FBMctrl}$ might be slightly lower than during the active phase. Here the burst frame duty cycle and burst mode frequency is fully controlled by means of V_{FB} .

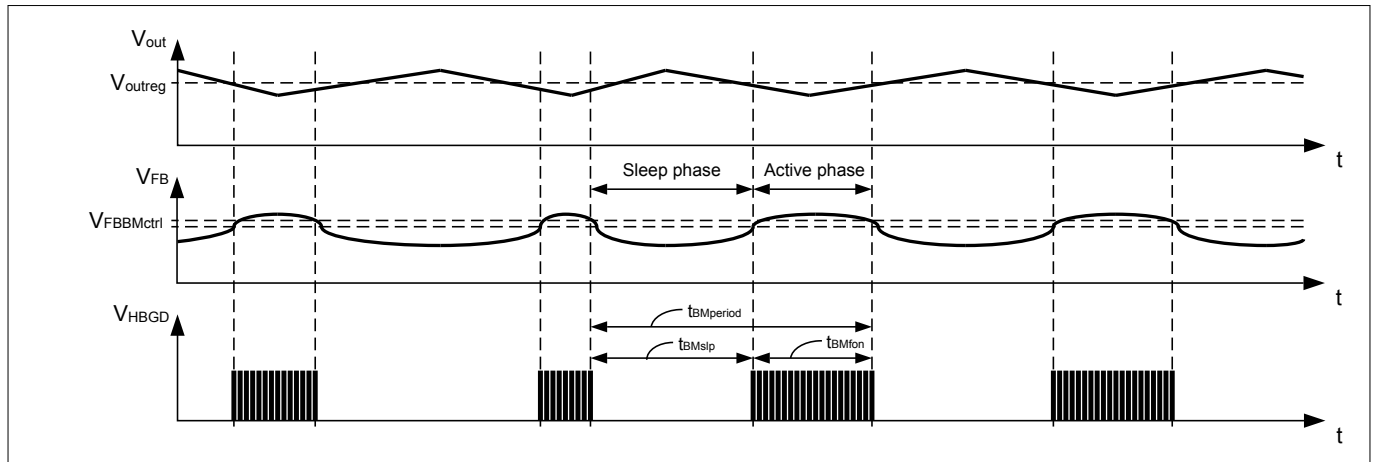


Figure 36 Pulse pattern during burst mode operation

During burst frame on-time t_{BMfon} the transferred energy is based on ZV-RVS mode switching cycles (see [Chapter 3.3.1.3.2](#)) with a peak current setting at CS pin only dependent on V_{out} and taking the first valley as base for initiating the ZVS pulse.

In burst mode the peak current setting I_{MAGpos} is fixed to $I_{MAGposRVS(+)} + I_{MAGneg}$ (see [Figure 30](#)). This results in a limited output current during the burst on-frame phase I_{outBM} :

$$I_{outBM} = \frac{t_{HBperiod}}{t_{HBperiodex}} \times \frac{1}{2} \times N \times (I_{MAGposRVS(+)} + I_{MAGneg})$$

Equation 40

The average output current is now depending on the burst on-frame duty cycle (see [Figure 37](#)):

$$I_{out} = \frac{t_{BMfon}}{t_{BMperiod}} \times I_{outBM}$$

Equation 41

Functional description

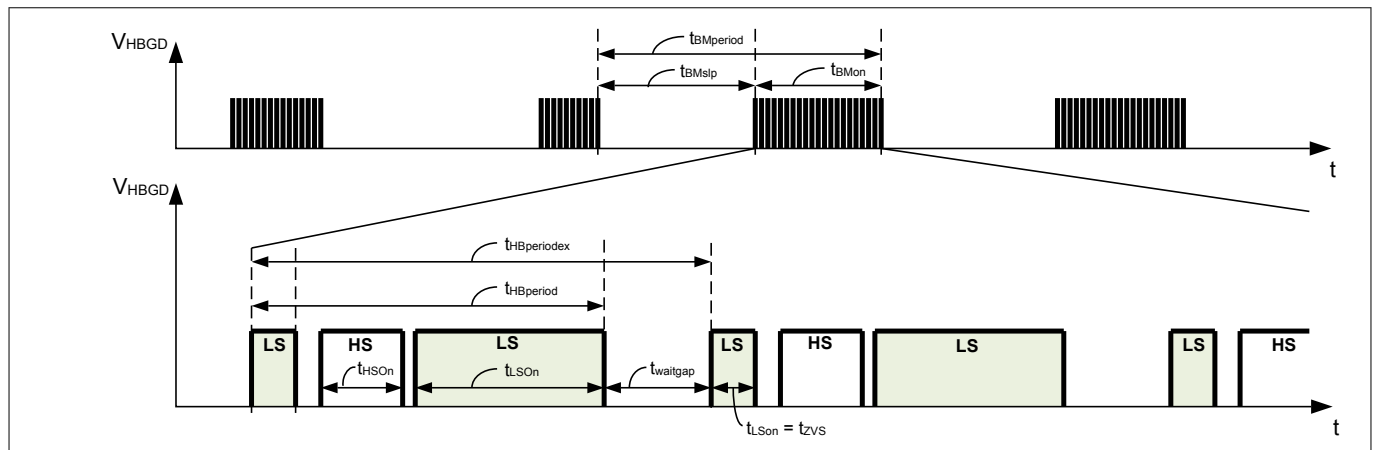


Figure 37 Burst mode timings for average current set-point calculation

3.3.4.3 Burst mode bootstrap precharge

Operation in burst mode at very light-load leads to long IC sleep phases without switching activities. During this sleep-time period t_{BMSlp} (see [Figure 36](#)) the HSVCC voltage is dropping below the off-threshold $V_{HSVCCoff}$ and deactivating the floating *HS* gate driver (HSUVOFF, see [Chapter 3.4.3](#)). When HSVCC is exceeding the on-threshold $V_{HSVCCon}$ the *HS* gate driver is enabled for turning on the power switch after a delay $t_{HSGDdelen}$ (see [Chapter 3.3.6](#)). To ensure that a proper HSVCC supply is in place for turning on the *HS* switch after a long IC sleep phase, a precharge pulse is introduced first before the ZV-RVS pattern is executed (see [Figure 38](#)). The precharge pulse shall only charge the HSVCC above $V_{HSVCCon}$ in order to get the *HS* gate driver prematurely enabled. Dimensioning the length of this precharge pulse $t_{BMprepulse}^{15}$ needs to consider the required delay time period $t_{HSGDdendel}$ for getting enabled the *HS* gate driver after the HSVCC voltage has exceeded the $V_{HSVCCon}$ threshold. During this delay time period also one half-bridge oscillation and one ZVS pulse period are taking place. The precharge pulse is only introduced at the beginning of the burst mode on-frame for a subsequent ZV-RVS switching cycle when the captured burst mode sleep-time period is exceeding the threshold $t_{BMSlpthrpp}^{15}$.

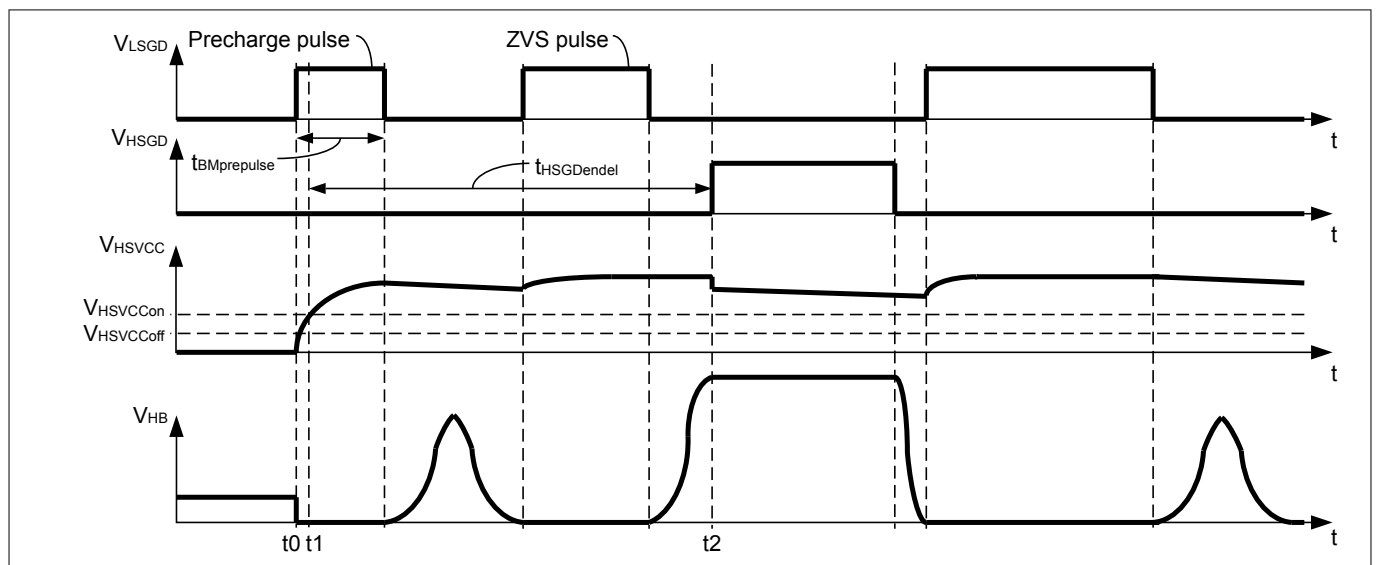


Figure 38 Precharge pulse pattern

¹⁵ configurable, see [Table 10](#)

Functional description

3.3.4.4 Burst mode exit control

The burst mode exit control supports a smooth switch-over for the closed feedback control loop when leaving burst mode due to load jump or load is slowly increasing beyond a burst mode exit current set-point threshold. There are two burst mode exit paths supported. A strong load jump requires a fast burst mode exit (see [Chapter 3.3.4.4.2](#)) and immediate full power delivery whereas a slightly increasing load shall be controlled for a smooth switch-over (see [Chapter 3.3.4.4.1](#)) for the feedback voltage control in order to avoid oscillations at the output. A smaller load jump that leads to a fast burst mode exit shall also not lead to oscillations at the output. Both requirements are covered by introducing an offset $\Delta V_{FBBM<x>exoffs}$ on the measured feedback voltage V_{FB} , when determining the correlated internal current set-point $I_{SET\%}$ based on the output current control law (see [Chapter 3.3.1.3](#)). Once tracking mode is entered (CRM or continuous ZV-RVS mode operation) $\Delta V_{FBBM<x>exoffs}$ is linearly reduced by every half-bridge switching cycle (see [Figure 39](#)).

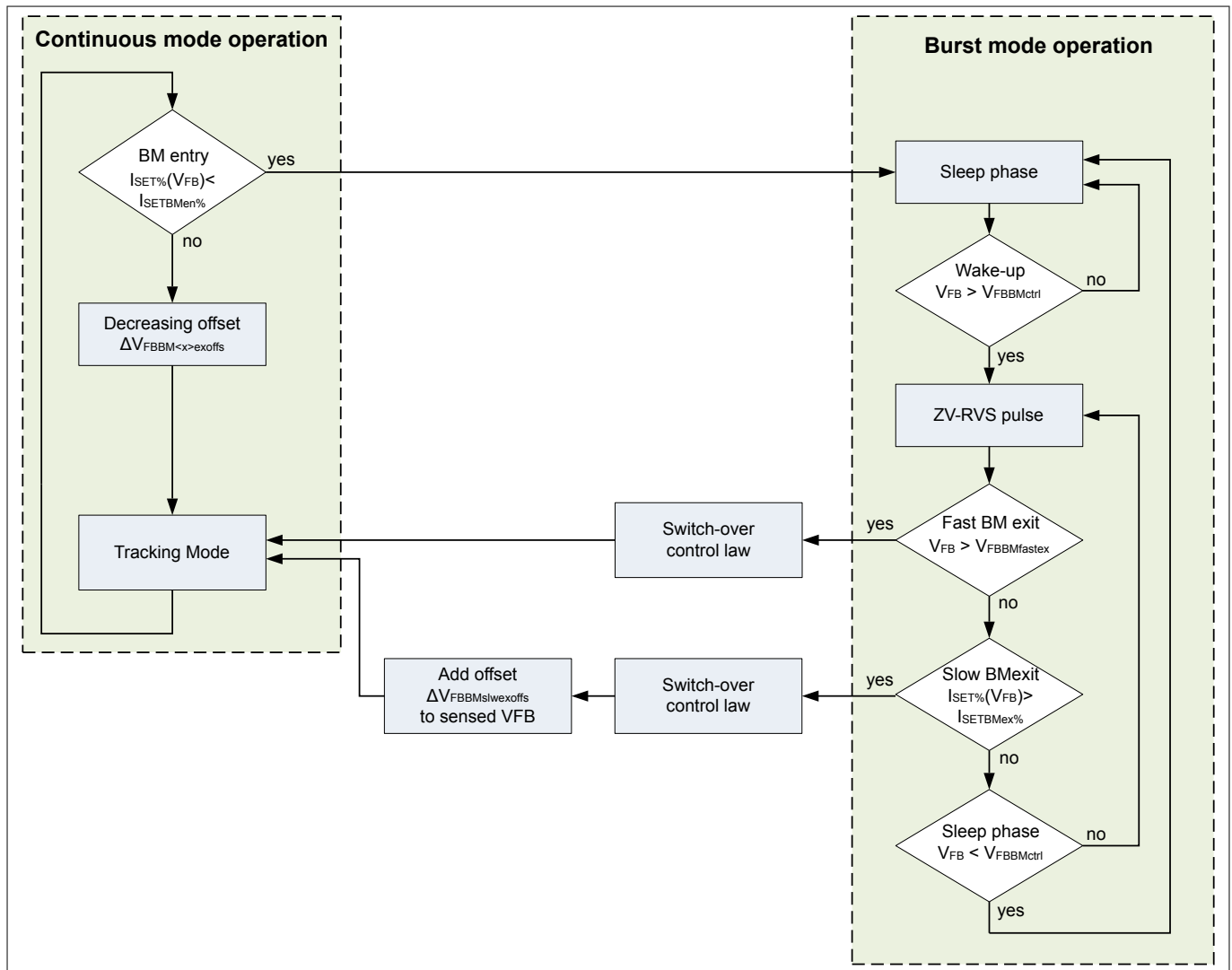


Figure 39 Burst mode exit flow diagram

During burst mode operation the feedback control law only contains two thresholds at FB pin and one for the internal current set-point $I_{SET\%}$ (see [Figure 40](#)):

- $V_{FBBMctrl}$ for controlling the burst on-frame and the sleeping phase
- $V_{FBBMfastex}$ for immediately leaving the burst mode
- $I_{SETBMex\%}$ based on output current estimation for slowly leaving the burst mode

When a burst mode exit condition is met a switch-over of the output current control law is taking place. The feedback voltage level corresponds at that point of time to a different current set-point compared to steady state continuous operation. E.g. if a slow burst mode exit takes place with $I_{SET\%}(V_{FB}) > I_{SETBMex\%}$, the feedback

Functional description

voltage is ca. $V_{FBBctrl}$, which is then close to the nominal current set-point $I_{SETnom\%}$. The normally required $I_{SETBMex\%}$ and associated V_{FBBMex} levels are much lower, which then can lead to an output voltage overshoot depending on how fast the external control loop is adjusting V_{FB} to the required lower level. The added offset on the measured V_{FB} is immediately ensuring the right internal current set-point for peak current control at CS pin. By afterwards linearly reducing every half-bridge switching cycle the offset the regulator is supported to smoothly settle to the target feedback point, which matches then to the required internal current set-point defined by the control law. The target feedback point after burst mode slow exit can be calculated by [Equation 13](#):

$$V_{FBBMex} = (I_{SETBMex\%} \times I_{SETnom\%} \times V_{FBOPmax}) + V_{FBOPmin}$$

Equation 42

The added offset after burst mode slow exit is therefore:

$$\Delta V_{FBBMslwexoffs} = V_{FBBMex} - V_{FBBctrl}$$

Equation 43

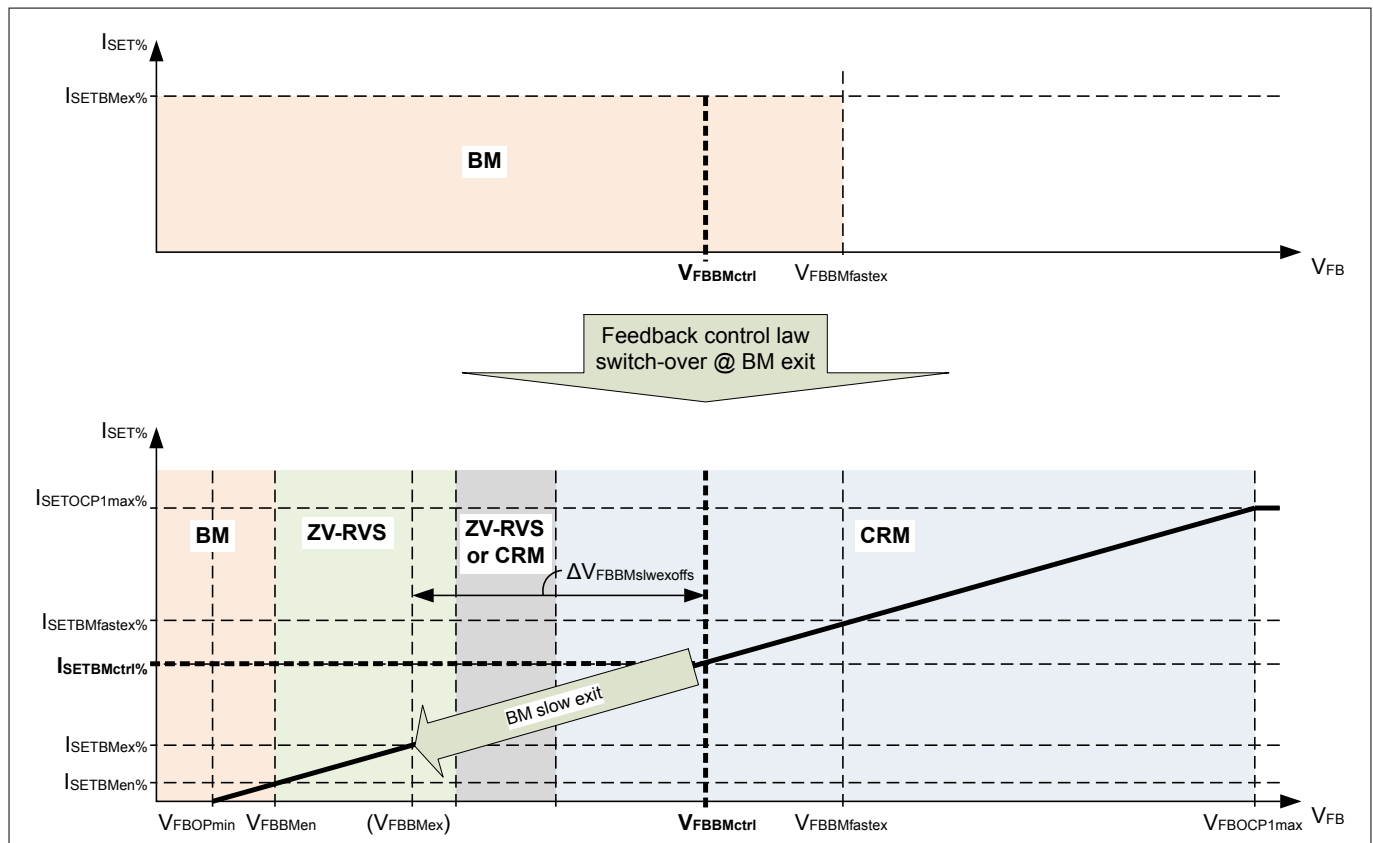


Figure 40 Control law switch-over from burst mode to continuous mode operation

3.3.4.4.1 Burst mode slow exit

Burst mode slow exit is based on output current estimation by capturing the burst frame duty cycle during burst mode operation (see [Equation 41](#)). When the estimated current is exceeding the current set-point $I_{SETBMex\%}$ ¹⁶⁾ for number of $N_{BMexreqthr}$ ¹⁶⁾ burst frame period cycles the burst mode is left by switching over the control law to continuous operation, activating the offset $\Delta V_{FBBMslwexoffs}$ and entering tracking mode with ZV-RVS mode operation.

¹⁶⁾ configurable, see [Table 10](#)

Functional description

3.3.4.4.2 Burst mode fast exit

Once a load jumps exceeds the fixed energy transmission level set during burst on-frame period the feedback voltage is further increasing. The fast burst mode exit threshold $V_{FBBMfastex}^{17}$ is then exceeded if not slow burst mode has been triggered so far. Afterwards the control law is switched over. The IC is then entering CRM operation for the first half-bridge switching cycles if V_{ZCD} is higher than the threshold $V_{ZCDRVS2CRM}$. This can be disabled by $EN_{BMfastexCRM}^{18}$.

3.3.5 Frequency jitter

The jitter function is only working in CRM operation. Furthermore it is depending on the voltage at VS pin. The jitter function is enabled once the voltage at VS pin exceeds the threshold $V_{VSJitteren}^{19}$. Frequency jitter is generated by modulating the magnetizing current for I_{MAGpos} and I_{MAGneg} in such a way that the sum of them I_{MAGtot} is kept constant. Then also I_{out} is kept constant not being impacted by modulating the switching period (see [Equation 5](#)).

$$I_{MAGtot} = I_{MAGpos} + I_{MAGneg}$$

Equation 44

The modulation of the peak to peak magnetizing current I_{MAGpp} is performed by directly adjusting the peak current threshold at CS pin for the positive magnetizing current level I_{MAGpos} and indirectly adjusting the negative magnetizing current level I_{MAGneg} by means of changing the on-time t_{Lson} (see [Chapter 3.1.1](#)).

$$I_{MAGpp} = I_{MAGpos} - I_{MAGneg}$$

Equation 45

Once the negative magnetizing current is changing, the closed control loop is adjusting I_{MAGpos} accordingly. The delta for the change of half-bridge switching frequency ΔF_{HBsw} is set by a constant for the target jitter spread $d_{Jitterspread\%}^{19}$, which is based on a percentage number of the switching frequency without Jitter.

$$\Delta F_{HBsw} = F_{HBsw} \times d_{Jitterspread\%}$$

Equation 46

$$\Delta t_{HBsw} = \frac{1}{\Delta F_{HBsw}}$$

Equation 47

The incremental step for changing the target switching period is one master clock period t_{MCLK} . This adjustment is taking place after a delay time $t_{Jitterstpdel}^{19}$ in order to provide time for the control loop to settle to the changed level for I_{MAGneg} . The jitter function starts first with increasing I_{MAGneg} step by step until the correlated switching period has exceeded the target maximum jitter switching period $t_{Jitterpermax}$.

$$t_{Jitterpermax} = t_{HBper} + \Delta t_{HBsw}$$

Equation 48

¹⁷ configurable, see [Table 10](#)

¹⁸ configurable, see [Table 10](#)

¹⁹ configurable, see [Table 20](#)

Functional description

Subsequently I_{MAGneg} is adjusted step by step back to the starting level for the switching period t_{HBper} (see [Figure 41](#))

Note: Increasing the amount of negative magnetization I_{MAGneg} is reducing the dead-time for turning on the high-side switch t_{deadHS} . Therefore the potential target delta for switching period spread $d_{Jitterspread\%}$ is limited by the target minimum time delay between the falling edge of LS switch and following zero-crossing detection $t_{LSdelZCDmin}$.

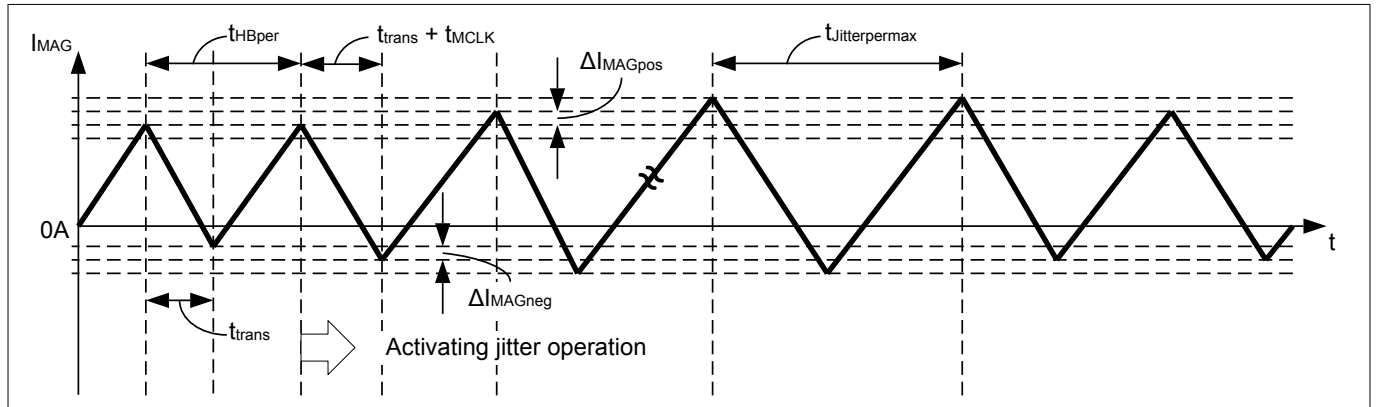


Figure 41 I_{MAG} modulation for frequency jittering

3.3.6 Half-bridge gate driver

The half-bridge gate driver consists of a low-side gate driver for *LS* switch, which is supplied by *VCC* and *GND* pin. The *HS* switch is driven by a floating high-side gate driver supplied by *HSVCC* and *HSGND*. The floating *HS* domain is galvanically isolated and steered via a coreless pulse transformer. The *LS* and *HS* gate drivers are enabled/disabled based on the corresponding undervoltage lockout thresholds (V_{VCCcon} , V_{VCCoff}) and ($V_{HSVCCcon}$, $V_{HSVCCoff}$) (see [Chapter 3.4.2](#) and [Chapter 3.4.3](#)). Both drivers are clamping the maximum gate driver output voltage to $V_{LSGDhigh}$; $V_{HSGDhigh}$. If disabled the gate driver outputs are actively kept shut down. When *HSVCC* exceeds the threshold $V_{HSVCCcon}$ the high-side gate driver is enabled after a time period of $t_{HSGDendel}$.

Functional description

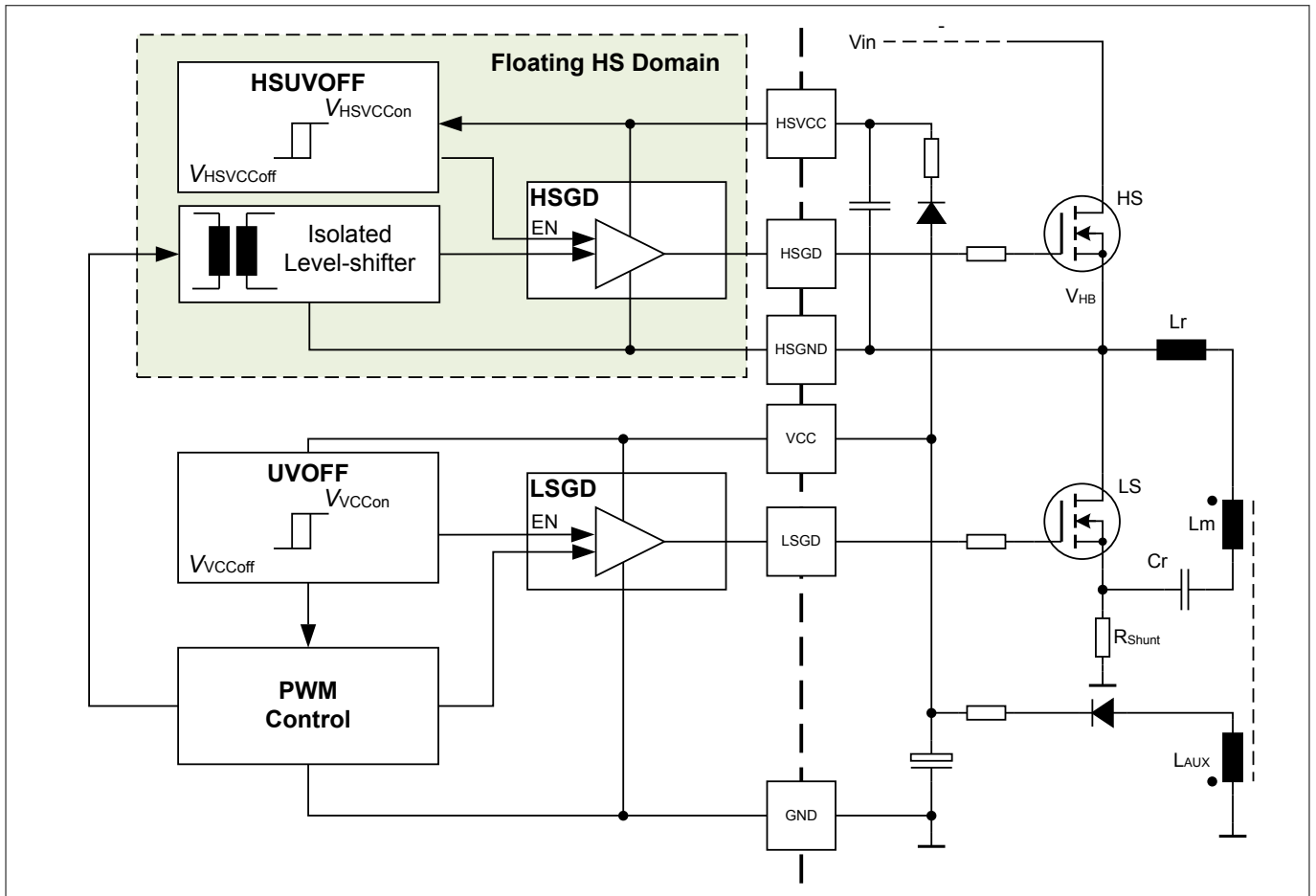


Figure 42 Half-bridge gate driver

Functional description

3.4 Protection features

Table 4 shows the protection features and their corresponding default reactions. Two protection modes (auto-restart mode and latch mode) as well as a UVOFF HW reset (IC deactivation by VCC undervoltage lockout) are implemented.

Note: All protection features w/o UVOFF and HSUVOFF only apply during normal operation. During sleep phase (in burst or protection mode), no pin protection is active.

Table 4 Protection features

| Feature | Symbol | Default reaction | Description |
|--|----------|--|---------------------------------|
| VCC undervoltage lockout | UVOFF | HW reset and restart | Chapter 3.4.2 |
| HSVCC undervoltage lockout | HSUVOFF | Disable HS gate driver | Chapter 3.4.3 |
| Brown-in protection | BIP | Bang-bang mode without start-up request | Chapter 3.4.4.1 |
| Slow brown-out protection | SBOP | Stop operation and enter bang-bang mode for brown-in phase | Chapter 3.4.4.3 |
| Fast brown-out protection | FBOP | Stop operation and enter bang-bang mode for brown-in phase | Chapter 3.4.4.2 |
| Vin overvoltage protection | VinOVP | Auto-restart mode | Chapter 3.4.4.4 |
| Start-up timeout protection | STTOP | Auto-restart mode | Chapter 3.4.5 |
| CS pin short circuit protection | CSSCP | Auto-restart mode | Chapter 3.4.6 |
| Output overcurrent protection OCP1 level 1 | OCP1lev1 | Auto-restart mode | Chapter 3.4.7.1 |
| Output overcurrent protection OCP1 level 2 | OCP1lev2 | Auto-restart mode | Chapter 3.4.7.2 |
| Output maximum current protection | OCP1max | Auto-restart mode | Chapter 3.4.7.3 |
| Peak overcurrent protection OCP2 | OCP2 | Latch mode ²⁰⁾ | Chapter 3.4.7.4 |
| Vout overvoltage protection | VoutOVP | Latch mode ²¹⁾ | Chapter 3.4.8.2 |
| Vout undervoltage protection | VoutUVP | Auto-restart mode | Chapter 3.4.8.1 |
| Vout short circuit protection | VoutSCP | Auto-restart mode ²²⁾ | Chapter 3.4.8.3 |
| External overtemperature protection | extOTP | Auto-restart mode & Latch mode | Chapter 3.4.9 |
| Watchdog timer | WDOG | Auto-restart | Chapter 3.4.10 |

²⁰ configurable with EV_{CSOCP2} , see [Table 16](#)

²¹ configurable with EV_{ZCDOVP} , see [Table 15](#)

²² Only active during start-up phase

Functional description

3.4.1 Protection modes

Once the protection mode is entered, the IC stops the gate driver switching at *LSGD* and *HSGD* pins and enters stand-by mode. During stand-by mode, the HV start-up cell is operating in the bang-bang mode (see [Chapter 3.2.3](#)) to keep the VCC voltage at a high level to have enough energy stored in the VCC capacitor for the system start-up. Two protection modes are supported as described in the sequel.

Latch mode (LM)

In latched operation the system keeps staying in stand-by mode without any restart attempt. The latched operation can only be reset by VCC dropping below the UVOFF HW reset threshold V_{VCCoff} .

Note: Reset of latch mode is done by disconnecting the AC line. By connecting the HV start-up cell via diodes in front of the rectifier the reset time is mainly determined by the size of the capacitor at VCC pin.

Auto-restart mode (ARM)

In auto-restart mode operation the IC triggers a restart after the approximated auto-restart sleep time t_{ARMslp} ²³⁾. The control IC resumes its operation with soft-start after the VCC capacitor is charged up and the VCC voltage has reached its turn-on threshold V_{VCCon} . t_{ARMslp} determines the number of set sleep cycles $N_{ARMstep}$, which are based on the time period $t_{ARMbase}$. (see [Chapter 3.2.3](#)).

$$t_{ARMslp} = N_{ARMstep} \times t_{ARMbase}$$

Equation 49

3.4.2 VCC undervoltage lockout (UVOFF)

The implemented VCC undervoltage lockout (UVOFF) ensures a defined activation and deactivation of the IC operation depending on the supply voltage at pin VCC. The UVOFF contains a hysteresis with the upper voltage threshold V_{VCCon} for activating the IC. A VCC voltage level dropping below the bottom threshold V_{VCCoff} resets and deactivates the IC during normal operation. In reset state the HV start-up cell is turned on, starting the next VCC charge cycle until VCC voltage exceeds V_{VCCon} (see [Chapter 3.2.1](#)).

3.4.3 HSVCC undervoltage lockout (HSUVOFF)

The implemented HSVCC undervoltage lockout (UVOFF) ensures a defined activation and deactivation of the floating high-side driver. The HSUVOFF contains a hysteresis with the upper voltage threshold $V_{HSVCCon}$ for activating the high-side gate driver. A HSVCC voltage level dropping below the bottom threshold $V_{HSVCCoff}$ turns off and deactivates immediately the high-side driver. During deactivation phase the high-side driver current consumption is reduced to $I_{HSVCCUVOFF}$.

3.4.4 Input voltage Vin protection

The IC contains 4 detection thresholds at VS pin for input voltage *Vin* protection to ensure a safe operation within a reliable input voltage range (see [Figure 43](#)). Following *Vin* protections are provided:

- Vin brown-in protection (BIP, see [Chapter 3.4.4.1](#))
- Vin slow brown-out protection (SBOP, see [Chapter 3.4.4.3](#))
- Vin fast brown-out protection (FBOP, see [Chapter 3.4.4.2](#))
- Vin overvoltage protection (VinOVP see [Chapter 3.4.4.4](#))

²³ configurable, see [Table 12](#)

Functional description

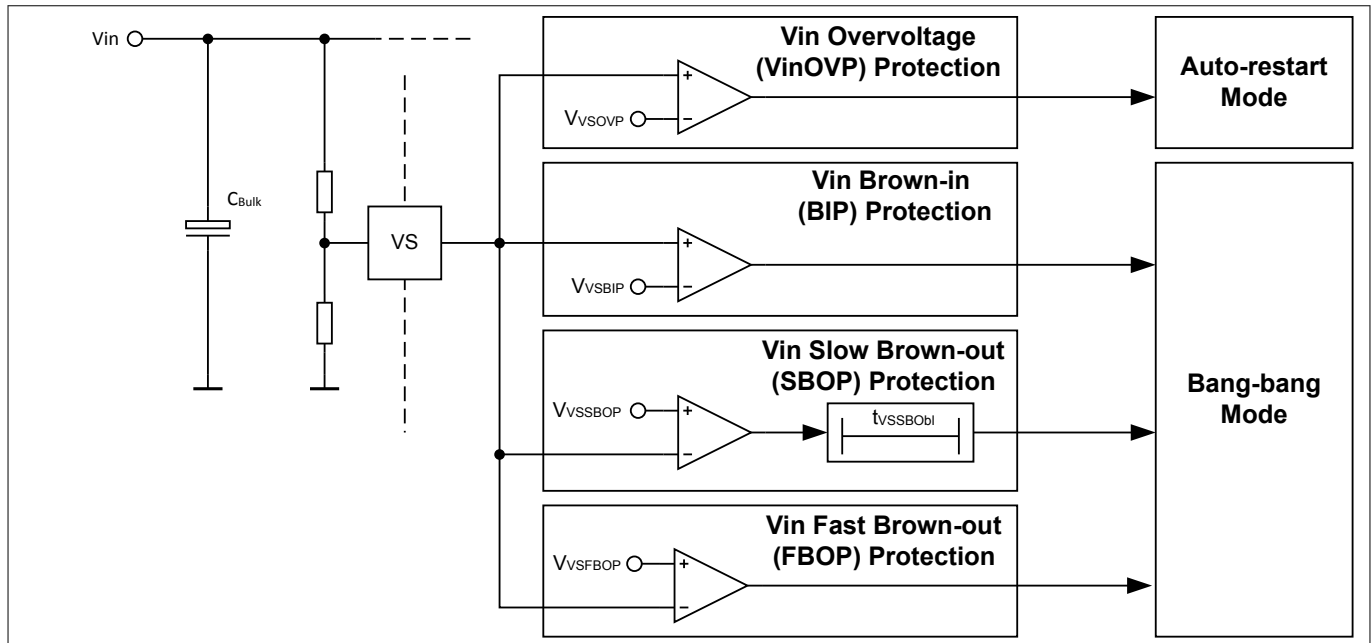


Figure 43 Input voltage V_{in} protection

3.4.4.1 Brown-in protection (BIP)

At initial power-up or auto-restart, the brown-in condition at VS pin must be fulfilled for initiating the switching start-up procedure. Brown-in conditions are met when voltage at VS pin exceeds the threshold $V_{VSBIP}^{24)}$ within the time period $t_{stupcheck}$ during start-up (see Chapter 3.3.3). If the IC is activated and V_{in} brown-in conditions are not reached the IC enters the bang-bang mode to keep the IC alive and ensure a high VCC level for immediate start-up once V_{in} brown-in conditions are detected (see Chapter 3.2.2).

3.4.4.2 Fast brown-out protection (FBOP)

The fast brown-out protection (FBOP) is realized by comparing the voltage at VS pin with the threshold $V_{VSFBOP}^{24)}$ that is set below the slow brown-out protection threshold V_{VSSBOP} (see Chapter 3.4.4.3). Fast brown-out occurrence is not blanked and sampled with a time period t_{sample} .

3.4.4.3 Slow brown-out protection (SBOP)

The slow brown-out protection (SBOP) is realized by comparing the voltage at VS pin with the threshold $V_{VSSBOP}^{24)}$ for a blanking time $t_{VSSBObI}$. Once triggered the bang-bang mode for V_{in} brown-in detection is entered (see Chapter 3.2.2).

3.4.4.4 Vin overvoltage protection (VinOVP)

V_{in} overvoltage protection (VinOVP) is taking place by comparing the voltage at VS pin with the threshold $V_{VSOVP}^{25)}$. The result is sampled with a time period t_{sample} . Once VinOVP is triggered the auto-restart mode is entered (see Chapter 3.4.1).

At V_{out} start-up the VinOVP is checked together with brown-in protection (BIP) (see Chapter 3.3.3). When a time period $t_{stupcheck}$ is exceeded and V_{in} voltage level is not within the target range the bang-bang mode during

²⁴ configurable, see Table 11

²⁵ configurable, see Table 13

Functional description

brown-in phase is entered (see [Chapter 3.3.3](#)). Furthermore also at wake-up during burst mode operation the start of burst on-frame is only initiated if no VinOVP is detected at wake-up.

3.4.5 Start-up timeout protection (STTOP)

In case of overload during start-up the output voltage V_{out} may not reach the regulation nominal voltage target V_{outnom} , preventing the system from entering regulation and staying permanently in start-up condition. To avoid such situation a timer is initiated at start-up request from the very first switching pulse to observe the ongoing start-up time t_{start} . A timeout is detected when after a maximum time period $t_{startto}$ ²⁶⁾ the current set-point determined by V_{FB} is not dropping below the current set-point determined by V_{out} start-up control (see [Chapter 3.3.3](#)).

3.4.6 CS pin short circuit protection (CSSCP)

During V_{out} start-up a short circuit detection at CS pin is activated for the very first HS switch pulse to protect the application operating with a shortened R_{shunt} . Hereby the maximum on-time of HS switch is limited to a precalculated time period $t_{HSonmax}$:

$$t_{HSonmax} = 2 \times t_{TRANSnom} \times \left(\frac{(V_{outnom} \times N) / k_{Rvs}}{V_{VS}} \right)$$

Equation 50

V_{VS} is the instantaneous input voltage measured at VS pin. Once the on-time of HS switch exceeds $t_{HSonmax}$ auto-restart mode is entered.

3.4.7 Overcurrent protection

The overcurrent protection contains several detection functions, which protect the application when exceeding a primary side peak current or operating under output overcurrent conditions (see [Figure 44](#)).

- Output overcurrent protection OCP1 level 1 (OCP1lev1, see [Chapter 3.4.7.1](#))
- Output overcurrent protection OCP1 level 2 (OCP1lev2, see [Chapter 3.4.7.2](#))
- Output maximum current protection (OCP1max, see [Chapter 3.4.7.3](#))
- Primary peak overcurrent protection OCP2 (OCP2, see [Chapter 3.4.7.4](#))

²⁶⁾ configurable, see [Table 14](#)

Functional description

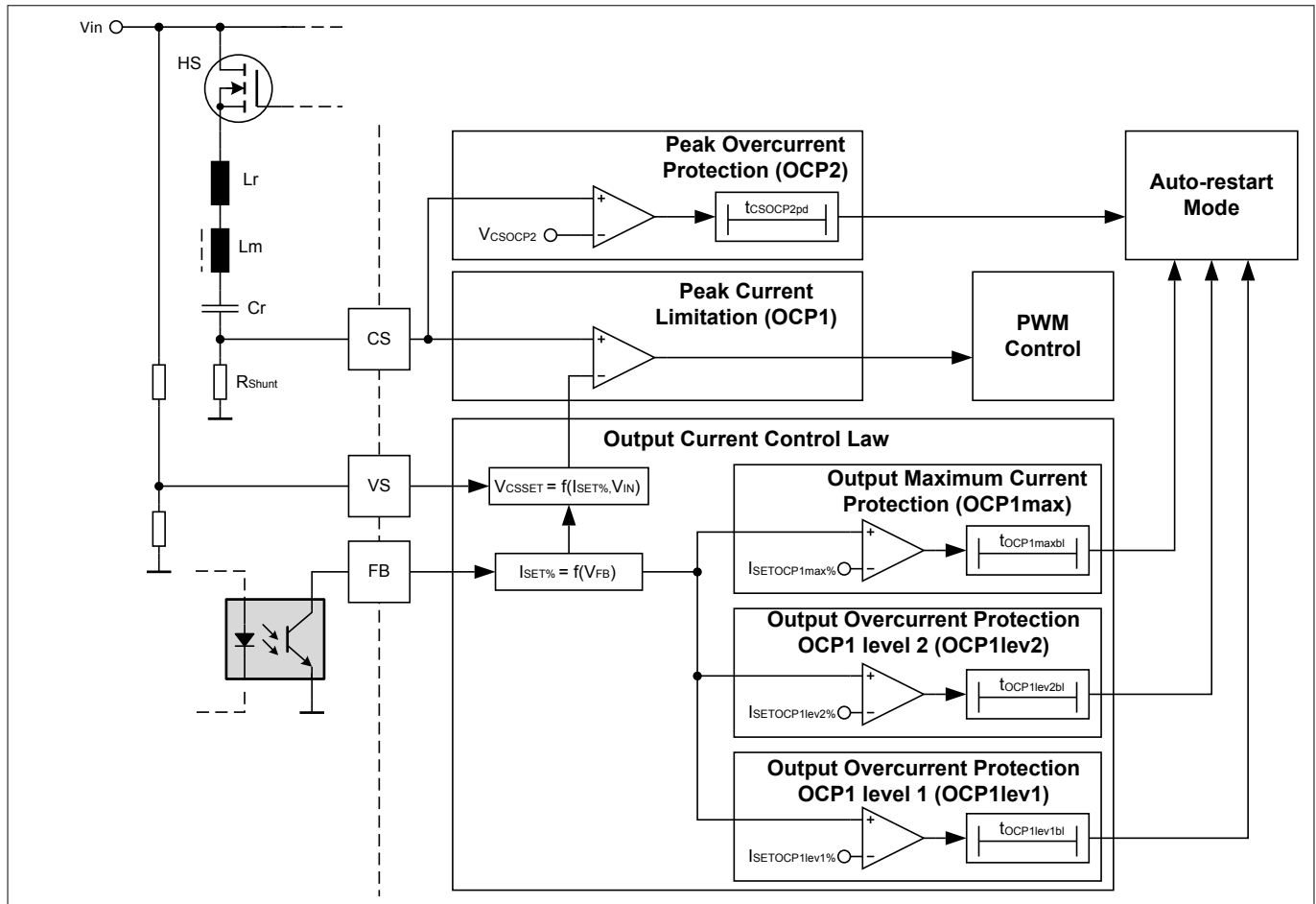


Figure 44 Overcurrent protection overview

3.4.7.1 Output overcurrent protection OCP1 level 1 (OCP1lev1)

The output overcurrent protection level $I_{SETOCP1lev1}^{27}$ is defined by the output current control law (see Figure 25). Once the current set-point $I_{SET\%}$ exceeds the threshold $I_{SETOCP1lev1\%}$ a timer is started. Auto-restart mode is triggered when the timer reaches the threshold $t_{OCP1lev1bl\%}^{27}$. The timer is also reset when $I_{SET\%}$ is dropping back below $I_{SETOCP1lev1\%}$.

The associated peak current setting at CS pin can be calculated with Equation 15 and Equation 16:

CRM operation

$$V_{CSOCP1lev1} = (I_{SETOCP1lev1\%} \times I_{SETnom\%} \times V_{CSOPmax}) + (I_{MAGneg}(V_{in}) \times R_{Shunt})$$

Equation 51

ZV-RVS operation

$$V_{CSOCP1lev1} = \frac{t_{HBperiodex}}{t_{HBperiod}} \times [(I_{SETOCP1lev1\%} \times I_{SETnom\%} \times V_{CSOPmax}) + (I_{MAGneg}(V_{in}) \times R_{Shunt})]$$

Equation 52

The associated feedback voltage at FB pin can be calculated with Equation 13:

²⁷ configurable, see Table 16

Functional description

$$V_{\text{FBOP1lev1}} = (I_{\text{SETOCP1lev1}\%} \times I_{\text{SETnom}\%} \times V_{\text{FBOPmax}}) + V_{\text{FBOPmin}}$$

Equation 53

3.4.7.2 Output overcurrent protection OCP1 level 2 (OCP1lev2)

The threshold $I_{\text{SETOCP1lev2}\%}$ ²⁸⁾ provides a 2nd output overcurrent protection level. Once the current set-point $I_{\text{SET}\%}$ exceeds the threshold $I_{\text{SETOCP1lev2}\%}$ the timer for OCP1lev2 is started. Auto-restart mode is triggered when the timer reaches the threshold $t_{\text{OCP1lev2bl}\%}$ ²⁸⁾. This timer is also reset when I_{SET} is dropping back below $I_{\text{SETOCP1lev2}\%}$

The associated peak current setting at CS pin can be calculated with [Equation 15](#) and [Equation 16](#):

CRM operation

$$V_{\text{CSOCP1lev2}} = (I_{\text{SETOCP1lev2}\%} \times I_{\text{SETnom}\%} \times V_{\text{CSOPmax}}) + (I_{\text{MAGneg}}(\text{Vin}) \times R_{\text{shunt}})$$

Equation 54

ZV-RVS operation

$$V_{\text{CSOCP1lev2}} = \frac{t_{\text{HBperiodx}}}{t_{\text{HBperiod}}} \times [(I_{\text{SETOCP1lev2}\%} \times I_{\text{SETnom}\%} \times V_{\text{CSOPmax}}) + (I_{\text{MAGneg}}(\text{Vin}) \times R_{\text{shunt}})]$$

Equation 55

The associated feedback voltage at FB pin can be calculated with [Equation 13](#):

$$V_{\text{FBOP1lev2}} = (I_{\text{SETOCP1lev2}\%} \times I_{\text{SETnom}\%} \times V_{\text{FBOPmax}}) + V_{\text{FBOPmin}}$$

Equation 56

3.4.7.3 Output maximum current protection (OCP1max)

The threshold $I_{\text{SETOCP1max}\%}$ ²⁹⁾ defines the maximum output current level of output current control. Once a higher output current is requested via V_{FB} control the output current is kept limited and a timer for I_{outMaxP} is started. During this phase output voltage is dropping because output current is higher than what is provided by the converter ($I_{\text{SETOCP1max}\%}$). Auto-restart mode is entered when the timer reaches the threshold $t_{\text{OCP1maxbl}\%}$ ²⁹⁾. The timer is reset when auto-restart mode is entered or I_{SET} is dropping below $t_{\text{OCP1maxbl}\%}$.

The associated peak current setting at CS pin can be calculated with [Equation 15](#) and [Equation 16](#):

CRM operation

$$V_{\text{CSOCP1max}} = I_{\text{SETOCP1max}\%} \times I_{\text{SETnom}\%} \times V_{\text{CSOPmax}} + (I_{\text{MAGneg}}(\text{Vin}) \times R_{\text{shunt}})$$

Equation 57

ZV-RVS operation

²⁸⁾ configurable, see [Table 16](#)

²⁹⁾ configurable, see [Table 16](#)

Functional description

$$V_{CSOCP1max} = \frac{t_{HBperiodx}}{t_{HBperiod}} \times [I_{SETOCP1max\%} \times I_{SETnom\%} \times V_{CSOPmax} + (I_{MAGneg}(Vin) \times R_{Shunt})]$$

Equation 58

The associated feedback voltage at *FB* pin can be calculated with [Equation 13](#):

$$V_{FBOCP1max} = I_{SETOCP1max\%} \times I_{SETnom\%} \times V_{FBOPmax} + V_{FBOPmin}$$

Equation 59

3.4.7.4 Primary peak overcurrent protection OCP2 (OCP2)

V_{CSOCP2} is a fixed threshold at *CS* pin and beyond the maximum operating range $V_{CSOPmax}$. The OCP2 function is not blanked during the leading edge blanking time t_{HSLeb} . Once exceeded the latch mode is entered as default.

3.4.8 Vout voltage protection

The IC provides 2 output voltage *Vout* protection threshold levels V_{ZCDUVP} (*VoutUVP*, see [Chapter 3.4.8.1](#)) and V_{ZCDOVP} (*VoutOVP*, see [Chapter 3.4.8.2](#)) to ensure a reliable operation within a defined *Vout* operating range. The measurement is done via the reflected voltage at the auxiliary winding of the transformer during the demagnetization phase when the LS switch is turned on (see [Figure 19](#)). Furthermore the zero-crossing detection during start-up phase is observed to detect short circuit conditions at the output (*VoutSCP*, see [Chapter 3.4.8.3](#)).

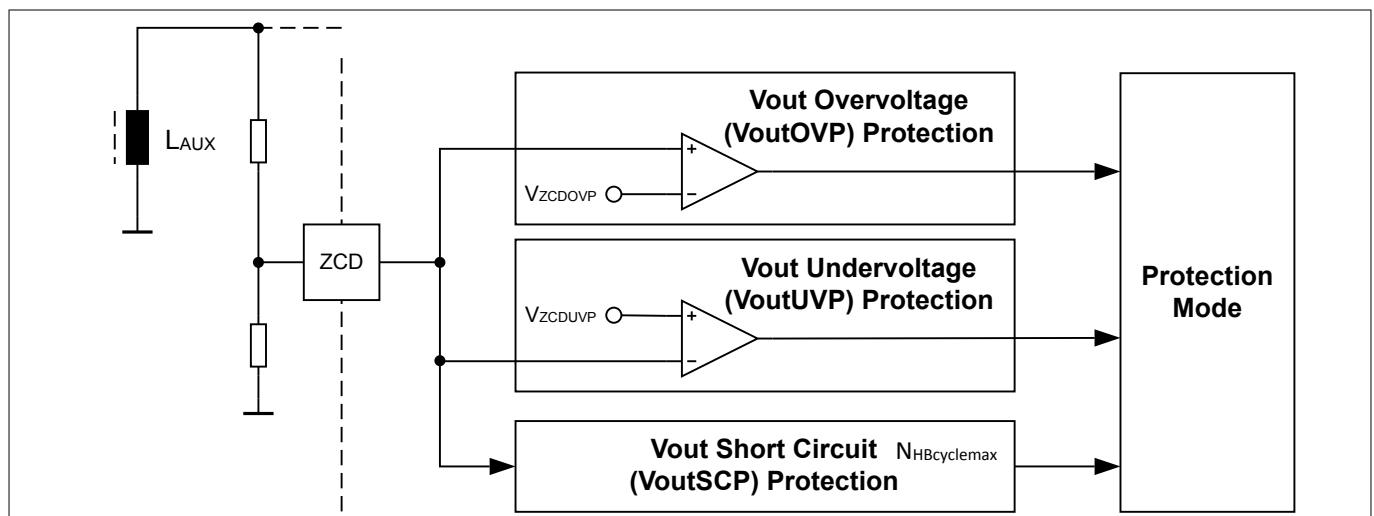


Figure 45

3.4.8.1 Vout undervoltage protection (VoutUVP)

Vout undervoltage is detected when the reflected output voltage measured via *ZCD* pin is dropping below the threshold V_{ZCDUVP} ³⁰⁾. Once detected the auto-restart mode is immediately triggered. *VoutUVP* can be disabled during burst mode operation by means of $EN_{BMVoutUVP}$ ³⁰⁾.

³⁰⁾ configurable, see [Table 15](#)

Functional description

3.4.8.2 Vout overvoltage protection (VoutOVP)

Vout overvoltage is detected when the reflected output voltage measured via ZCD pin is exceeding the threshold V_{ZCDOVP} ³¹⁾. Once detected a protection mode is immediately triggered. The default reaction is set to latch mode and can be changed to auto-restart mode with EV_{ZCDOVP} ³¹⁾.

3.4.8.3 Vout short circuit protection (VoutSCP)

The Vout short circuit protection is only active during start-up phase in order to limit the number of half-bridge switching cycles during the auto-restart. When operating under short circuit condition at the output the magnitude of reflected voltage is too low, which inhibits a proper zero-crossing detection at ZCD pin. After start-up request only a maximum of $N_{HBcyclemax}$ ³²⁾ consecutive half-bridge switching cycles without zero-crossing detection are allowed. If $N_{HBcyclemax}$ is exceeded the restart phase is stopped and auto-restart mode sleeping phase is prematurely entered.

3.4.9 External overtemperature protection (extOTP)

The external overtemperature protection is based on measuring an external NTC resistor. The external NTC is biased by the internal VREF supply via the internal pull-up resistor R_{MFIOpu} . The voltage at MFIO pin is measured and taken for calculation of the external resistor connected to MFIO pin. The calculated resistor is then compared with 2 resistor thresholds. When the external resistor R_{EXT} is falling below the threshold $R_{MFIOOTPre}$ ³³⁾ auto-restart mode is entered. An auto-restart cycle can only take place if R_{EXT} value is exceeding the threshold $R_{MFIOOTPre}$. The auto-restart cycles after being triggered with an external overtemperature event are counted. When the number of external OTP events exceeds the threshold $N_{OTPeVmax}$ ³³⁾ latch mode is entered, which can be only released by VCC dropping below V_{VCCoff} .

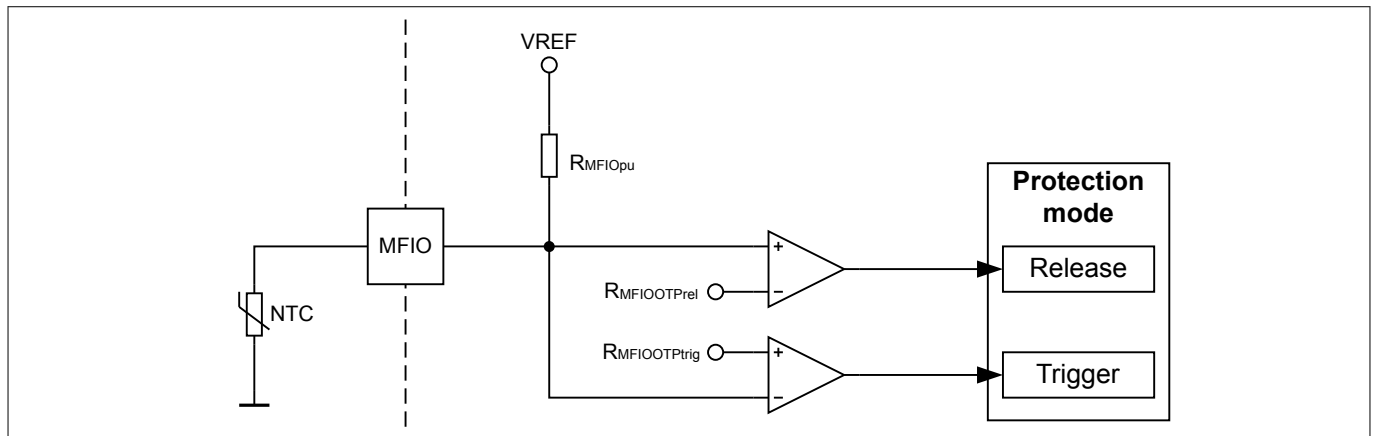


Figure 46

3.4.10 Watchdog timer

A watchdog timer is observing the internal control procedure by being continuously reset within a set time period. Once the timer is not reset in time a protection mode is entered, which is determined by the parameter EV_{WDOG} ³⁴⁾.

31 configurable, see [Table 15](#)
 32 configurable, see [Table 11](#)
 33 configurable, see [Table 17](#)
 34 configurable see [Table 18](#)

Configuration

4 Configuration

The configuration of XDPS2201 is supported by the GUI tool .dp Vision provided by Infineon. This chapter gives an overview about the configurable parameters, which are programmable via the UART interface at MFIO pin. [Chapter 4.1](#) shows the relationship between the parameter symbols described in the functional description and the parameter names shown in .dp Vision GUI tool. Furthermore the associated tolerance classes are assigned to the configurable typical parameters, which can be found in [Chapter 4.2](#).

4.1 Configurable parameters and functions

The following tables show the IC configurable parameters and their default programmed values, which some of them are either derived from or being configurable system parameters defined in XDP™ Vision tool.

4.1.1 System settings

Table 5 System settings

| Symbol | Description | Value | Unit | Tol.-Class | Chapter |
|--------------|---|--------|------|------------|-------------------------------|
| N | Transformer turns ratio of primary winding N_p and secondary winding N_s , defined by N_p/N_s | 2.83 | — | — | Chapter 3.4.6 |
| k_{RVS} | Ratio of resistor divider connected at VS pin and bulk voltage | 168.25 | — | — | |
| V_{outnom} | Maximal nominal regulated output voltage | 20 | V | — | |
| I_{outnom} | Maximal nominal output current without over-current condition | 3.25 | A | — | |

4.1.2 Dimensioning

Table 6 Dimensioning for output current control

| Symbol | Description | Value | Unit | Tol.-Class | Chapter |
|----------------------|--|--------|------|------------|---------------------------------|
| $I_{MAGnegnom}\%$ | Nominal negative magnetizing current level in percentage in relation to $I_{outnom} \times 2/N$ | 17.4 | % | — | Chapter 3.3.1 |
| $I_{MAGnegmaxCRM}\%$ | Maximum negative magnetizing current level in percentage in relation to $I_{outnom} \times 2/N$ required to achieve ZVS at maximum input voltage V_{in} during CRM operation | 31.6 | % | — | |
| $I_{MAGnegmaxRVS}\%$ | Maximum negative magnetizing current level in percentage in relation to $I_{outnom} \times 2/N$ required to achieve ZVS at maximum input voltage V_{in} during ZV-RVS mode operation | 39.5 | % | — | |
| $I_{MAGposRVS0V}\%$ | Minimum peak current setting determined by $I_{MAGposRVS}$ for $V_{out} = 0V$ in percentage in relation to $I_{MAGposnom}$ | 75 | % | — | Chapter 3.3.2.1 |
| V_{ZCDnom} | ZCD pin nominal voltage during LS switch turn-on at V_{outnom} ³⁵⁾ | 1.3984 | V | TC_V3a | Chapter 3.3.1.2 |

Configuration

Table 6 Dimensioning for output current control (continued)

| Symbol | Description | Value | Unit | Tol.-Class | Chapter |
|--------------------|--|-------|---------|------------|---------|
| $t_{TRANSnom}$ | Minimum LS switch on-time during energy transfer at V_{outnom} | 2.8 | μs | TC_T1 | |
| $t_{TRANSRVS0V\%}$ | Representing the value t_{TRANS} in RVS mode for $V_{out} = 0V$ in percentage in relation to $t_{TRANSnom}$ for t_{TRANS} modulation depending on output voltage measured via ZCD pin. | 166 | % | — | |

4.1.3 Half-bridge

Table 7 Half-bridge timings

| Symbol | Description | Value | Unit | Tol.-Class | Chapter |
|-------------------|--|-------|------|------------|---------------------------------|
| $t_{LS2ZCDnom}$ | Target time delay target for LS pulse falling edge to ZCD pulse falling edge at minimum V_{in} | 650 | ns | TC_T1 | Chapter 3.3.2.1 |
| $t_{LS2ZCDmin}$ | Target time delay target for LS pulse falling edge to ZCD pulse falling edge at maximum V_{in} | 234 | ns | — | |
| t_{deadLS} | Dead-time between HS pulse falling edge and LS pulse rising edge | 150 | ns | TC_T1 | |
| $t_{ZCDrefilCRM}$ | Time delay between falling edge ZCD and HS pulse rising edge in CRM operation | 172 | ns | TC_T1 | |
| t_{HSleb} | HS switch leading edge blanking (LEB) determining minimum on-time | 300 | ns | TC_T1 | |

Table 8 Half-bridge timings only for ZV-RVS mode

| Symbol | Description | Value | Unit | Tol.-Class | Chapter |
|-------------------|--|-------|------|------------|-----------------------------------|
| $t_{deadHSRVS}$ | Dead-time between LS (ZVS pulse) falling edge and HS pulse rising edge in ZV-RVS mode | 400 | ns | TC_T1 | Chapter 3.3.2.2 |
| t_{ZVSmin} | Minimum ZVS pulse width during ZV-RVS mode operation | 600 | ns | TC_T1 | |
| $t_{ZCDrefilRVS}$ | Filtering time between ZCD pulse rising edge and HS pulse rising edge in ZV-RVS mode operation | 410 | ns | TC_T1 | |
| $t_{ZCDrefilRVS}$ | Filtering time for ZCD pulse falling edge for valley detection in ZV-RVS mode operation | 210 | ns | TC_T1 | Chapter 3.3.2.2.1 |

³⁵ for wide output voltage range

Configuration

4.1.4 ZV-RVS/DCM operation

Table 9 Transition between ZV-RVS mode and DCM operation

| Symbol | Description | Value | Unit | Tol.-Class | Chapter |
|-----------------|--|---------|------|------------|---------------------------------|
| EN_{DCM} | Enable for DCM operation (when maximum valley in RVS operation is reached) | Enabled | — | n.a. | Chapter 3.3.2.3 |
| F_{DCMmin} | Minimum switching frequency limit during DCM operation | 20 | kHz | TC_T1 | |
| $N_{RVSvalmax}$ | Maximum number of valleys during ZV-RVS operation | 10 | — | n.a. | Chapter 3.3.2.4 |

4.1.5 Burst

Table 10 Burst mode operation

| Symbol | Description | Value | Unit | Tol.-Class | Chapter |
|--------------------|---|---------|------|------------|---------------------------------|
| $I_{SETBMen\%}$ | Burst mode entry current set-point in percentage of nominal set-point | 4 | % | — | Chapter 3.3.4.1 |
| $I_{SETBMex\%}$ | Burst mode exit current set-point in percentage of nominal set-point | 15 | % | — | Chapter 3.3.4.1 |
| $N_{BMexreqthr}$ | Number of burst frames with average current level higher than $I_{SETBMex\%}$ to leave burst mode | 3 | — | — | |
| $V_{FBMfastex}$ | FB pin fast burst mode exit threshold | 1.82 | V | TC_V4 | Chapter 3.3.4.2 |
| $EN_{BMfastexCRM}$ | Allow for CRM operation directly after burst mode fast exit. If disabled, ZV-RVS mode is first used after burst mode fast exit. | Enabled | — | — | |
| $t_{BMprepulse}$ | Pulse width to precharge the bootstrap capacitor after a pause longer than $t_{BMslpthrpp}$ | 1.3 | μs | TC_T1 | Chapter 3.3.4.3 |
| $t_{BMslpthrpp}$ | Burst pause time threshold for enabling precharge pulse | 1.0 | ms | TC_T2 | |

4.1.6 Start-up

Table 11 Start-up operation

| Symbol | Description | Value | Unit | Tol.-Class | Chapter |
|------------------|---|-------|------|------------|---------------------------------|
| V_{VSBIp} | VS pin threshold for input voltage V_{in} brown-in protection | 0.737 | V | TC_V1b | Chapter 3.4.4.1 |
| $I_{SETstmax\%}$ | Maximum target current set-point during start-up phase in percentage of nominal set-point | 140 | % | — | Chapter 3.3.3 |
| $t_{startramp}$ | Output voltage ramp-up target time period during start-up phase ³⁶⁾ | 12 | ms | TC_T1 | |

Configuration

Table 11 Start-up operation (continued)

| Symbol | Description | Value | Unit | Tol.-Class | Chapter |
|------------------|---|-------|---------|------------|---------|
| $N_{HBcyclemax}$ | Maximum number of allowed half-bridge switching cycles without subsequent zero-crossing detection (ZCD) during ZCD search phase at V_{out} start-up | 150 | — | — | |
| $t_{startzcdto}$ | Maximum time period without zero-crossing detection for generating next pulse ³⁷⁾ only during ZCD search phase | 70 | μs | TC_T1 | |
| $t_{ZVSst1st}$ | Very first ZVS pulse initial length at to precharge the HS bootstrap capacitor | 7 | μs | TC_T1 | |

4.1.7 Protections

Table 12 Auto-restart mode [ARM]

| Symbol | Description | Value | Unit | Tol.-Class | Chapter |
|--------------|---|-------|------|------------|-------------------------------|
| t_{ARMslp} | Approximated auto-restart mode sleep time period ³⁸⁾ | 3.0 | s | TC_T2 | Chapter 3.4.1 |

Table 13 Input voltage V_{in} protection at VS pin

| Symbol | Description | Value | Unit | Tol.-Class | Chapter |
|--------------|---|-------|------|------------|---------------------------------|
| V_{VSSBOP} | VS pin threshold for input voltage V_{in} slow brown-out protection | 0.713 | V | TC_V1b | Chapter 3.4.4.3 |
| V_{VSFBOP} | VS pin threshold for input voltage V_{in} fast brown-out protection | 0.392 | V | TC_V1b | Chapter 3.4.4.2 |
| V_{VSOVP} | VS pin threshold for input voltage V_{in} overvoltage protection | 2.270 | V | TC_V1b | Chapter 3.4.4.4 |

Table 14 Start-up timeout protection

| Symbol | Description | Value | Unit | Tol.-Class | Chapter |
|---------------|---|-------|------|------------|-------------------------------|
| $t_{startto}$ | Maximum allowed start-up time until start drop of feedback voltage ³⁶⁾ | 48 | ms | TC_T3 | Chapter 3.3.3 |

³⁶⁾ based on $t_{SLWTASK}$, see [Table 35](#)

³⁷⁾ based on t_{MCLK} , see [Table 35](#)

³⁸⁾ based on $t_{ARMbase}$, see [Table 35](#)

Configuration

Table 15 **Vout voltage protection**

| Symbol | Description | Value | Unit | Tol.-Class | Chapter |
|------------------|--|--------|------|------------|---------------------------------|
| V_{ZCDUVP} | ZCD pin undervoltage protection threshold for output voltage | 0.220 | V | TC_V3b | Chapter 3.4.8.1 |
| $EN_{BMVoutUVP}$ | Activation of V_{out} UVP in burst mode operation | Enable | — | — | |
| EV_{ZCDOVP} | Reaction event for ZCD pin overvoltage detection | Latch | — | — | Chapter 3.4.8.2 |

Table 16 **Overcurrent protection**

| Symbol | Description | Value | Unit | Tol.-Class | Chapter |
|---------------------|--|-------|------|------------|---------------------------------|
| $I_{SETOCP1lev1\%}$ | Current set-point threshold in percentage of nominal set-point for OCP1 overcurrent protection level 1 | 125 | % | — | Chapter 3.4.7.1 |
| $t_{OCP1lev1bl}$ | OCP1 overcurrent protection level 1 blanking time ³⁹⁾ | 12 | s | TC_T4 | |
| $I_{SETOCP1lev2\%}$ | Current set-point threshold in percentage of nominal set-point for OCP1 overcurrent protection level 2 | 140 | % | — | Chapter 3.4.7.2 |
| $t_{OCP1lev2bl}$ | OCP1 overcurrent protection level 2 blanking time ³⁶⁾ | 1000 | ms | TC_T3 | |
| $I_{SETOCP1max\%}$ | Current set-point in percentage of nominal set-point for OCP1 maximum current limitation | 160 | % | — | Chapter 3.4.7.3 |
| $t_{OCP1maxbl}$ | OCP1 maximum current limitation blanking time ³⁶⁾ | 6 | ms | TC_T3 | |
| EV_{CSOCP2} | Reaction on exceeding OCP2 overcurrent threshold | Latch | — | — | |

Table 17 **Overtemperature protection**

| Symbol | Description | Value | Unit | Tol.-Class | Chapter |
|-------------------|--|-------|------------|------------|-------------------------------|
| $R_{MFIOOTptrig}$ | MFIO pin external overtemperature protection trigger resistor threshold | 7.7 | k Ω | TC_R1 | Chapter 3.4.9 |
| $R_{MFIOOTprel}$ | MFIO pin external overtemperature protection release resistor threshold | 51.4 | k Ω | TC_R2 | |
| $N_{OTPeVmax}$ | MFIO pin external overtemperature protection number of allowed triggered events before entering latch mode | 2 | — | — | |

³⁹⁾ based on $t_{VSLWTASK}$, see [Table 35](#)

³⁶⁾ based on $t_{SLWTASK}$, see [Table 35](#)

Configuration

Table 18 Watchdog timer

| Symbol | Description | Value | Unit | Tol.-Class | Chapter |
|----------------|---|--------------|------|------------|--------------------------------|
| $E_{V_{WDOG}}$ | Reaction if watchdog timer is not reset in time | Auto-restart | — | — | Chapter 3.4.10 |

4.1.8 Mode thresholds

Table 19 CRM and ZV-RVS mode thresholds

| Symbol | Description | Value | Unit | Tol.-Class | Chapter |
|--------------------|---|-------|------|------------|---------------------------------|
| $I_{SETRVS2CRM\%}$ | Current set-point threshold in percentage of nominal set-point for switching over from ZV-RVS mode to CRM | 70 | % | — | Chapter 3.3.2.4 |
| $I_{SETCRM2RVS\%}$ | Current set-point threshold in percentage of nominal set-point for switching over from CRM to ZV-RVS mode | 50 | % | — | |
| $V_{ZCDRVS2CRM}$ | ZCD pin threshold for switching over from ZV-RVS mode to CRM | 0.81 | V | TC_V3a | |
| $V_{ZCDCRM2RVS}$ | ZCD pin threshold for switching over from CRM to ZV-RVS mode | 0.74 | V | TC_V3a | |

4.1.9 Jitter

Table 20 Frequency Jitter

| Symbol | Description | Value | Unit | Tol.-Class | Chapter |
|----------------------|---|-------|------|------------|-------------------------------|
| $V_{VSJitteren}$ | VS pin Input voltage V_{in} jitter enable threshold | 1.486 | V | TC_V1a | Chapter 3.3.5 |
| $d_{Jitterspread\%}$ | Frequency jitter spread on a percentage base of switching frequency | 10 | % | TC_T1 | |
| $t_{Jitterstpdel}$ | Time delay for next frequency jitter step based on time period ³⁶⁾ | 1.3 | ms | TC_T1 | |

4.1.10 Others

Table 21 Propagation delay compensation (PDC)

| Symbol | Description | Value | Unit | Tol.-Class | Chapter |
|-----------|--|-------|------|------------|---------------------------------|
| t_{PDC} | Total propagation delay period to compensate OCP1 peak current control | 200 | ns | — | Chapter 3.3.1.4 |

³⁶⁾ based on $t_{SLWTASK}$, see [Table 35](#)

Configuration

4.2 Tolerance classes for configurable parameters

The are several configurable parameters for voltages, currents, timings, and frequencies and temperatures available, which are correlated with different tolerance ranges. The configurable parameters can be clustered based on the associated hardware peripheral. This clustering is done by means of tolerance classes, which are assigned to each configurable parameter. Parameters defining events, configuration registers, digital numbers or constants are not assigned to tolerance ranges.

The available tolerance classes are named with TC_xxx and listed in the following [Table 22](#). Described is how minimum and maximum tolerance values can be derived for the typical value X_{typ} of the configurable parameters.

Table 22 Tolerance classes

| Tol.-Class | Description | Min. value | Max. value |
|------------|--|--------------------------------------|--------------------------------------|
| TC_T1 | Timing parameter below 1215ns ⁴⁰⁾ | $t_{typ} \times 0.95 - 15.8ns$ | $t_{typ} \times 1.05 + 15.8ns$ |
| | Timing parameter above 1215ns ⁴⁰⁾ | $t_{typ} \times 0.937$ | $t_{typ} \times 1.063$ |
| | Frequency parameter below 500kHz ⁴⁰⁾ | $F_{typ} \times 0.937$ | $F_{typ} \times 1.063$ |
| TC_T2 | Timing parameter based on stand-by clock ⁴¹⁾ | $t_{typ} \times 0.90$ | $t_{typ} \times 1.12$ |
| TC_T3 | Timing parameter (integer multiple of 0.1ms) based on slow task period ⁴²⁾ | $t_{typ} \times 0.937 - 0.11ms$ | $t_{typ} \times 1.063 + 0.11ms$ |
| TC_T4 | Timing parameter (integer multiple of 5ms) based on very slow task period ⁴³⁾ | $t_{typ} \times 0.937 - 5.5ms$ | $t_{typ} \times 1.063 + 5.5ms$ |
| TC_V1a | Voltage threshold at pin VS | $(V_{VStyp} \times 0.994) - 0.099V$ | $(V_{VStyp} \times 1.006) + 0.099V$ |
| TC_V1b | Voltage threshold at pin VS | $(V_{VStyp} \times 0.994) - 0.040V$ | $(V_{VStyp} \times 1.006) + 0.040V$ |
| TC_V2 | Voltage threshold for OCP1 comparator at pin CS | $V_{CSOCP1typ} - 0.034V$ | $V_{CSOCP1typ} + 0.034V$ |
| TC_V3a | Voltage threshold at pin ZCD | $(V_{ZCDtyp} \times 0.995) - 0.091V$ | $(V_{ZCDtyp} \times 1.005) + 0.091V$ |
| TC_V3b | Voltage threshold at pin ZCD | $(V_{ZCDtyp} \times 0.995) - 0.024V$ | $(V_{ZCDtyp} \times 1.005) + 0.024V$ |
| TC_V4 | Voltage threshold at pin FB | $(V_{FBtyp} \times 0.984) - 0.084V$ | $(V_{FBtyp} \times 1.016) + 0.084V$ |
| TC_R1 | Range 1 for resistor threshold at pin MFIO | see Figure 47 | see Figure 47 |
| TC_R2 | Range 2 for resistor threshold at pin MFIO | see Figure 48 | see Figure 48 |

⁴⁰⁾ based on main clock $t_{MCLK} = 15.8ns(typ.)$

⁴¹⁾ $t_{STBCLK} = 10\mu s(typ.)$

⁴²⁾ $t_{SLWTASK} = 0.1ms (typ.)$

⁴³⁾ $t_{VSLWTASK} = 5ms (typ.)$

Configuration

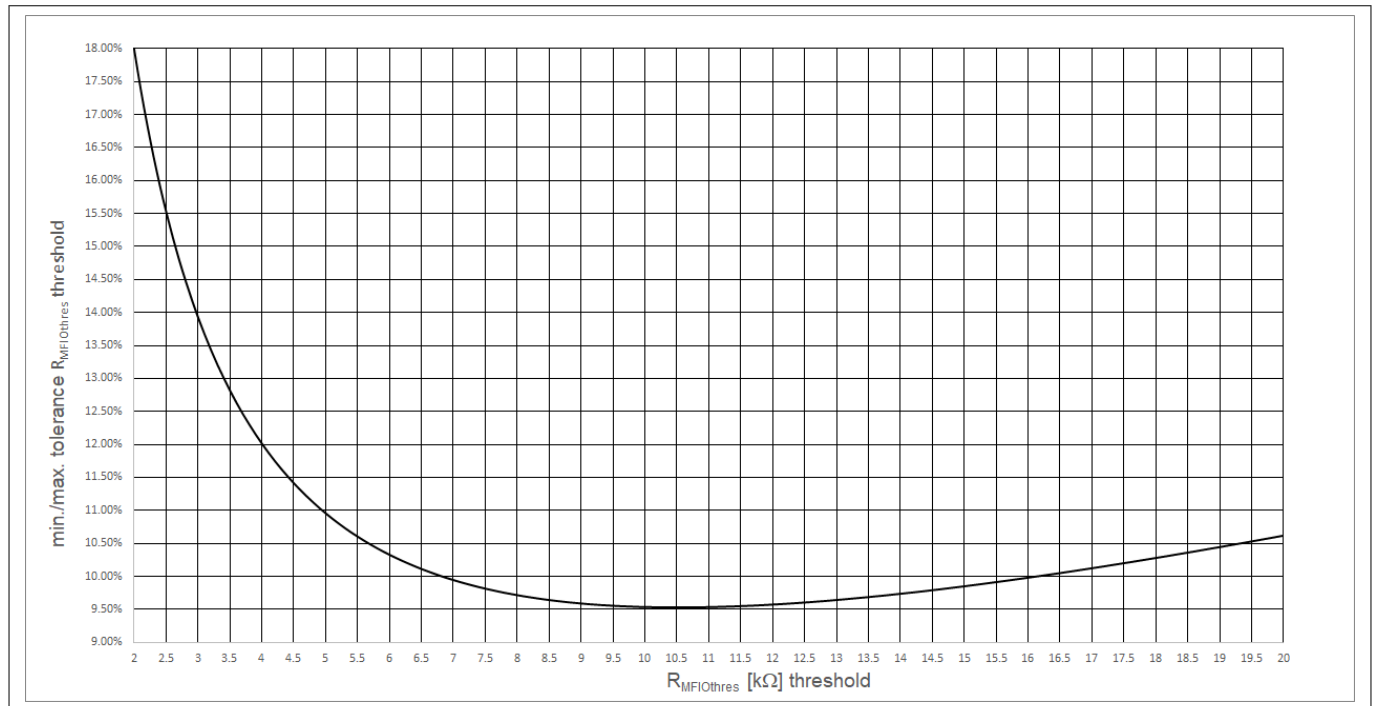


Figure 47 Tolerance class TC_R1 for resistor threshold $R_{MFIOthres}$ at pin MFIO

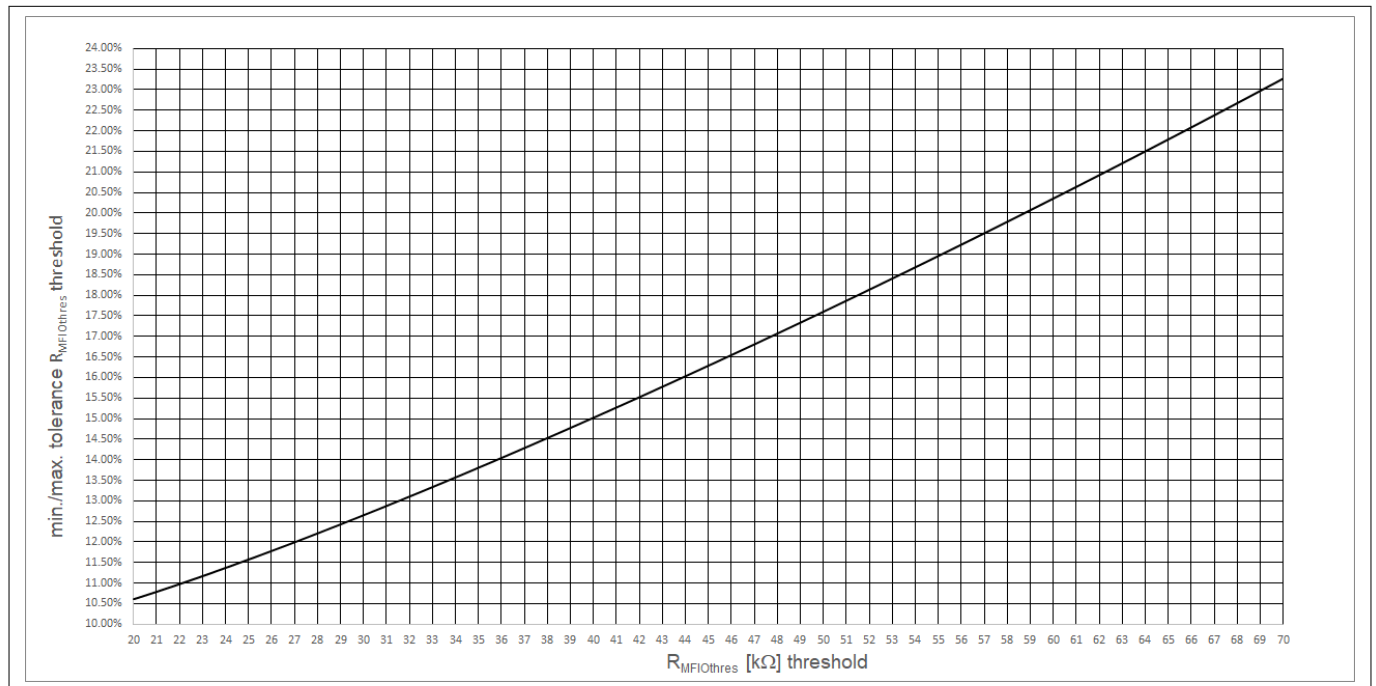


Figure 48 Tolerance class TC_R2 for resistor threshold $R_{MFIOthres}$ at pin MFIO

Electrical characteristics

5 Electrical characteristics

All signals are measured with respect to ground pin *GND*, except the high-side signals at pins *HSVCC* and *HSGD*, which are measured with respect to pin *HSGND*. The voltage levels are valid if other ratings are not violated.

5.1 Definitions

Figure 49 illustrates the definition for the voltage and current parameters used in this data sheet.

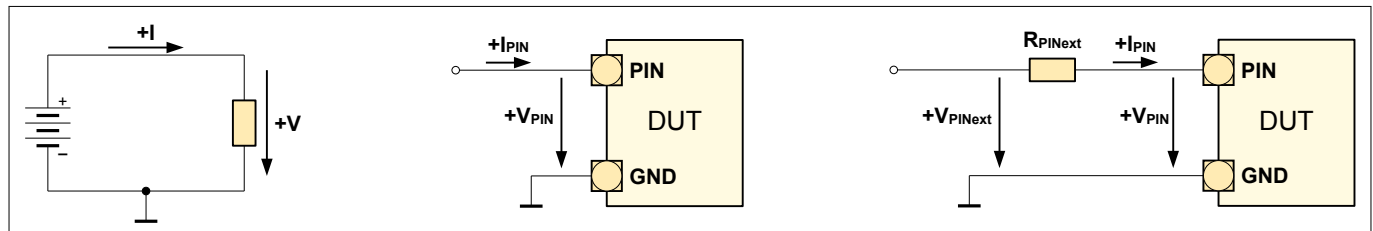


Figure 49 Voltage and current definitions

Values indicated under “absolute maximum ratings” must not be exceeded.

Values indicated under “operating conditions” can be exceeded if a corresponding explicit “absolute maximum rating” is given for this parameter, but the related function of the device is not ensured.

5.2 Absolute maximum ratings

Attention: Stresses above the values listed below may cause permanent damage to the device. Exposure to absolute maximum rating conditions for extended periods may affect device reliability. Maximum ratings are absolute ratings; exceeding only one of these values may cause irreversible damage to the integrated circuit. These values are not tested during production test. For the same reason make sure that any capacitors that will be connected to pins *VCC* and *HSVCC* are discharged before assembling the application circuit.

Table 23 Absolute maximum ratings

| Parameter | Symbol | Limit values | | Unit | Remarks |
|--|-------------------|--------------|------|------|---------------|
| | | Min. | Max. | | |
| Voltage at pin <i>HV</i> | V_{HV} | -0.3 | 600 | V | 44) |
| Current into pin <i>HV</i> | I_{HV} | — | 10 | mA | 44) |
| Voltage at pin <i>VCC</i> | V_{VCC} | -0.5 | 26 | V | 44) |
| Voltage at pin <i>MFIO</i> | V_{MFIO} | -0.5 | 3.6 | V | 44) |
| Voltage at pin <i>VS</i> | V_{VS} | -0.5 | 3.6 | V | 44) |
| Voltage at pin <i>FB</i> | V_{FB} | -0.5 | 3.6 | V | 44) |
| Voltage at pin <i>ZCD</i> | V_{ZCD} | -0.5 | 3.6 | V | 44) |
| Maximum negative transient voltage at pin <i>ZCD</i> | $-V_{ZCDN_TR}$ | — | 1.5 | V | pulse < 500ns |
| Maximum permanent negative clamping current for pin <i>ZCD</i> | $-I_{ZCDCLN_DC}$ | — | 2.5 | mA | RMS |

44 Permanently applied as DC value.

Electrical characteristics

Table 23 Absolute maximum ratings (continued)

| Parameter | Symbol | Limit values | | Unit | Remarks |
|---|-------------------|--------------|-----------------|------|--|
| | | Min. | Max. | | |
| Maximum transient negative clamping current for pin ZCD | $-I_{ZCDCLN_TR}$ | — | 10 | mA | pulse < 500ns |
| Voltage at pin CS | V_{CS} | -0.5 | 3.6 | V | ⁴⁴⁾ |
| Maximum negative transient voltage at pin CS | $-V_{CSN_TR}$ | — | 3.0 | V | pulse < 500ns |
| Maximum permanent negative clamping current for pin CS | $-I_{CSCLN_DC}$ | — | 2.5 | mA | RMS |
| Maximum transient negative clamping current for pin CS | $-I_{CSCLN_TR}$ | — | 10 | mA | pulse < 500ns |
| Maximum permanent positive clamping current for pin CS | I_{CSCLP_DC} | — | 2.5 | mA | RMS |
| Maximum transient positive clamping current for pin CS | I_{CSCLP_TR} | — | 10 | mA | pulse < 500ns |
| Voltage at pin LSGD | V_{LSGD} | -0.5 | $V_{VCC}+0.3$ | V | Limited by internal clamping |
| Voltage at pin HSGND | V_{HSGND} | -650 | 650 | V | referred to GND |
| Voltage at pin HSVCC | V_{HSVCC} | -0.5 | 26 | V | referred to HSGND |
| Voltage at pin HSGD | V_{HSGD} | -0.5 | $V_{HSVCC}+0.3$ | V | referred to HSGND |
| Slew-rate for floating high-side domain | dV_{HS}/dt | -50 | 50 | V/ns | |
| Junction operation temperature | T_J | -40 | 125 | °C | |
| Storage temperature | T_S | -55 | 150 | °C | |
| Maximum power dissipation | P_{TOT} | — | 0.63 | W | $T_A = 50\text{ °C}$, $T_J = 125\text{ °C}$, $R_{thJA} = 119\text{ K/W}$ |
| Soldering temperature | T_{Sold} | — | 260 | °C | ⁴⁵⁾ Wave soldering |
| ESD capability | V_{HBM} | — | 1500 | V | ⁴⁶⁾ Human body model |
| | V_{CDM} | — | 500 | V | ⁴⁷⁾ Charged device model |
| Latch-up capability | I_{LU} | — | 150 | mA | ⁴⁸⁾ Pin voltages acc. to abs. max. ratings |

⁴⁴ Permanently applied as DC value.

⁴⁵ According to JESD22-A111

⁴⁶ According to ANSI/ESDA/JEDEC JS-001

⁴⁷ According to JESD22-C101

⁴⁸ According to JESD78, 85 °C (Class II) temperature

Electrical characteristics

5.3 Package characteristics

Table 24 Package characteristics

| Parameter | Symbol | Values | | Unit | Remarks |
|--|------------|--------|------|------|--------------------------|
| | | Min. | Max. | | |
| Thermal resistance from junction to ambient | R_{thJA} | — | 119 | K/W | PG-DSO-14, JEDEC 1s0p |
| Creepage distance between HV and HSxxx pins vs. GND-related pins | D_{CR} | 2.1 | — | mm | |

5.4 Operating range

Table 25 shows the recommended operating range.

Table 25 Operating conditions

| Parameter | Symbol | Limit values | | Unit | Remarks |
|---|-----------------|--------------|-------------------|------|---|
| | | Min. | Max. | | |
| Junction operation temperature | T_J | -25 | 125 | °C | |
| Voltage at pin <i>HV</i> | V_{HV} | -0.3 | 600 | V | |
| External voltage at pin <i>VCC</i> | V_{VCC} | 11 | 24 | V | Max. value needs to consider internal power losses |
| Voltage at pin <i>MFIO</i> | V_{MFIO} | -0.3 | 3.3 | V | |
| Voltage at pin <i>FB</i> | V_{FB} | -0.3 | 3.3 | V | |
| Voltage at pin <i>ZCD</i> | V_{ZCD} | -0.3 | 3.3 | V | |
| Voltage at pin <i>CS</i> | V_{CS} | -0.3 | 3.3 | V | |
| Voltage at pin <i>LSGD</i> | V_{LSGD} | -0.3 | $V_{VCC} + 0.3$ | V | Internally clamped at $V_{LSGDhigh}$ |
| Low state output reverse current at pin <i>LSGD</i> | $-I_{LSGDLREV}$ | — | 100 | mA | ⁴⁹⁾ Applies if $V_{LSGD} < 0\text{ V}$ and driver at low state |
| Voltage at pin <i>HSGD</i> | V_{HSGD} | -0.3 | $V_{HSVCC} + 0.3$ | V | Internally clamped at $V_{HSGDhigh}$ |
| Low state output reverse current at pin <i>HSGD</i> | $-I_{HSGDLREV}$ | — | 100 | mA | ⁴⁹⁾ Applies if $V_{HSGD} < 0\text{ V}$ and driver at low state |
| Voltage at pin <i>HSVCC</i> | V_{HSVCC} | 10 | 24 | V | Referred to <i>HSGND</i> |
| Voltage at pin <i>HSGND</i> | V_{HSGND} | -0.3 | 600 | V | |
| UART Baudrate at pin <i>MFIO</i> | t_{BD} | 10k | 115k | Bd | |

⁴⁹⁾ Assured by design.

Electrical characteristics

5.5 DC electrical characteristics

The electrical characteristics involve the spread of values given within the specified supply voltage and junction temperature range T_J from $-25\text{ }^\circ\text{C}$ to $125\text{ }^\circ\text{C}$. Typical values represent the median values related to $T_J = 25\text{ }^\circ\text{C}$. All voltages refer to *GND*, *HSGND* and the assumed supply voltage is $V_{VCC} = 12\text{ V}$ and $V_{HSVCC} = 12\text{ V}$, if not otherwise mentioned.

The following characteristics are specified:

- Pin *HV* (Table 26)
- Pin *VCC* (Table 27)
- Floating HS domain (Table 28)
- Pin *LSGD* (Table 29)
- Pin *VS* (Table 30)
- Pin *CS* (Table 31)
- Pin *FB* (Table 32)
- Pin *MFIO* (Table 33)
- Pin *ZCD* (Table 34)
- Central control functions (Table 35)

Table 26 Electrical characteristics of Pin *HV*

| Parameter | Symbol | Values | | | Unit | Note or test condition |
|---------------------------------------|-------------------|--------|------|------|---------------|---|
| | | Min. | Typ. | Max. | | |
| HV peak VCC charge current capability | $I_{HVchargeVCC}$ | 2.4 | 5.0 | 7.5 | mA | ⁵⁰⁾ $V_{VCC} = 1\text{ V}$, $V_{HV} = 30\text{ V}$ |
| Leakage current at HV pin | I_{HVLK} | — | — | 10 | μA | $V_{HV} = 600\text{ V}$, HV start-up cell disabled |

Table 27 Electrical characteristics of Pin *VCC*

| Parameter | Symbol | Values | | | Unit | Note or test condition |
|---|------------------|--------|-------|-------|---------------|--|
| | | Min. | Typ. | Max. | | |
| VCC turn-on threshold | V_{VCCon} | 19.0 | 20.5 | 22.0 | V | Rising slope |
| VCC turn-off threshold | V_{VCCoff} | 7.98 | 8.40 | 8.82 | V | Falling slope |
| VCC threshold for turning on the HV start-up cell during sleep mode | $V_{VCCslpHVon}$ | 9.97 | 10.50 | 11.03 | V | Falling slope |
| VCC UVOFF current | $I_{VCCUVOFF}$ | — | 20 | 40 | μA | $V_{VCC} < V_{VCCoff(min)} - 0.3\text{ V}$ |
| VCC operating current | I_{VCCop} | — | 11.0 | 14.5 | mA | Without gate driver gate charge losses and during brown-in phase |
| VCC quiescent current during burst mode power saving-phase | $I_{VCCBpsm0}$ | — | 0.7 | 3.4 | mA | Burst mode entered; pin <i>MFIO</i> and <i>FB</i> open |
| | | — | — | 1.5 | mA | as for $I_{VCCBpsm0}$, $T_J = 85\text{ }^\circ\text{C}$ |

⁵⁰⁾ Max. peak charge current will be limited in the application by an external resistor connected to HV pin.

Electrical characteristics

Table 27 Electrical characteristics of Pin VCC (continued)

| Parameter | Symbol | Values | | | Unit | Note or test condition |
|---|-------------|--------|------|------|------|---|
| | | Min. | Typ. | Max. | | |
| VCC quiescent current during bang-bang mode | I_{VCCBB} | — | 0.32 | 0.58 | mA | Protection mode entered; pin <i>MFIO</i> and <i>FB</i> open |

Table 28 Electrical characteristics of Floating HS domain

| Parameter | Symbol | Values | | | Unit | Note or test condition |
|--|------------------|--------|------|------|---------------|---|
| | | Min. | Typ. | Max. | | |
| HSVCC turn-on threshold | $V_{HSVCCon}$ | 8.7 | 9.2 | 9.7 | V | Rising slope |
| HSVCC turn-off threshold | $V_{HSVCCoff}$ | 6.2 | 6.7 | 7.2 | V | Falling slope |
| HSVCC idle current | $I_{HSVCCidle}$ | — | 0.3 | 0.8 | mA | Without gate driver gate charge losses, $V_{HSVCC} = 14\text{ V}$ |
| HSGD enabling delay time after HSVCC voltage is exceeding $V_{HSVCCon(max)}$ | $t_{HSGDendel}$ | — | 2.3 | 4.1 | μs | $V_{HSVCC} = 11\text{ V}$ |
| HSGD voltage at high state | $V_{HSGDhigh}$ | 10 | 11 | 12 | V | $I_{HSGD} = -20\text{ mA}$ |
| | | 7 | — | — | V | $I_{HSGD} = -20\text{ mA}$, $V_{HSVCC} = 8\text{ V}$ |
| HSGD voltage at active shutdown | $V_{HSGDaSD}$ | — | 25 | 200 | mV | $I_{HSGD} = 20\text{ mA}$, $V_{HSVCC} = 5\text{ V}$ |
| HSGD peak source current | $-I_{HSGDpksrc}$ | 130 | — | — | mA | |
| HSGD peak sink current | $I_{HSGDpksnk}$ | 450 | — | — | mA | |

Table 29 Electrical characteristics of Pin LSGD

| Parameter | Symbol | Values | | | Unit | Note or test condition |
|---------------------------------|------------------|--------|------|------|------|---|
| | | Min. | Typ. | Max. | | |
| LSGD voltage at high state | $V_{LSGDhigh}$ | 9.9 | 10.5 | 11.1 | V | $I_{LSGD} = -20\text{ mA}$ |
| | | 7.5 | — | — | V | $I_{LSGD} = -20\text{ mA}$, $V_{VCC} = 8\text{ V}$ |
| LSGD voltage at active shutdown | $V_{LSGDaSD}$ | — | — | 1.6 | V | $I_{LSGD} = 5\text{ mA}$, $V_{VCC} = 5\text{ V}$ |
| LSGD peak source current | $-I_{LSGDpksrc}$ | — | 360 | — | mA | |
| LSGD peak sink current | $I_{LSGDpksnk}$ | 800 | — | — | mA | |

Table 30 Electrical characteristics of Pin VS

| Parameter | Symbol | Values | | | Unit | Note or test condition |
|-----------------------------------|---------------|--------|------|-----------|---------------|--------------------------------------|
| | | Min. | Typ. | Max. | | |
| VS leakage current | I_{VSlk} | -0.2 | — | 0.2 | μA | $0\text{ V} < V_{VS} < 2.9\text{ V}$ |
| VS dynamic voltage range | V_{VS} | 0 | — | V_{REF} | V | |
| VS brown-in detection time period | $t_{VSBldet}$ | — | 5.2 | — | ms | Brown-in phase |

Electrical characteristics

Table 30 Electrical characteristics of Pin VS (continued)

| Parameter | Symbol | Values | | | Unit | Note or test condition |
|---|----------------|--------|------|------|------|------------------------|
| | | Min. | Typ. | Max. | | |
| VS pin blanking time for input voltage V_{in} slow brown-out protection | $t_{VSSBOPbl}$ | 41.1 | 44.0 | 46.9 | ms | $V_{VS} < V_{VSSBOP}$ |

Table 31 Electrical characteristics of Pin CS

| Parameter | Symbol | Values | | | Unit | Note or test condition |
|---|----------------|--------|------|------|---------|---|
| | | Min. | Typ. | Max. | | |
| CS leakage current | I_{CSlk} | -10 | — | 10 | μA | $0 V < V_{CS} < 2.8 V$ |
| CS OCP1 maximum operating current range | $V_{CSOPmax}$ | 405 | 437 | 469 | mV | |
| CS OCP1 propagation delay | $t_{CSOCP1pd}$ | 121 | 213 | 305 | ns | input signal slope, $dV_{CS}/dt = 150 \text{ mV}/\mu s$ |
| CS OCP2 threshold | V_{CSOCP2} | 550 | 600 | 650 | mV | |
| CS OCP2 propagation delay | $t_{CSOCP2pd}$ | 125 | 135 | 190 | ns | $dV_{CS}/dt = 100 \text{ V}/\mu s$ |

Table 32 Electrical characteristics of Pin FB

| Parameter | Symbol | Values | | | Unit | Note or test condition |
|---|-----------------|--------|-------|-------|------------|-----------------------------------|
| | | Min. | Typ. | Max. | | |
| FB open circuit output voltage | V_{FBoc} | 3.04 | 3.20 | 3.36 | V | |
| FB pull-up resistor | R_{FBpu} | 24 | 30 | 36 | k Ω | |
| FB minimum operating range | $V_{FBOPmin}$ | 0.309 | 0.400 | 0.491 | V | |
| FB threshold maximum usable range | $V_{FBOPmax}$ | — | — | 2.428 | V | |
| FB burst mode wake-up and sleep control threshold | $V_{FBBMctrl}$ | 1.48 | 1.60 | 1.72 | V | During active phase in burst mode |
| | | 1.36 | 1.55 | 1.61 | V | During sleep phase in burst mode |
| FB burst mode wake-up delay | $t_{FBBMWKdel}$ | — | 25 | 31 | μs | Burst mode, rising slope |

Table 33 Electrical characteristics of Pin MFIO

| Parameter | Symbol | Values | | | Unit | Note or test condition |
|----------------------------------|--------------|--------|------------|------|------------|--|
| | | Min. | Typ. | Max. | | |
| MFIO open circuit output voltage | V_{MFIOoc} | — | V_{VREF} | — | V | During active phase |
| MFIO pull-up resistor | R_{MFIOpu} | — | 11 | — | k Ω | Active phase, internally calibrated for OTP resistor thresholds $R_{MFIOOTPx}$ |
| MFIO input capacitance | C_{MFIOIN} | — | — | 10 | pF | |

Electrical characteristics

Table 33 Electrical characteristics of Pin MFIO (continued)

| Parameter | Symbol | Values | | | Unit | Note or test condition |
|------------------------------------|----------------|--------|------|------|------|------------------------------|
| | | Min. | Typ. | Max. | | |
| MFIO input threshold for logic “0” | V_{MFIOIL} | — | — | 1.0 | V | |
| MFIO input threshold for logic “1” | V_{MFIOIH} | 2.0 | — | — | V | |
| MFIO output voltage for logic “0” | V_{MFIOOL} | — | — | 0.8 | V | $I_{MFIOOL} = 2 \text{ mA}$ |
| MFIO output voltage for logic “1” | V_{MFIOOH} | 2.2 | — | — | V | $I_{MFIOOH} = -2 \text{ mA}$ |
| MFIO output sink current | I_{MFIOOL} | — | — | 2 | mA | |
| MFIO output source current | $-I_{MFIOOH}$ | — | — | 2 | mA | |
| Output rise time (0 → 1) | $t_{MFIOrise}$ | — | — | 25 | ns | 20 pF load |
| Output fall time (1 → 0) | $t_{MFIOfall}$ | — | — | 25 | ns | 20 pF load |

Table 34 Electrical characteristics of Pin ZCD

| Parameter | Symbol | Values | | | Unit | Note or test condition |
|---|-------------------|--------|-------|-------|---------------|---|
| | | Min. | Typ. | Max. | | |
| ZCD leakage current | I_{ZCDIk} | -10 | — | 10 | μA | $V_{ZCD} = 0 \text{ V} / 3.0 \text{ V}$ |
| | | -1 | — | 1 | μA | $T_J = 85^\circ\text{C}$ $V_{ZCD} = 0 \text{ V} / 3.0 \text{ V}$ |
| ZCD threshold for Vout overvoltage protection | V_{ZCDOVP} | 1.511 | 1.600 | 1.632 | V | |
| ZCD voltage threshold for determining ZVS pulse length based on V_{ZCD} | $V_{ZCDtZVSstap}$ | 0.194 | 0.220 | 0.246 | V | Start-up phase, rising slope |
| ZCD zero-crossing detection threshold | V_{ZCDTHR} | 15 | 40 | 70 | mV | Falling slope |
| ZCD input voltage negative clamping | $-V_{ZCDCLN}$ | 140 | 180 | 220 | mV | |

Table 35 Electrical characteristics of Central control functions

| Parameter | Symbol | Values | | | Unit | Note or test condition |
|--|----------------|--------|-------|-------|---------------|---|
| | | Min. | Typ. | Max. | | |
| VDDP power supply | V_{VDDP} | 3.04 | 3.20 | 3.36 | V | |
| VREF reference voltage | V_{VREF} | 2.391 | 2.428 | 2.465 | V | |
| Main clock oscillation period time base | t_{MCLK} | 15.0 | 15.8 | 16.6 | ns | |
| Stand-by clock oscillation period time base | t_{STBCLK} | 9.0 | 10.0 | 11.2 | μs | |
| Slow task period time base | $t_{SLWTASK}$ | 93 | 100 | 107 | μs | |
| Very slow task period time base | $t_{VSLWTASK}$ | 4.68 | 5.00 | 5.32 | ms | |
| Sampling time period | t_{sample} | 93 | 100 | 107 | μs | |
| Restart step time base for auto-restart mode | $t_{ARMbase}$ | 270 | 300 | 336 | ms | Base for configurable auto-restart time t_{ARMslp} when auto-restart mode entered |

Electrical characteristics
Table 35 **Electrical characteristics of Central control functions (continued)**

| Parameter | Symbol | Values | | | Unit | Note or test condition |
|--|-------------------------|--------|------|------|------|--|
| | | Min. | Typ. | Max. | | |
| HW initialization time period after IC activation for VCC turn-on | t_{HWini} | — | 3.2 | — | ms | $V_{VCC} > V_{VCCon}$ after UVOFF |
| Time period for initial start-up conditions check | $t_{stupcheck}$ | 1.80 | — | 2.13 | ms | Start-up after $V_{VCC} > V_{VCCon}$ |
| Limited maximum change in on-time control for HS switch during CRM operation | $\Delta t_{HSonmaxCRM}$ | 75 | 80 | 85 | ns | CRM operation, t_{HSon} not limited by V_{CSSET} |

Revision history

Revision history

| Document version | Date of release | Description of changes |
|------------------|-----------------|--|
| R1.0 | 30.10.20 | <ul style="list-style-type: none"> Release of final datasheet |
| R1.1 | 20.01.21 | <ul style="list-style-type: none"> Corrected default value for V_{ZCDUVP} in table 15 Added specification for I_{ZCDIk} in table 34 Corrected tolerances for $V_{ZCDtZVSstup}$ in table 34 Corrected TC_V3a and TC_V3b in table 22 |
| R1.2 | 10.06.21 | <ul style="list-style-type: none"> Editorial corrections in Table 1 Corrected "mode transmission" to "mode transition" in Chapter 3.3.2 Corrected parameter names in Figure 19 Corrected default values of N in Table 5 Corrected default values of V_{ZCDnom} and $t_{Transnom}$ in Table 6 Corrected default value and description of $t_{LS2ZCDnom}$, description and tolerance class of $t_{LS2ZCDmin}$ in Table 7 Corrected description of $t_{ZCDrefilRVS}$ and $t_{ZCDfifilRVS}$ in Table 8 Corrected default value of $N_{RVSvalmax}$ in Table 9 Corrected default value of $I_{SETBMen\%}$, $I_{SETBMex\%}$, and $V_{FBBMfastex}$ in Table 10 Corrected default value of $N_{HBcyclemax}$ in Table 11 Corrected default value of V_{VSFBOP} in Table 13 Corrected tolerance class of $t_{startto}$ in Table 14 Corrected tolerance classes of $t_{OCP1lev1bl}$, $t_{OCP1lev2bl}$, and $t_{OCP1maxbl}$ in Table 16 Corrected default values of $I_{SETRVS2CRM\%}$ and $I_{SETCRM2RVS\%}$ in Table 19 Corrected default value of $d_{Jitterspread\%}$ in Table 20 Corrected default value of t_{PDC} in Table 21 Corrected LSGD peak source current $-I_{LSGDpksrc}$ in Table 29 Corrected VS pin blanking time for input voltage V_{in} slow brown-out protection $t_{VSSBOPbl}$ in Table 30 Corrected tolerance classes TC_T1 and TC_T2, added tolerance classes TC_T3 and TC_T4 in Table 22 Corrected Slow task period time base $t_{SLWTASK}$, Very slow task period time base $t_{VSLWTASK}$, Sampling time period t_{sample}, Time period for initial start-up conditions check $t_{stupcheck}$, in Table 35 Removed Minimum HS switch on-time $t_{HSonmin}$ from Table 35 which is configurable and duplicates t_{HSleb} in Table 7 <p>(refer to errata sheet ES_2105_PL21_2105_051535)</p> |

Trademarks

All referenced product or service names and trademarks are the property of their respective owners.

Edition 2021-06-10

Published by

Infineon Technologies AG

81726 Munich, Germany

© 2021 Infineon Technologies AG

All Rights Reserved.

Do you have a question about any aspect of this document?

Email: erratum@infineon.com

Document reference

IFX-mwt1553183552776

IMPORTANT NOTICE

The information given in this document shall in no event be regarded as a guarantee of conditions or characteristics ("Beschaffheitsgarantie").

With respect to any examples, hints or any typical values stated herein and/or any information regarding the application of the product, Infineon Technologies hereby disclaims any and all warranties and liabilities of any kind, including without limitation warranties of non-infringement of intellectual property rights of any third party.

In addition, any information given in this document is subject to customer's compliance with its obligations stated in this document and any applicable legal requirements, norms and standards concerning customer's products and any use of the product of Infineon Technologies in customer's applications.

The data contained in this document is exclusively intended for technically trained staff. It is the responsibility of customer's technical departments to evaluate the suitability of the product for the intended application and the completeness of the product information given in this document with respect to such application.

WARNINGS

Due to technical requirements products may contain dangerous substances. For information on the types in question please contact your nearest Infineon Technologies office.

Except as otherwise explicitly approved by Infineon Technologies in a written document signed by authorized representatives of Infineon Technologies, Infineon Technologies' products may not be used in any applications where a failure of the product or any consequences of the use thereof can reasonably be expected to result in personal injury.